Improving System Throughput Based on Multiuser Cooperative Mobility in Ad hoc Networks

XIE Jiquan

June 15th, 2021

Abstract

It is indispensable for Society 5.0 to build an economic and efficient high-speed wireless communication network. With the large-scale popularization of intelligent devices, the era of Internet of Things (IoT) is coming. Due to the intrinsic properties of IoT devices, resource factors such as transmission power, bandwidth, and coverage are often subject to constraints when implementing applications with high quality of service (QoS) requirements. System throughput is a vital criterion for judging the user experience to ensure that QoS requirements are met. In this thesis, we consider the improvement of the system throughput as a whole, and not only the improvement of transmission rates for individual users.

In recent years, users have been able to roam with IoT devices by virtue of the widespread deployment of 5th-Generation (5G) networks. However, the current 5G technology has many limitations. Base stations, for example, are expensive to deploy and have a small coverage. Wi-Fi technology can provide cheaper and wider coverage communication than 5G cellular base stations. On the other hand, Wi-Fi has a small coverage area, and the key to its practicality is to expand the coverage area by using multi-hop. For comfortable communication anytime and anywhere, ad hoc networks can be formed based on Wi-Fi and Device-to-Device (D2D) communication by relaying users, as a necessary complement to 5G technology.

Currently, there are still some problems for achieving high QoS in ad hoc networks as follows. First, radio waves have varying throughput performance depending on the relay user's physical distance. Since physical distance often determines the fading characteristics of the signal as it propagates through space, the farther the distance the greater the signal fading, resulting in poorer throughput performance. Additionally, the degree of interference is a factor in determining throughput performance, which varies depending on the location of other users. Therefore, moving a user to a location where there is minimal interference and optimizing the physical distance between each user will optimize its throughput performance. We collectively refer to this control method for mobile users as user cooperative mobility mechanism. Finally, given the motivation and incentives for users to move, we consider social intimacy among users as a reason they are willing to move. There are two aspects to be solved, i) the motivation to forward other users' data, and ii) the best selection of mobile users, i.e., which users should be moved. In summary, the following three problems are addressed in this research.

1. How to maximize throughput in a small number of users application scenario while considering radio wave propagation and signal interference between each user?

2. How to leverage user mobility strategy to achieve high throughput performance and low algorithmic complexity in complex application scenarios?

3. How to maximize throughput considering the motivation for cooperation of movable users, i.e. given the social relationships and satisfying the high social intimacy between each other in the social-physical ad hoc networks?

To address these problems, previous approaches are limited to considering the single user mobility, i.e., an *independent* mobility strategy. The reason is that the complexity is extremely high due to the huge diversity of the solution space, and in the case of multiuser mobility, both user interference and signal strength need to be considered. This diversity makes it difficult to achieve optimality, so few researches have overcome this challenge so far. The originality of this thesis is to overcome the diversity for achieving the optimal solution by proposing a multiuser mobility control mechanism with *cooperative* behavior. To our best knowledge, we are the first to study the throughput performance maximization problem based on multiuser cooperative mobility in ad hoc networks. To this end, we present the following three contents, which are summarized as follows:

- First, we propose an interaction position game (IPG) to maximize throughput based on multiuser cooperative mobility. The multiuser cooperative mobility and the different geographical locations and distances between all users are jointly considered. For the conventional game-theoretic approaches, they always exploit self-centered behaviors among players and maximizes their own benefits. In this game, we use the cooperative behavior among movable users to maximize the overall system throughput performance, rather than being self-centered like the traditional game models. In summary, this research contributes to obtaining the best mobility strategy for maximizing throughput while considering the radio wave propagation and signal interference between each user.

- Second, we propose a new algorithm, called Maximum Throughput algorithm for Optimal Position (MTOP), based on the known geographic location information of fixed users. Different from previous studies, the lower and upper bounds are derived to determine the search space domain based on feasible location assembles. Furthermore, a conflict set of locations graph is defined to prove this proposition that the domain includes the optimal location allocation. In summary, this research contributes to yielding an efficient multiuser cooperative mobility strategy in a large number of users to achieve high throughput performance and low algorithmic complexity.

- Finally, we propose the Relay selection and Link Interference Degree Graph (RS-LIDG) algorithm to obtain an optimal social relay selection scheme with high intimacy requirements to maximize the system throughput for social-physical ad hoc networks. Feasible relays and multiuser cooperative mobility with satisfactory link reliability for throughput maximization are jointly considered. In summary, this research contributes to maximizing throughput while satisfying high social intimacy in social-physical ad hoc networks.

Through this thesis, we contribute to maximizing throughput performance based on multiuser cooperative mobility in ad hoc networks. First, this thesis demonstrates that the proposed IPG method achieves the best throughput by *cooperative* behavior different from the conventional game approaches. Second, this thesis strongly explains that the proposed MTOP algorithm achieves excellent throughput performance and lowest complexity for a large number of users. Finally, the proposed RS-LIDG algorithm is also expected to provide support for social networks to enable the best communication experience of wireless wearable devices in Society 5.0.

Keywords: *System throughput*, *Ad hoc networks*, *Multiuser cooperative mobility*, *Cooperative behavior*, *Game-theoretic approaches*, *Computational complexity*, *Social relay selection*, *Social intimacy*.

Contents

List of Figures

List of Tables

Chapter 1

Introduction

1.1 Background

Ad hoc networks have attracted massive attention from researchers with the rapidly growing mobile devices. Ad hoc network protocol is widely adopted in the small-scale area (hotel, house, etc.) and population gathering community (business center, commercial office, etc.) for assisting in individual and commercial usage [1]. With the widespread of IoT, the increasing demand for ad hoc networks for high transmission rate and QoS [2] is a significant issue that requires further exploration. For supporting high QoS, system throughput is a vital parameter to advance the transmission rate; that is, the amount of data traffic per unit slot received by the access point (AP) [3]. Therefore, pursuing the maximum system throughput is always a worthy research hotspot.

1.2 Conventional methods to improve throughput in ad hoc networks

There are a number of conventional methods to improve throughput in ad hoc networks. The throughput improvement methods of ad hoc network mainly focus on three layers, namely physical layer, medium access control (MAC) layer, and network layer. Conventional methods to improve throughput are shown in Table 1.1.

Table 1.1 Summary of conventional methods to improve throughput

Layer	Category	Problems	Related work
Physical layer	MIMO-OFDM	High spectrum costs	[4]-[9]
	Aggregation schemes	High bandwidth costs	[10]
	Block acknowledgement	High complexity	[11]-[12]
MAC layer	Enhanced MAC layer technology	High complexity	[13]-[14]
	MAC scheduling mechanisms	Low traffic density	[15]-[17]
	Admission control mechanisms	High bandwidth costs	[18]-[20]
Network layer	Route discovery	High overhead	[21]
	Route selection	Low traffic density	[22]-[23]

For the physical layer, [4]-[12] suggested that the throughput can be improved by employing multiple-input multiple-output with orthogonal frequency division modulation (MIMO-OFDM) technology, aggregation mechanism and block acknowledgement. MIMO technol-

ogy improves performance due to its reliance on antenna diversity and spatial multiplexing, which allows it to transmit and receive from multiple spatial channels simultaneously [4]-[6]. In addition, OFDM overcomes the performance degradation of traditional IEEE 802.11 in a multipath environment [7]- [9]. [10] proposed aggregation schemes to transmit some frames together into aggregated packets. In [11]-[12], they proposed block acknowledgement, which consists of grouping frames and sharing the access time in the channel among several frames that have the same destination. Unfortunately, these schemes require high spectrum resources, and consume large amounts of bandwidth resources with a high degree of complexity during signal modulation and demodulation process.

For the MAC layer, most of the researchers focus on three points, i.e., enhanced MAC layer technology, MAC scheduling mechanisms, and admission control mechanisms, respectively [13]-[20]. [13]-[14] developed an enhanced MAC layer, including aggregation schemes and service differentiation, to support the throughput requirements of real-time users. Additionally, some researchers focused on scheduling methods that improve throughput performance and guarantee fairness of real-time streams in ad hoc networks [15]-[17]. The proposed scheduling methods are performed at the access point that maintain the list of time slots reserved by the transmitter for the next transmission, which reduces the collisions in the network and consequently effectively improves the throughput performance. A distributed admission control mechanism is proposed for contention-based channel access to protect higher priority data streams by incorporating a transmission budget for each admission control [18]. [19]-[20] proposed two local data control schemes and an admission control scheme for ad hoc wireless networks with considering the MAC standard. However, these MAC layer schemes are only applicable when the traffic load is not very heavy and do not consider the bandwidth reduction in a multi-hop ad hoc environment.

For the network layer, some researchers concentrated on the routing protocol, including route discovery and route selection [21]-[23]. [21] proposed a ticket-based throughput routing protocol that uses tickets to find delay-constrained or bandwidth-constrained routes. Based on it, [22]-[23] proposed trigger-based distributed-QoS routing methods, which are location-based routing protocol. These protocols distinguish from others by using a local neighborhood database and based on outage prediction during route discovery, thereby increasing throughput. Unfortunately, these network layer protocols incur a large communication overhead and require additional information, such as the strength of the received signal, and throughput performance is unstable when data traffic density is high.

Consequently, conventional studies to improve throughput focus on nothing more than three points: adopting advanced techniques at the physical layer (i.e., MIMO-OFDM), enhancing the efficiency of mechanisms at the MAC layer, and boosting the routing accuracy of network layer routing protocols. However, these methods always consume significant economic and physical resources, or add significant complexity to protocol standards or network architectures.

1.3 A new method: user cooperative mobility

In order to deal with these implementation problems, some researchers proposed a new method, called user cooperative mobility, to improve the overall throughput. It allows a movable user to change its geographical position to adapt links and eliminate performance anomalies. Fig.1 depicts the application scenario for user cooperative mobility. We note that some fixed users on the city's periphery might experience a low transmission rate and poor throughput performance due to their distance from the nearest AP. Meanwhile, for work or business reasons, people close to an AP may move toward the edge of the city. These mobile users are able to carry data traffic and act as relays forwarding data to fixed users. Considering the signal-to-interference-plus-noise ratios (SINRs) between all users, it is worth addressing the issue of how to move these mobile users to the optimum positions.

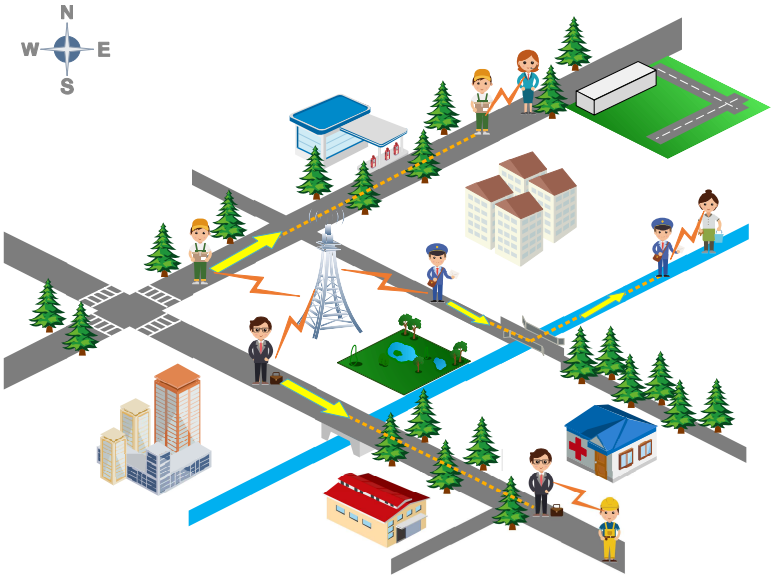

Fig. 1.1 Application scenario of user cooperative mobility.

Considering the effects of interference and SINR between all users, these movable relays can move to the best location within a limited range to help the fixed users and increase the throughput performance, especially in the earthquake, fire, and other emergencies. User cooperative mobility approach is not only used in disaster or emergency scenarios, but also can be applied in common scenarios. For example, in daily life, when fixed users are far away from the access point or cannot access Internet directly because of strong outside interference or low receive power, they can access Internet with the help of other movable users as relays. In summary, this method is able to enhance throughput by simply moving users to the right location at a negligible cost of execution compared to the traditional methods of increasing bandwidth or improving protocol efficiency.

In recent years, many researchers focused on algorithms for improving system throughput through user mobility methods. M. Grossglauser *et al.* [24] first theoretically proved that user mobility behavior can be exploited to dramatically enhance the system throughput

through path diversity. Subsequently, B. Baron *et al.* [25] demonstrated that the random mobility of portable devices can be viewed as providing opportunistic access to data that can effectively overcome base station constraints and increase throughput. Later, T. Murase [26] and A. Chaintreau *et al.* [27] showed that cooperative user mobility can reduce the resource consumption of service providers and effectively increase throughput. Thus, it can be effective to design an efficient algorithm based on human mobility paths to improve throughput at a low complexity.

The independent mobility approach was proposed to boost SINR and throughput significantly. It requires the movable users to consider the interference between all the devices interacting with each other, not just to increase their own transmission rate or reduce others' interference, i.e., the movable users have to behave cooperatively concerning system throughput, rather than with selfish or greedy incentives. Sumiko Miyata *et al.* [28] proposed an optimal AP selection algorithm for maximizing throughput while keeping newly arrived user throughput stable. In [28], this algorithm should be applied within the movable distance and acceptable throughput threshold. Ryo Hamamoto *et al.* [29] introduced an AP selection method based on collaboration among APs and user's mobility under the single user and the limited distances. In addition, Tianran Luo *et al.* [30], [31] evaluated system throughput features of the single movable user and validated the best location under capture effect or dynamic back-off time. However, these related work only centered on single-user mobility strategies, which are limited in mobility distance and energy consumption.

To make this new approach simple to implement, some researchers introduced the intuitive method [32]-[33]. It means that these movable users move to an intermediate location between the two assisted users for connecting each link. J. Li *et al.* [32] analyzed ad hoc wireless networks' capacity. They discovered a reasonable location scheduling; that is, the average distance between the source user and the destination user must be equal to make the network expands total throughput. R. Ohmiya *et al.* [33] investigated the throughput properties of three different ad hoc network topologies and revealed that the best locations are in the middle of two users. These papers verified that the intuitive method could improve throughput.

1.4 Problems

These previous researches have not considered the motivation for these movable users, i.e., why these users would want to act as relays to assist others with poor data rate. As a result, the problems of the related work are summarized as follows:

1. Most researchers have only evaluated the features and performance of single-user mobility without jointly considering the problem of multiuser cooperative mobility and user interference in ad hoc networks [28]-[31].

2. Many proposed algorithms for throughput enhancement have not considered the complexity of the practical execution process, and high complexity can lead to excessive computing time [24]-[27]. The trade-off between the best throughput performance and the least algorithmic complexity is a problem to be explored.

3. Few researchers have comprehensively studied the consideration of user motivation for cooperation to maximize the throughput of social-physical ad hoc networks [32]-[33]. A relevant practical algorithm for a multiuser cooperative mobility scheme in a physical-social network has not previously been investigated due to the complex transmission strategies and social intimacy requirements involved.

1.5 Challenges, approaches, and contributions

This thesis aims to solve the three problems of related work, which are pointed out in the above sub-chapter. To this end, we challenge to study the throughput performance considering interference between each other, and investigate the useful mathematical theories to solve an NP-hard problem. First, we study the relationship between signal attenuation and spatial distance, as well as throughput. Additionally, we should consider how to move these users to the best position in different locations, with multiple users interfering with each other. The challenges in this thesis are summarized as follows:

1. We study a multiuser cooperative mobility approach for maximizing throughput considering the signal attenuation and interference with different positions of users.

2. We investigate a feasible and effective approach to achieve high throughput and low algorithmic complexity for larger number of user application scenarios.

3. We explore an approach to improve the system throughput of social networks through multiuser cooperative mobility, i.e., to maximize throughput with high intimacy for relay selection.

To approach the above challenges, we firstly focus on multiple movable user mobility and ad hoc networks considering the interference influence among users in different position scenarios. In particular, a system throughput maximization problem is formulated for optimizing and finding the best position of multiple movable users. We propose an interaction position game (IPG) to realize maximization throughput performance. The originality of this game lies in the exploitation of cooperative behavior between movable users, unlike the selfish behavior in traditional games. As a result, this approach can obtain the global optimum rather than suboptimal or local values, and then achieve better throughput than the traditional game-theoretic approaches.

For reducing the complexity of mobility control algorithms and enabling high-throughput performance, we utilize the coordinate information of cooperative users to propose a Maximum Throughput for Optimal Position (MTOP) algorithm, which not only maximizes system throughput but also reduces computation cost and communication overhead. Specifically, the key idea of the algorithm is that by defining the conflict set of the location graph and proving the upper and lower bounds, the solution space can be partitioned so that the algorithm converges to the optimal or suboptimal solution with extremely low complexity.

For explaining the reasons and motivations for moving users, we consider a social network based on multiuser cooperative mobility and formulate a throughput maximization problem that specifies the requirements for both the social and physical layers. We propose the Relay Selection and Link Interference Degree Graph (RS-LIDG) algorithm. The originality of the algorithm lies in creatively exploiting graph theory to prove that the nonconvex problem can be transformed into a convex one by iteratively partitioning the mobility region to find the optimal locations of the mobile relays. As a result, the proposed RS-LIDG algorithm can achieve a significant throughput gain and a reduction in relay selection time compared to previous methods.

In summary, we focus on the following approaches and presents the following contributions:

1. We propose an Interaction Position Game (IPG) with jointly considering different geographical places and distances among all of the users to maximize throughput in Chapter 3. Unlike traditional game-theoretic approaches, this game exploits cooperative behavior among movable users to obtain a global optimum rather than a sub-optimum.

2. We introduce a new algorithm, called Maximum Throughput for Optimal Position (MTOP), to obtain high throughput with low complexity based on multiuser cooperative mobility in Chapter 4. Through this algorithm, the solution space can be partitioned to achieve parallel search and rapidly converge to the optimal or suboptimal, which greatly reduces the complexity. Therefore, in order to reduce complexity in the presence of a large number of users, a compromise between optimal throughput and minimum algorithmic complexity is required.

3. We propose the Relay Selection and Link Interference Degree Graph (RS-LIDG) algorithm considering feasible relays and multiuser cooperative mobility with satisfactory high social intimacy for throughput maximization in Chapter 5. This proposed algorithm achieves a significant throughput gain and a reduction in relay selection compared to conventional methods by iteratively partitioning the mobility region to find the optimal locations of the mobile relays.

The chapters of this thesis are organized as follows. Chapter 2 shows related technologies (i.e., the definition ad hoc networks and user cooperative mobility) and related work

about this thesis. Chapter 3 introduces an interaction position game based on multiuser cooperative mobility in ad hoc networks. Chapter 4 presents an optimal location allocation based on multiuser cooperative mobility for high throughput with low complexity. Chapter 5 introduces an effective collaboration method to maximize throughput based on multiuser cooperative mobility in social-physical ad hoc networks. Finally, the conclusion and future work are presented in Chapter 6. This thesis is based on my three published open access journals [34]-[36]. These three journals give me their copyrights.

Chapter 2

Related Technologies

This chapter shows related technologies, the definition of ad hoc networks and user cooperative mobility, and related work for this thesis. This chapter highlights the problem of these related technologies and the novelty of this thesis. The following subchapters summarize challenges, approaches, and contributions in each chapter.

2.1 Throughput improvement in ad hoc networks

2.1.1 Ad hoc networks

As smartphones become massively popular, the information explosion has arrived, and the amount of data will grow geometrically over the next decade. Device-to-device (D2D) technology has received comprehensive attention to address this challenge to overcome the shortcomings of traditional cellular networks [37]. D2D allows users to communicate directly without the base station to provide services. Additionally, D2D improves the user experience of short-range communications and address data flooding disasters in information-centric networks to enhance the robustness of the infrastructure [38]. Recently, ad hoc networks that can be easily established leveraging D2D attributes have been widely deployed in small areas and populated organizations to aid personal and business usage.

Ad hoc networks are traditionally structured and decentralized independent networks that maintain each device function as an independent router and generates independent data without the need for any network infrastructure based on a base station [39]. Wireless transmitters and receivers are equipped with ad hoc networks nodes by using a cooperative transmission protocol, which may use broadcast [40], amplify-and-forward (AF), or decode-and-forward (DF) [41] transmission. IEEE 802.11 standard presents ad hoc network as an indispensable class of local area networks [42] that can be widely adopted in small-scale environments and communities, such as meeting rooms, exhibition halls, and hotels.

Fig. 2 describes the basic concept of ad hoc networks. In a limited area, movable devices play the role of intermediate nodes that can send and receive data packages from the access point or source device and then relay to other required devices. It can be noted that an ad hoc network is an infrastructure-less wireless network of single-hop or multihop paths of mobile nodes that are free to move in any direction and operate as both hosts and routers.

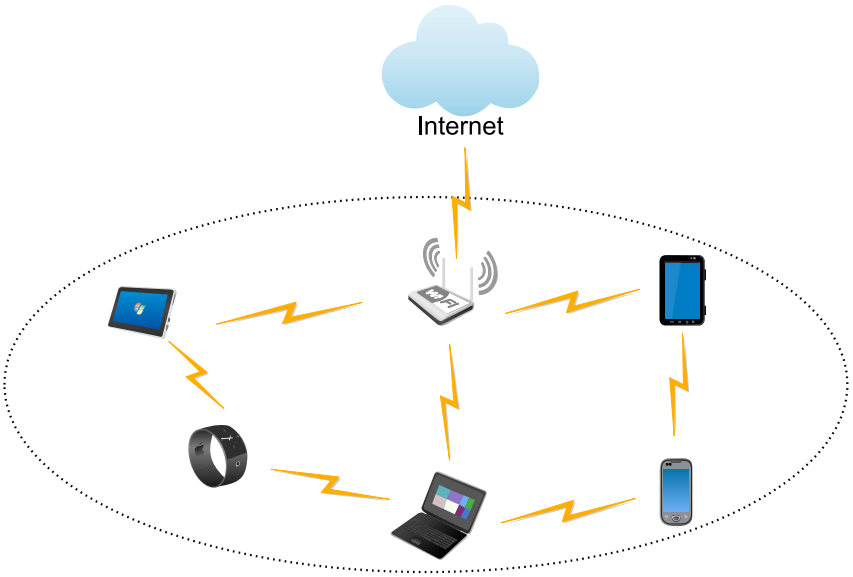

Fig. 2.1 The concept of ad hoc networks.

2.1.2 Throughput requirements

The current ubiquitous access to smart devices and the huge traffic generated by emerging multimedia applications, such as YouTube and Netflix, urgently requires the construction of high-speed communication networks. The increasing demand for ad hoc networks for high transmission rate, low latency, and quality of service (QoS) is a significant issue that requires further exploration. Thus, it is necessary to maintain the QoS in ad hoc netwroks.

System throughput is a vital criterion for judging the user experience to ensure that QoS requirements are met. Generally, the system throughput is defined as the amount of data traffic per unit slot received by the access point (AP). How to maximize throughput in ad hoc networks is always a topical issue to be explored.

However, due to the unpredictable link properties, node mobility, and bandwidth resource limitations, it is challenging to improve throughput as a result. First, physical distance often determines throughput among users at the interference area, error rate, and transmission rate, which are calculated by bandwidth and protocol behavior. Additionally, during the transmitting process period, the interference among different users causes a performance anomaly [43], which degrades the transmission rate and system throughput to poor performance due to the carrier sense multiple access with collision avoid (CSMA/CA) protocol. Finally, the waste of transmission time because of channel capture for one user causes not only a delay but also increases communication overhead in the operational process.

Therefore, we seek to construct network architectures and propose protocol mechanisms that can satisfy demands for throughput maximization in ad hoc networks.

2.1.3 Conventional approaches for throughput improvement

Currently, there are a large number of conventional approaches for achieving throughput improvement in the physical layer, network layer, and medium access control (MAC) layer [44]. The MAC layer plays the most critical role for throughput enhancement since it is a medium for communication and support of other layer services, especially service differentiation, minimum latency, and fairness in bandwidth allocation. Overall, we mainly discuss the proposed MAC mechanisms that lead to achieving high throughput, which are shown in Table 2.1.

Table 2.1 Summary of conventional approaches for improving throughput in the MAC layer

Category	Approach	Problems	Related work
Enhanced MAC layer technology	Congestion control	High complexity	[13]
	Contention mechanism		[14]
MAC scheduling mechanisms	TXOP sharing method	Low traffic density, No fairness	[15]
	Transmit to multiple users simultaneously		[16]
	Block acknowledgment of frame aggregation		[17]
Admission control mechanisms	WGPD algorithm	High bandwidth costs, Management overhead	[18]
	Distributed topology management algorithm		[19]
	POPR protocol		[20]

Providing high throughput through an enhanced MAC layer, Sandip *et al.* [13] proposed a design for achieving gain in transmission control protocol (TCP) throughput for different congestion control schemes, which combines 802.11e Hybrid Coordination Function (HCF) and 802.11n frame aggregation schemes. The proposed design includes several mechanisms such as admission control, calculation of the transmission opportunity (TXOP), and a scheduler that aims to increase the throughput of best-effort traffic. However, this design only guarantees that this mechanism supports small real-time traffic, and no consideration was given to the different interference and noise levels. Zhiqun *et al.* [14] focused on bandwidth allocation schemes for distributed wireless LANs based on the IEEE 802.11ac contention mechanism. For this purpose, they proposed Markov chains under non-saturated conditions, but they only consider ideal channel conditions, and all the enhanced PHY/MAC characteristics are not included.

MAC scheduling mechanism aims to design an effective scheduler for frame aggregation to achieve high throughput at the upper layer. Aajami *et al.* [15] proposed a TXOP sharing method based on throughput awareness. In this method, the ant colony optimization mechanism is applied to achieve the scheduling and joint link adaptation of the TCP downlink, but this TXOP does not support dynamic channel management. In [16], Mounir *et al.* proposed a method that can transmit to multiple users simultaneously and provide appropriate transmission parameters for selected users. Then, it is helpful to select different transmis-

sion parameters and improve user throughput. However, the interference of noise and the fairness of channel bonding is not considered. In [17], Mustafa *et al.* implemented the block acknowledgment of frame aggregation and tuning the TCP congestion algorithm to improve the algorithm's performance and increase the packet transmission rate. Yet, the authors did not consider the different channel conditions while implementing the TCP congestion algorithm. In brief, most algorithms or mechanisms did not consider different channel access conditions, as well as sacrifice significant bandwidth or management resources to boost limited throughput. Hence, they are sometimes inefficient in practical applications.

Akyol *et al.* [18] proposed the wireless greedy primal-dual (WGPD) algorithm for combined congestion control and scheduling to solve the utility maximization problem. In [19], Bao and Garcia-Luna-Aceves proposed a distributed topology management algorithm that constructs and maintains a backbone topology, which makes the provision of QoS services more stationary by topology management. Rajesh *et al.* [20] presented a path observation-based physical routing protocol named POPR, which improves physical forwarding and intersection. Unfortunately, both of those algorithms sacrifice considerable bandwidth or management resources to elevate finite throughput and would be inefficient to apply in practice.

Consequently, conventional studies of throughput improvement in MAC layer focus on nothing more than three points: queue scheduling and congestion control mechanisms, topology management, and increasing protocol efficiency. Unfortunately, these methods always consume a substantial amount of economic and physical resources, high overhead or add a great deal of complexity to protocol standards.

2.2 User cooperative mobility approach

2.2.1 Single-user cooperative mobility

To reduce economic costs and implementation challenges, some researchers have proposed cooperative user mobility approaches to improve throughput. It allows a movable user to change its geographical position to adapt links and eliminate performance anomalies. Thus, it can be effective to design an efficient algorithm based on human mobility paths to improve throughput at a low resource cost.

Fig. 2.2 depicts the operation of the single-user cooperative mobility approach. A data package is received by the movable user and relayed to the fixed user and then retransmitted to other devices that cannot receive radio or signal directly from the AP. The QoS of many users cannot be satisfied to meet the typical requirements due to the distance away from AP. When many users are far away from AP, the transmission rate is low due to the signal attenuation, especially for remote nodes. According to the abnormal performance, the lower rate nodes will seriously affect the system throughput. The movable user can select the best position to improve system throughput considering the effects of interference and signal to interference plus noise ratio (SINR) among all users.

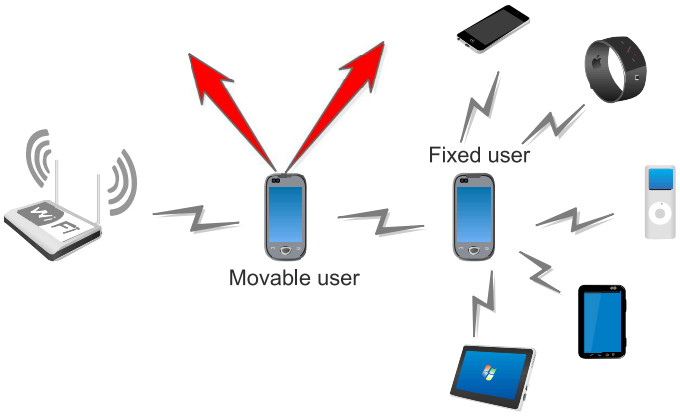

Fig. 2.2 Single-user cooperative mobility.

In recent years, many researchers have been working on methods to improve throughput through single-user mobility approach. S. Miyata *et al.* [28] introduced an algorithm for selecting the optimal AP based on user mobility to maximize throughput. Hamamoto *et al.* [29] introduced an AP selection method based on movable APs and users. T. Luo *et al.* [30], [31] experimentally verified the system throughput gain for a single mobile user at the optimal location and validated the range of throughput variation under the capture effect. In addition, K. Okumura *et al.* [45] proposed direct and indirect methods of analyzing the throughput performance of multiple networks in the presence of link bottlenecks.

However, these papers only verified that single-user mobility can improve throughput and did not consider the interference interactions between different users.

2.2.2 Multiuser cooperative mobility

Fig. 2.3 depicts the scenario and operation of the multiuser cooperative mobility approach. There exist many movable users, all of which can act as relays or hosts to transmit data. These mobile users can act as relays to help fixed users who are unable to establish a connection with the AP, enabling them to successfully transmit data with the AP. However, moving these mobile users to the optimal location is a challenge, since users in different locations can interact with each other on SINR and ultimately affect throughput.

At present, most of these previous approaches are only centered on single-user mobility strategies, which are limited in mobility distance and energy consumption. Moreover, multiple user mobility leads to the NP-hard problem and high complexity in traditional algorithms. Currently, the effective algorithm of multi-user cooperative mobility strategy has not been proposed. According to the knowledge, this thesis is the first to using the multiuser cooperative mobility to maximize throughput.

In this thesis, the multi-user cooperative mobility approach is demonstrated to significantly improve SINR and throughput. It requires the multiple movable users to consider the interference between all the devices interacting with each other, not just to increase their own transmission rate or reduce others' interference, i.e., the movable users have to behave

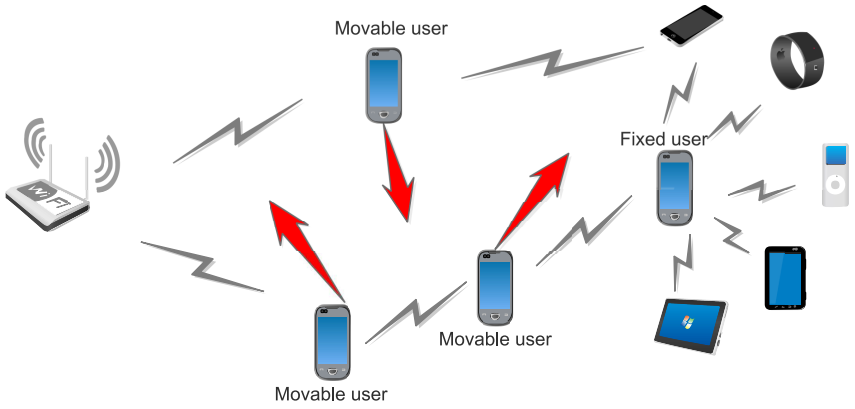

Fig. 2.3 Multiuser cooperative mobility.

cooperatively concerning system throughput, rather than with selfish or greedy incentives.

2.3 Challenges, approaches, and contributions in each chapter

2.3.1 Challenges, approaches, and contributions in Chapter 3

In Chapter 3, we focus on multiple movable user mobility and ad hoc networks without limiting transmission time and distance. We challenge the interaction between signal fading and spatial distance for movable users, and considers the problem of interference between users. Unlike the non-cooperative game described above, the cooperative behavior is exploited by the utility function of position mobility to maximize the throughput performance. Different from a traditional specific position of single-user mobility, we consider the interference influence among users in different position scenarios. The contributions of Chapter 3 is summarized as follows:

- We jointly consider different geographical places and distances among all users. A system throughput maximization problem is formulated for optimizing and finding the best position of multiple movable users.
- We propose an interaction position game (IPG) based on system throughput and user position information. For the conventional game-theoretic approach, it exploits selfish decentralized behaviors among players and maximizes their own benefits. In this game, we exploit cooperative behaviors among movable users rather than assuming selfishness as in traditional game models. This IPG game-theoretic approach considers the interference impacts on other players in the optimal position while maximizing their throughput.
- We introduce the simulated annealing (SA) algorithm to solve this NP-hard problem as a comparison. Finally, a simulation is conducted to evaluate and compare the performance in terms of the proposed interaction position game (IPG) method, intuitive method, SA algorithm, and exhaustive global search by NS3.

2.3.2 Challenges, approaches, and contributions in Chapter 4

From the above, it is clear that most previous algorithms for improving throughput performance have high complexity and high communication overhead, which are sometimes not efficient in existing communication systems. Nevertheless, the relevant practical algorithms for cooperative multi-user mobility schemes have not been explored due to the complex transmission strategies and optimization conditions.

In Chapter 4, we challenge a feasible and effective approach to achieve high throughput and low algorithmic complexity for larger number of user application scenarios. Different from previous mobility strategies, we utilize the coordinate information of cooperative users to propose a new heuristic algorithm, which not only maximizes system throughput but also reduces algorithmic complexity. The contributions can be summarized as follows:

- We employ the Poisson point process (PPP) and calculate the cumulative distribution function to present the property of fixed nodes positions. From this, the Decode-and-Forward (DF) transmission technique is exploited in formulation of system throughput maximization problem, which is a mixed-integer with non-linear and non-convex problem aimed at finding the optimal location for multiple moveable users.

- For solving this NP-hard problem, we define a domain concept in which the optimal locations for movable nodes can definitely be found. Furthermore, this domain is classified as two boundaries, called as lower and upper bounds, to delineate the domain scope.

- We propose a Maximum Throughput for Optimal Position (MTOP) algorithm. A conflict set of locations graph (CSLG) is proposed to clarify and calculate the values of lower bound and upper bound. Different with the previous conflict graph methods, we allocate the feasible location partitions as exploitable resources to movable nodes in CSLG. Moreover, the allocation policy is specified based on the conflict conditions of the SINR. It is proved that the optimal locations for movable nodes must be located in the domain.

2.3.3 Challenges, approaches, and contributions in Chapter 5

In Chapter 5, a relay selection scheme and a multiuser cooperative mobility strategy are employed to ensure link reliability and stability in terms of physical link (high throughput) and social link (good intimacy). To the best of our knowledge, in the context of social-physical ad hoc networks, this is the first to comprehensively challenge an optimal scheme based on both relay selection and a multiuser cooperative mobility strategy to address the above issue. The contributions of this thesis are summarized as follows:

- We model a social-physical network based on multiuser cooperative mobility and formulate a throughput maximization problem that specifies the requirements for both

the social and physical layers. Specifically, we define the concept of link reliability by jointly considering both social intimacy and the probability of successful data transmission. A nonlinear and nonconvex (NCNL) optimization problem is then constructed, which is a classical NP-hard problem.

- We propose the Relay Selection and Link Interference Degree Graph (RS-LIDG) algorithm. The original optimization problem is decomposed into two subproblems: a relay selection scheme and a multiuser cooperative mobility strategy. For the relay selection scheme, it is demonstrated that high intimacy is achieved first while ensuring cooperation, and then optimal stopping theory is used to select the user who maximizes the effective transmission time as the optimal relay.

- We creatively exploit graph theory and prove that the nonconvex problem can be transformed into a convex one by iteratively partitioning the mobility region to find the optimal locations of the mobile relays. In the multiuser cooperative mobility strategy, the relays' different locations and the interference between users are jointly considered. Simulation results show that the proposed RS-LIDG algorithm can achieve a significant throughput gain and a reduction in relay selection time compared to previous methods.

Chapter 3

An Interaction Position Game for Maximizing Throughput

3.1 Related work

In recent years, game theory methodology has been widely applied in the field of wireless communication. Quang Duy Lã *et al.* [46] summarized game theory applications in radio resource management for wireless communications systems and networking. This book initiated formulating game theory applications in solving NP-hard problems. Koji Yamamoto *et al.* [47] introduced the properties of potential games and discussed a variety of channel assignment problems that can be solved by potential games. The summary of related work for maximizing throughput by game theory methodology is shown in Table 2.2.

Table 3.1 Summary of related work for maximizing throughput by game theory

Behavior	**Multiuser cooperative mobility**	**Ad hoc networks**	**Related work**
Noncooperative	×	✓	[46]-[47]
Noncooperative	×	×	[50]-[52]
Cooperative	×	✓	[48]-[49]
Cooperative	✓	✓	**Our work**

For ad hoc network applications, Zhangyu Guan *et al.* [48] used Nash equilibrium (NE) points to obtain nonlinear and nonconvex problem solutions in cognitive ad hoc networks. Moreover, in [49], Yuhua Xu *et al.* proposed a local altruistic game that can maximize the network throughput by considering payoffs both for each user and its neighbors. Zhang, Yan, and Mohsen Guizani [50] summarized multiuser games in wireless communications and networking, including the definitions and conditions of the noncooperative games and cooperative games. Further, they analyzed the Nash equilibrium and Nash bargaining in the examples of the power and channel allocation games. However, the authors did not elaborate on cooperative strategies in detail and did not introduce the properties of the final solution of cooperative manners.

For conventional noncooperative game-theoretical methods, D. Goodman *et al.* [51] presented utility functions for voice and data, and then proposed a new algorithm to obtain Nash equilibrium by power control for maximum utility. This thesis early introduced the concept of game theory into the research field of power control. Furthermore, Tsiropoulou, E.E., *et al.* [52] proposed a non-convex noncooperative game to make a trade-off between the uplink throughput performance and power consumption. In this noncooperative game, each user

is associated with power control utility to maximize uplink throughput performance. In the noncooperative game, the users can selfishly maximize their utility throughput performance under the limitations.

In summary, few research papers have jointly considered the different geographical positions and interference among all of the users in ad hoc networks. Furthermore, a productive algorithm or game method has not been proposed and adopted in multiple cooperative user mobility systems for maximization throughput.

3.2 System model and problem formulation

In this subchapter, we illustrate a detailed system modeling of multiple user cooperative mobility. Additionally, we formulate the system throughput maximization as an NP-hard problem and qualitatively analyze the different position cases.

3.2.1 System model

As described in earlier sections, the intermediate nodes of ad hoc networks can act as both receivers and transmitters in the communication link by D2D or peer-to-peer (P2P) technology. The multiple user cooperative mobility transmission system is shown in Fig. 3.1, in which there are multiple movable users and fixed users within the coverage of a destination user. The source user wants to send data packets to the wireless access point. However, due to limiting factors, such as long-distance or poor communication circumstances, this user cannot directly connect with the AP. The fixed users and movable users decide to cooperate with others as helpers or participants to help data transmission for the destination user and their own data uploading. In other words, the source user sends data packets by helpers (fixed and movable users) to AP in this data flow. Finally, an ad hoc network is formed as a result.

In this transmission system, we set all users to generate data traffic toward the AP, and all links are saturated. Then, the system throughput is defined as the amount of traffic per unit time received by the AP, which is equal to the average harmonic value of the transmission rate of all users. The transmission link assumed here is a multihop chain topology. The topology, that is, connectivity of the users, does not change even though the users move. The reason is that the communication link between each user is determined by social intimacy [66]. Social intimacy means that if two users are friends and form a social relationship, then the wireless link can be established between these two users in social network. This social relationship ensures the transmission route among users unchanged. The transmission route logic is that two users with a high degree of relationship transfer, otherwise not transfer. Thus, social intimacy among users can guarantee the uniqueness of the transmission link and keep the topology unchanged. Therefore, we can assume that the topology keeps unchanged even if users move dramatically.

For simplicity, we assume that movable users can move within a limited area where the

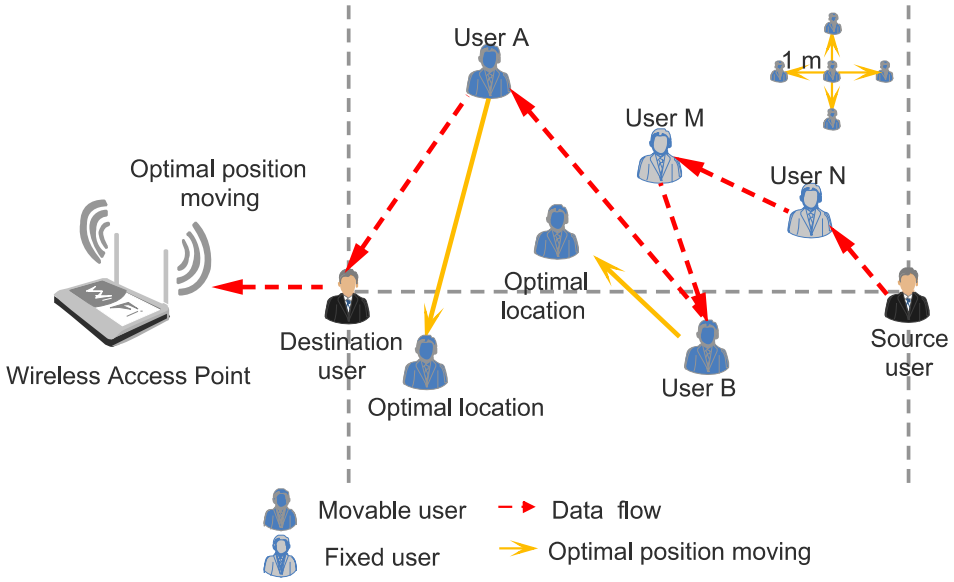

Fig. 3.1 Multiple user cooperative mobility transmission system.

location is between the source user and destination user. Without loss of generality, we define the unit length of each user's mobility as one meter, and movable users move in four directions. This is because our purpose is throughput improvement instead of the accuracy of the step unit, which is not related to the objective.

The best strategy for maximizing system throughput is to find the best position of movable users considering receiving power and interference overall among users, i.e., the optimal geographical positions of users have enough to maintain maximized throughput due to system signal to interference plus noise ratio (SINR). As a result, movable users A and B select optimal positions within the range area to achieve maximum system throughput. To precisely determine users' positions and calculate interference easily, we design the mathematical location model, as shown in Fig. 3.2.

The angle difference $\hat{\Theta}_{X,Y}$ between user X and Y can be expressed as

$$\hat{\Theta}_{X,Y} = |\Theta_X - \Theta_Y|, \Theta_X \neq 0, \Theta_Y \neq 0 \tag{3.1}$$

where Θ_X and Θ_Y are the angles between the fixed users and the horizontal line, respectively. We assume that all of the users are not located on a same line if and only if $\Theta_X \neq \Theta_Y$, $\Theta_X \neq 0, \Theta_Y \neq 0$. The research makes no sense since the optimal location for the scheduling and finding of movable users can be easily found by intuitive methods when all of the users

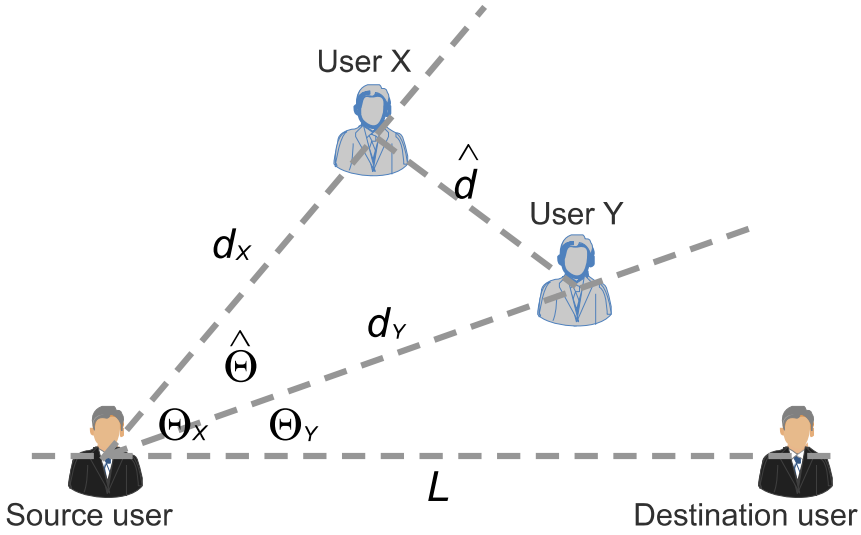

Fig. 3.2 Mathematical location model.

are at the same line [14]. Then, the distance between fixed users $\hat{d}_{X,Y}$ can be derived as

$$\begin{aligned}\hat{d}_{X,Y} &= \|d_X - d_Y\| \\ &= \begin{cases} |d_X - d_Y|, \Theta_X = \Theta_Y, \Theta_X \neq 0, \Theta_Y \neq 0 \\ \sqrt{d_X^2 + d_Y^2 - 2d_X d_Y \cos\hat{\Theta}_{X,Y}}, \Theta_X \neq \Theta_Y \end{cases}\end{aligned} \tag{3.2}$$

where d_X and d_Y denote the location of user X and user Y, respectively. L is the distance from the source user to the destination user, which is a constant, $d_X \leqslant \frac{\sqrt{5}L}{2}$, $d_Y \leqslant \frac{\sqrt{5}L}{2}$ and $\hat{d}_{X,Y} \leqslant \sqrt{2}L$. Therefore, we can accurately calculate every position case of users based on the above location model.

3.2.2 Problem formulation

In [67], Singhal, Chetna *et al.* introduced two transmission models, the model of two-tier femtocell and the model of Visible-Light Communication Local Area Networks (VLC-LANs). We refer to the representation of their model schema.

In this ad hoc network system, the communication mode is adopted in the outdoor and shadowed urban places, e.g., large squares, playgrounds, museums. Consider the actual implement site of mobility users, then the fading of the signal is mainly due to multi-path propagation. There are a lot of scattering, reflection, and refraction bodies around the movable users, causing the multi-path transmission of the signal. Therefore, we set the path loss model as the not line of sight (NLOS), so the multi-path signals superimpose. The strength of the total signal obeys the Rayleigh distribution approximately. The signal of SINR is short-term fading (fast fading) obeys the Rayleigh distribution.

Next, we describe the transmission model. It is assumed that all of the users can communicate with other users in the range of radio transmission through the same channel, which

would cause interchannel interference and capture effects. We set the number of fixed users and movable users as $|\mathcal{S}|$, $|\mathcal{M}|$, respectively, in this ad hoc network, where all users located at a limited area (the square with side length L). Denote $\mathcal{S}$ and $\mathcal{M}$ as the set of fixed and movable users, respectively, $s \in \mathcal{S}$, $m \in \mathcal{M}$. Besides, Sor and Des denote source user and destination user, respectively. Let $\boldsymbol{H} = \{Sor\} \cup \mathcal{M} \cup \mathcal{S} \cup \{Des\}$ as the total set of all users.

Assume user i sends data packets to user j , the transmission power from user i is denoted as P_i, and the distance between two users can be expressed as $\hat{d}_{i,j}$; then, the received power P_j at user j is given by

$$P_j = g_{i,j} \frac{P_i}{\hat{d}_{i,j}^{\alpha}} \tag{3.3}$$

where $g_{i,j}$ is the antenna gain and the parameter α is the path loss exponent, $2 < \alpha \leqslant 4$, which is the usual model outside a small neighborhood of the transmitter [68]. In this system, consider the actual implement site is the outdoor and shadowed urban area of mobility users. Then, we refer to the path loss model by shadowing model [69], which could be better close to reality and match with the NLOS setting parameter. The path loss is usually measured in dB, which can be expressed as

$$\left(\frac{P_i}{P_j}\right)_{\text{dB}} = -10\alpha \log_{10} \frac{\hat{d}_{i,j}}{d_0} + \Delta \tag{3.4}$$

where d_0 is determined by measurements for microcellular systems and vary between 1m and 100m, Δ is a Gaussian random variable with zero mean and standard deviation σ [69]. At the shadowed urban area, the value of σ is from 4 to 12. Then, the antenna gain $g_{i,j}$ can be calculated by (3.4). The SINR of user j can be expressed as

$$SINR_j^i = \frac{P_j}{N_0 + \sum_{k \neq i} g_{k,j} \frac{P_{k,j}}{\hat{d}_{k,j}^{\alpha}}} \tag{3.5}$$

where N_0 is the background noise power, and $k \in \mathcal{S} \cup \mathcal{M}$. For the capture effect, if the received power of the signal from user i is more significant than others, then the other weak signals are ignored as noise. We can describe this physical model as the SINR should be larger than a certain threshold, which can be given by

$$SINR \geqslant \beta \tag{3.6}$$

where the SINR threshold β is necessary for successful reception for receiving users.

We assume that the transmission link will not cause a bottleneck and guarantees flow balance because the chain topology is stable, and all links are saturated. Thus, the system capacity is approximately equal to the transmission rate. According to the Shannon's capacity

theorem, we can obtain the maximum transmission data rate of sender i

$$R_i = W \log_2 \left(1 + SINR_j^i\right) \tag{3.7}$$

where W is the physical channel bandwidth, which can be normalized as 1. In this transmission link, the total throughput is defined as the average harmonic value of every user because all links are saturated [70]. Therefore, the system throughput can be defined as

$$U_{network} = \frac{|\mathcal{S}| + |\mathcal{M}| + 2}{\sum_{s\in\mathcal{S}} \left(\frac{1}{R_s}\right) + \sum_{m\in\mathcal{M}} \left(\frac{1}{R_m}\right) + \frac{1}{R_{Sor}} + \frac{1}{R_{Des}}} \tag{3.8}$$

where R_{Sor} and R_{des} denote the transmission rates of the source user and destination user, respectively. For the sake of brevity, it is assumed that all of the users have the same transmitting power and antenna gain as P and g , respectively.

In this ad hoc system, movable users move in a small area and the relationship between convergence radius r and transmission power P is $P \propto r^2 \sim r^5$. Consider the movable distance is short and convergence radius slightly changed, then transmission power for every user can be regarded as nearly unchanged. In addition, the topology always keeps chain-type and does not change to star or tree type. We can assume all of the users have the same transmitting power and antenna gain because of fixed senders and receivers in the route.

Let $\hat{\boldsymbol{D}}_{i,j}$ denote the matrix distance between user i and user j, which can be expressed as

$$\hat{\boldsymbol{D}}_{i,j} = \|\boldsymbol{d}_i - \boldsymbol{d}_j\| \tag{3.9}$$

where $\boldsymbol{d}_i$ and $\boldsymbol{d}_j$ denote the location set of user i and user j, respectively. The distance matrix for fixed users is denoted with $\hat{\boldsymbol{D}}_{s,j} = \left(\hat{d}_{s,j}\right)$, $s \in \mathcal{S}$, $j \in \boldsymbol{H} \setminus \mathcal{M} \cup \{m\}$, where $\hat{d}_{s,j}$ represents the distance between fixed user s and other user j except for movable user. Similarly, the distance matrix for movable users is denoted with $\hat{\boldsymbol{D}}_{m,m'} = \left(\hat{d}_{m,m'}\right)$, $m \in \mathcal{M}$, $m \in \mathcal{M} \setminus \{m\}$, where $\hat{d}_{m,m'}$ represents the distance between movable user m and other movable user m'. Denote the distance matrix for movable and fixed users as $\hat{\boldsymbol{D}}_{m,j} = \left(\hat{d}_{m,j}\right)$, $m \in \mathcal{M}$, $j \in \boldsymbol{H} \setminus \mathcal{M} \cup \{m\}$, where $\hat{d}_{m,j}$ represents the distance between movable user m and other user j except for movable user.

For fixed users, source user and destination user, the location set for them is defined as $\mathbf{d} = (d_i)$, $i \in \boldsymbol{H} \setminus \mathcal{M} \cup \{m\}$. $\mathbf{d}$ is a set of constants, because the location information of these users is known. Let $\tilde{\boldsymbol{d}} = \left(\tilde{d}_m\right)$, $m \in \mathcal{M} \setminus \{m\}$ denote the location information set of movable users, which is a set of variables.

From above, it is noted that $\hat{\boldsymbol{D}}_{m,i}$ and $\hat{\boldsymbol{D}}_{m,m'}$ are the unknown matrixes of variable, and $\hat{\boldsymbol{D}}_{s,i}$ is the known matrix of constants. $\hat{\boldsymbol{D}}_{m,i}$ and $\hat{\boldsymbol{D}}_{m,m'}$ can be expressed as $\hat{\boldsymbol{D}}_{m,j} = \|\tilde{\boldsymbol{d}} - \mathbf{d}\|$, $\hat{\boldsymbol{D}}_{m,m'} = \|\tilde{d}_m - \tilde{d}_{m'}\|$, respectively, so both of them are the functions of the variable set of $\tilde{\boldsymbol{d}}$.

When a fixed user s, $s \in \mathcal{S}$ is a sender, the SINR Γ_j^s of a receiver j, $j \in \boldsymbol{H}$, can be derived as

$$\Gamma_j^s = \frac{1}{N_0 \frac{\hat{\boldsymbol{D}}_{s,i}^{\alpha} + \hat{\boldsymbol{D}}_{s,m}^{\alpha}}{gP} + \sum_{k \neq s} \left(\frac{\hat{\boldsymbol{D}}_{s,i} + \hat{\boldsymbol{D}}_{s,m}}{\hat{\boldsymbol{D}}_{j,k}} \right)^{\alpha}}, \quad i \in \mathcal{M} \setminus \{j\}, m \in \mathcal{M} \tag{3.10}$$

where $\hat{\boldsymbol{D}}_{s,i}$ is a matrix of constant, $\hat{\boldsymbol{D}}_{s,m}$ and $\hat{\boldsymbol{D}}_{j,k}$ are the functions of the variable set of $\tilde{\boldsymbol{d}}$, so Γ_j^s can be rewritten as $\Gamma_s\left(\tilde{\boldsymbol{d}}\right)$. Similarly, if a fixed user m, $m \in \mathcal{M}$ is a sender, the SINR Γ_j^m of a receiver j, $j \in \boldsymbol{H}$, can be derived as

$$\Gamma_j^m = \frac{1}{N_0 \frac{\hat{\boldsymbol{D}}_{m,i}^{\alpha} + \hat{\boldsymbol{D}}_{m,m'}^{\alpha}}{gP} + \sum_{k \neq m} \left(\frac{\hat{\boldsymbol{D}}_{m,i} + \hat{\boldsymbol{D}}_{m,m'}}{\hat{\boldsymbol{D}}_{j,k}} \right)^{\alpha}}, \quad i \in \boldsymbol{H} \setminus \mathcal{M}, m' \in \mathcal{M} \tag{3.11}$$

where $\hat{\boldsymbol{D}}_{m,i}$, $\hat{\boldsymbol{D}}_{m,m'}$ and $\hat{\boldsymbol{D}}_{j,k}$ are the functions of a variable set of $\tilde{\boldsymbol{d}}$, then Γ_j^m also can be rewritten as $\Gamma_m\left(\tilde{\boldsymbol{d}}\right)$.

Substituting (3.10) and (3.11) into (3.7), we obtain the transmission rate of a fixed user s,$s \in \mathcal{S}$, $R_s\left(\tilde{\boldsymbol{d}}\right)$, and a movable user m, $m \in \mathcal{M}$, $R_m\left(\tilde{\boldsymbol{d}}\right)$, respectively as

$$R_s\left(\tilde{\boldsymbol{d}}\right) = \log_2\left(1 + \Gamma_s\left(\tilde{\boldsymbol{d}}\right)\right) \tag{3.12}$$

$$R_m\left(\tilde{\boldsymbol{d}}\right) = \log_2\left(1 + \Gamma_m\left(\tilde{\boldsymbol{d}}\right)\right) \tag{3.13}$$

For the source user and destination user transmission rate, substituting (3.3) and (3.5) into (3.7), $R_{Sor}\left(\tilde{\boldsymbol{d}}\right)$ and $R_{Des}\left(\tilde{\boldsymbol{d}}\right)$ can be expressed respectively as

$$R_{Sor}\left(\tilde{\boldsymbol{d}}\right) = \log_2\left[1 + \frac{1}{N_0 \frac{\hat{\boldsymbol{D}}_{s,Sor}^{\alpha} + \hat{\boldsymbol{D}}_{m,Sor}^{\alpha}}{gP} + \sum_{k \neq Sor} \left(\frac{\hat{\boldsymbol{D}}_{s,Sor} + \hat{\boldsymbol{D}}_{m,Sor}}{\hat{\boldsymbol{D}}_{j,k}} \right)^{\alpha}}\right], \quad j \in \boldsymbol{H}, m \in \boldsymbol{H} \cap \mathcal{M}, s \in \boldsymbol{H} \cap \mathcal{S} \cup \{Des\} \tag{3.14}$$

$$R_{Des}\left(\tilde{\boldsymbol{d}}\right) = \log_2\left[1 + \frac{1}{N_0 \frac{\hat{\boldsymbol{D}}_{s,Des}^{\alpha} + \hat{\boldsymbol{D}}_{m,Des}^{\alpha}}{gP} + \sum_{k \neq Des} \left(\frac{\hat{\boldsymbol{D}}_{s,Sor} + \hat{\boldsymbol{D}}_{m,Des}}{\hat{\boldsymbol{D}}_{j,k}} \right)^{\alpha}}\right], \quad j \in \boldsymbol{H}, m \in \boldsymbol{H} \cap \mathcal{M}, s \in \boldsymbol{H} \cap \mathcal{S} \cup \{Sor\} \tag{3.15}$$

The global objective is to find and select the best position for movable users to maximize the ad hoc network system throughput. Then, the system throughput is a function of the location information of movable users, i.e., a function of a variable set of $\tilde{\boldsymbol{d}}$, which can be

rewritten as

$$U_{network}\left(\tilde{\boldsymbol{d}}\right)=\frac{|\mathcal{S}|+|\mathcal{M}|+2}{\sum_{s\in\mathcal{S}}\frac{1}{R_s\left(\tilde{\boldsymbol{d}}\right)}+\sum_{m\in\mathcal{M}}\frac{1}{R_m\left(\tilde{\boldsymbol{d}}\right)}+\frac{1}{R_{Sor}\left(\tilde{\boldsymbol{d}}\right)}+\frac{1}{R_{Des}\left(\tilde{\boldsymbol{d}}\right)}} \tag{3.16}$$

Summarizing (3.12), (3.13), (3.14) and (3.15) into (3.16), the system throughput optimization problem can be derived as

$$\begin{aligned}
&\max_{\mathbf{D}} \quad U_{network}\left(\tilde{\boldsymbol{d}}\right)\\
&s.t. \quad \Gamma_s\left(\tilde{\boldsymbol{d}}\right)\geqslant\beta\\
&\qquad \Gamma_m\left(\tilde{\boldsymbol{d}}\right)\geqslant\beta\\
&N_0\frac{\hat{\boldsymbol{D}}_{s,Sor}^{\alpha}+\hat{\boldsymbol{D}}_{m,Sor}^{\alpha}}{gP}+\sum_{k\neq Sor}\left(\frac{\hat{\boldsymbol{D}}_{s,Sor}+\hat{\boldsymbol{D}}_{m,Sor}}{\hat{\boldsymbol{D}}_{j,k}}\right)^{\alpha}\geqslant\beta\\
&N_0\frac{\hat{\boldsymbol{D}}_{s,Des}^{\alpha}+\hat{\boldsymbol{D}}_{m,Des}^{\alpha}}{gP}+\sum_{k\neq Des}\left(\frac{\hat{\boldsymbol{D}}_{s,Sor}+\hat{\boldsymbol{D}}_{m,Des}}{\hat{\boldsymbol{D}}_{j,k}}\right)^{\alpha}\geqslant\beta\\
&0\leqslant\|\hat{\boldsymbol{D}}_{i,j}\|\leqslant\sqrt{2}L,\ i,j\in\boldsymbol{H}
\end{aligned} \tag{3.17}$$

However, finding the optimal position of movable users under the limitation based on the above problem (3.17) is nontrivial. In this problem formulated in (3.3)-(3.17), the expressions defined in (3.3)-(3.7) are nonlinear functions of the problem variables. Furthermore, the search space is $L^{2|\mathcal{M}|}$ profiles in variable vector $\tilde{\boldsymbol{d}}$. These factors cause the problem to be a nonconvex problem, which is generally NP-hard. The traditional exhaustive global search method is not favorable in the ad hoc network due to the high complexity and computational cost. Therefore, the demand for adaptability and small computational cost burden requires a high-accuracy and low-cost solution for the throughput maximization problem.

In chapter 3.2, we first propose an Interaction Position Game (IPG), then design the payoff function based on the derived objective function of the global maximum throughput, which must guarantee the existence of the Nash equilibrium, and optimal NE points coincide with the optimal solution. Moreover, we prove that the IPG is a bilateral symmetric interaction (BSI) game based on the proposed payoff function. BSI has at least one pure strategy NE point, and previous learning algorithms can find the global maximum of the potential function.

3.2.3 Qualitative analysis of different position cases

Since movable users move to random locations within the square range, it would cause different cases consisting of interference and capture effects among all of the users. To validate the above mathematical derivation, it is necessary to qualitatively analyze the best position for maximizing throughput according to the interference and SINR variance.

Table 3.2 Different position cases for fixed users.

CASE	$\hat{d}_{M,N}$	d_M	d_N
I	*short*	*short*	*short*
II	*short*	*long*	*long*
III	*long*	*long*	*short*
IV	*long*	*short*	*long*
V	*long*	*long*	*long*

For convenient analysis, we consider only two fixed users, user M and user N, and then define *short* and *long* distances as the qualitative distance standard. If the distance between two users is larger than $0.5L$, it can be defined as *long*; otherwise, it is *short*. There are five position cases, which are shown in Table 3.1. d_M and d_N denote the distance from the destination user to the user M and user N, respectively. These cases do not include $\hat{d}_{M,N}$ marked as *short*, while d_M and d_N are marked as *long* or *short* because of their unsatisfactory distance limitations and definitions. Besides, the case where $\hat{d}_{M,N}$ marked as *long* while both d_M and d_N are marked as *short*, is also not included in the correct situation. Thus, there are only five cases other than eight cases that need to be considered.

As shown in Fig. 3.3, we present two movable users' best position cases under the different positions of fixed users. For case I shown in Fig. 3.3 (a), the main impact for the first movable user A is the interference from user M and N, so the optimal position for user A is to keep too far away from user M and N and remain close to the source node. The main impact for movable user B is interference from the source node and user N and increasing receive power from user A. Therefore, the optimal position for user B is the place where it is located at the line between user A and user M but is closer to user A.

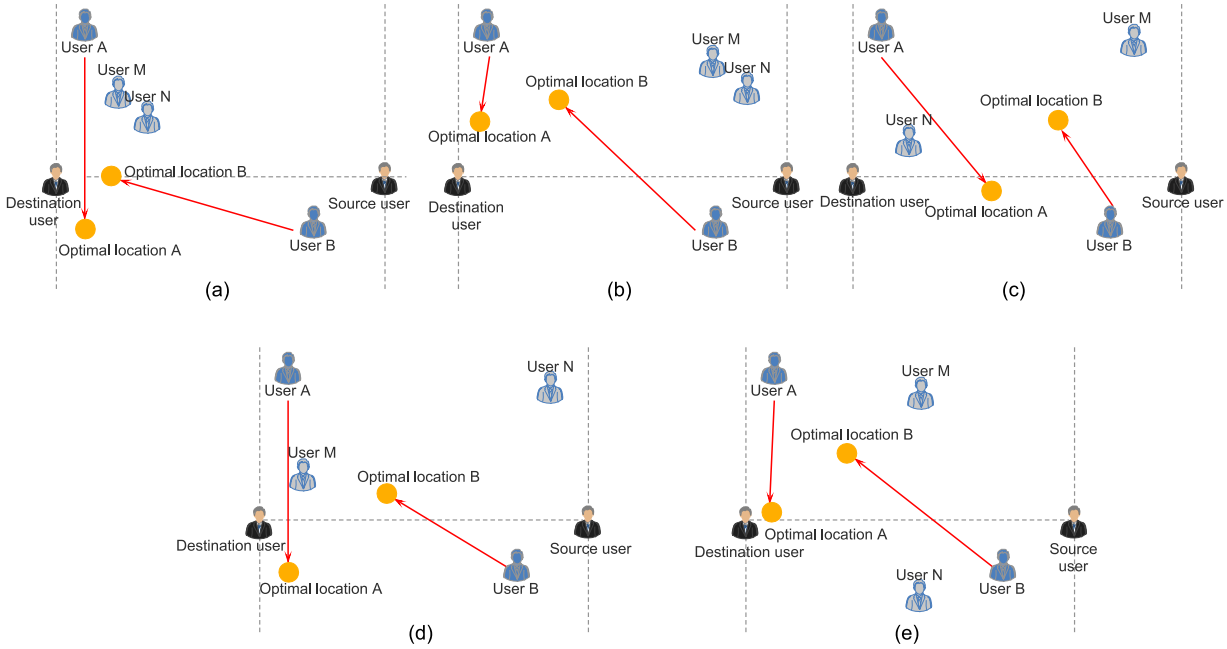

Fig. 3.3 Qualitative analysis of different position cases.

Cases II and IV are shown in Fig. 3.3 (b) and (d). Movable user A should remain close to the source node and not far away from user M because it could enhance the receiving power from the source node, maintain the SINR from user B and diminish the interference from user M. Movable user B should also mitigate the receiving power from user A. Thus, the optimal position for user B is the place located at the line between user A and user M but closer to user A.

For case III in Fig. 3.3 (c), user A should remain too far away from user N because of the interference from user M. The optimal position of user B is located at the middle of the line between user A and user M, where it can maintain the traffic balance between A and M and prevent bottlenecks. Finally, for case V in Fig. 3.3 (e), user A should remain close to the source node and not far away from user M, which increases the receiving power from the source node and maintains the high SINR of user B. Meanwhile, the optimal position of user B is located at the middle of the line between user A and user M considering the traffic balance and bottleneck.

We can summarize that the optimal position for movable users should mitigate the interaction interference and strengthen receiving power simultaneously at the different locations for fixed users. The above qualitative analysis can be used as a basis for determining the correct results of the simulation.

3.3 Game theory method and SA algorithm

In this subchapter, we propose an interaction position game and then design the utility function of this game, which has proven to be a bilateral symmetric interaction (BSI) game. In addition, we introduce the conventional simulated annealing algorithm as a comparison.

3.3.1 Game theory method

Game theory is an analytical tool for helping to formulate and observe results when decision makers cooperate and interact in this ad hoc network, which can be a helpful method for solving NP-hard problems. To demonstrate the game method, we further define an IPG and refer to the basics therein of the potential game [71], [72]. Not all optimization problems can be solved by game theory, because the problem might not exist in Nash equilibrium. We define this new game based on throughput problems and make use of three theorems to prove the existence of Nash equilibrium in this game.

The notation of this game theory method is shown in Table 3.2. A standard cooperative strategic game can be established by a structure $\mathcal{G} := \left(\mathcal{M}, (\mathcal{A}_i)_{i\in\mathcal{M}}, (u_i)_{i\in\mathcal{M}}\right)$, or simply given by $\mathcal{G} := (\mathcal{M}, \mathcal{A}_{i\in\mathcal{M}}, \boldsymbol{U}_{i\in\mathcal{M}})$, where $\mathcal{M}$ is a finite set of players or decision makers and $\mathcal{A}_i$ is the set of strategies for player $i \in \mathcal{M}$. The payoff function for each player $i \in \mathcal{M}$ can be denoted as $u_i : \prod \mathcal{A}_i \to \mathbb{R}$, which must be maximized. If $\mathcal{K} \subseteq \mathcal{M}$, the Cartesian product can be denoted as $\mathcal{A}_\mathcal{K}$. If $\mathcal{K} = \mathcal{M} \setminus \{i\}$, then let $\mathcal{A}_{-i}$ denote $\mathcal{A}_\mathcal{K}$. For simplicity, we

define $u_i(\boldsymbol{a}) := u_i(a_i, \boldsymbol{a}_{-i})$, which is the standard notation on game theory, where $\boldsymbol{a}_{-i} := \left(a_1, \cdots, a_{i-1}, a_{i+1}, \cdots, a_{|\mathcal{M}|}\right) \in \mathcal{A}_{-i}$, $\boldsymbol{a}_{-i}$ refers to the joint strategy adopted by player i's opponents.

Table 3.3 Notation.

Parameters	Description
$\mathcal{G}$	Strategic form game
$\mathcal{M}$	Finite set of movable players, $\mathcal{M} = \{1,2,...,\lvert\mathcal{M}\rvert\}$
$\mathcal{A}_i$	Set of strategies for player $i \in \mathcal{M}$
$\mathcal{A}$	Strategy space, $\prod_{i\in\mathcal{M}}\mathcal{A}_i$
a_i	Strategy of player i, $a_i \in \mathcal{A}_i$
$a_i^{'}$	Other strategy of player i except for a_i, $a_i^{'} \in \mathcal{A}_i$
u_i	Payoff function for player i, $i \in \mathcal{M}$
$\boldsymbol{U}$	Set of utility functions
ϕ	Potential function
$\mathcal{A}_{-i}$	$\mathcal{K} = \mathcal{M} \setminus \{i\}$, $\mathcal{A}_{\mathcal{K}}$
a_{-i}	Strategy of player j, $j \in \mathcal{M} \setminus \{i\}$
ϵ	Selection function of feasible movable users
$u1$	Utility function of system throughput
$u2$	Intermediate utility function
$\phi1$	Potential function corresponding to $u1$
$\phi2$	Potential function corresponding to $u2$
$\zeta1$	BSI game utility function of system throughput
$\zeta2$	BSI game intermediate utility function
$\psi1$	BSI game potential function corresponding to $\zeta1$
$\psi2$	BSI game potential function corresponding to $\zeta2$
$\lvert\mathcal{S}\rvert$	Number of fixed users
$\lvert\mathcal{M}\rvert$	Number of movable users

Definition 1 (Interaction Position Game (IPG)): An interaction position game is a tuple $\mathcal{G} := (\mathcal{M}, \mathcal{A}, \boldsymbol{U})$ where:

- $\mathcal{M}$ denotes the set of movable users, in which each user $i := (1,2,\cdots,|\mathcal{M}|)$ corresponds to a player.
- $\mathcal{A}$ denotes the set of strategies for different positions, which are Cartesian products of all individual strategy sets. Here, we let the strategy profile a_i denote the location of user d_i. Each individual strategy $\mathcal{A}_i$ has L^2 profiles. Thus, the strategy space of this game $\mathcal{A}$ includes $L^{2|\mathcal{M}|}$ profiles.
- $\boldsymbol{U}$ represents the set of utility functions for all movable players. Specifically, the utility function of each player $i \in \mathcal{M}$ is given by $u_i(a_i, \boldsymbol{a}_{-i})$. The function denotes the system throughput utility or payoff for each movable user. □

The IPG is a kind of strategic game in which all movable users select the best position, and the utility function is only dependent on its own strategy or their opponents' actions.

Definition 2 (Nash Equilibrium): The action strategy profile $\boldsymbol{a}^* = (a_1^*, a_2^*, \cdots, a_M^*)$ is a Nash equilibrium if and only if it satisfies the following inequality for any $i \in \mathcal{M}$, $a_i \in \mathcal{A}_i$

$$u_i\left(a_i^*, \boldsymbol{a}_{-i}^*\right) \geqslant u_i\left(a_i, \boldsymbol{a}_{-i}^*\right) \tag{3.18}$$

□

Although the proposed IPG satisfies the standard game definition in this ad hoc network, the existence of NE points is not guaranteed unless this game can prove as a potential game that has at least one pure strategy NE.

Definition 3 (Potential Game [73]): A strategic form game is an exact potential game if there exists an exact potential function $\phi : \mathcal{A} \to \mathbb{R}$ such that

$$u_i\left(a_i^{'}, \boldsymbol{a}_{-i}\right) - u_i\left(a_i, \boldsymbol{a}_{-i}\right) = \phi\left(a_i^{'}, \boldsymbol{a}_{-i}\right) - \phi\left(a_i, \boldsymbol{a}_{-i}\right) \tag{3.19}$$

for every $i \in \mathcal{M}$, $a_i, a_{-i}^{'} \in \mathcal{A}_i$ and $\boldsymbol{a}_{-i} \in \mathcal{A}_{-i}$. □

According to (3.17), we define two functions f_i and g_i to denote the receiving power and interference from opponents. The functions can be characterized as $f_i : \mathcal{A}_i \times \mathcal{A}_{\mathcal{M}_i} \to \mathbb{R}$ and $g_i : \mathcal{A}_i \times \mathcal{A}_{\mathcal{M}_i} \to \mathbb{R}$, where $\mathcal{M}_i := \{j \in \mathcal{M} \setminus \{i\}\}$ denotes the set of user i 's opponents, and $\boldsymbol{a}_{\mathcal{M}_i} := \left\{a_j \mid j \in \mathcal{M}_{\{i\}}\right\}$ represents the position strategies of the other users. For each movable user $i \in \mathcal{M}$, the receiving power function $f_i\left(a_i, \boldsymbol{a}_{\mathcal{M}_i}\right)$ can be defined as

$$f_i\left(a_i, \boldsymbol{a}_{\mathcal{M}_i}\right) = f_i\left(a_i, a_j\right) = N_0 \frac{\|a_j - a_i\|^\alpha}{gP}, i \in \mathcal{M}, j \in \mathcal{M} \setminus \{i\} \tag{3.20}$$

The interference function $g_i\left(a_i, \boldsymbol{a}_{\mathcal{M}_i}\right)$ can be given by

$$\begin{aligned} g_i\left(a_i, \boldsymbol{a}_{\mathcal{M}_i}\right) &= g_i\left(a_i, a_j, a_k\right) \\ &= \sum_{i \neq j, j \neq k} \left(\frac{\|a_j - a_i\|}{\|a_i - a_k\|}\right)^\alpha, i \in \mathcal{M}, j \in \mathcal{M} \setminus \{i\}, k \in \mathcal{M} \setminus \{i\} \cup \{j\} \end{aligned} \tag{3.21}$$

where $\boldsymbol{a}_{-i}$ and $\boldsymbol{a}_{\mathcal{M}_i}$ have the same meaning. For ease of expression, $\boldsymbol{a}_{-i}$ is used uniformly to denote $\boldsymbol{a}_{\mathcal{M}_i}$ subsequently.

Consider the limited condition in the optimal formula in (3.17); all users' SINR should be larger than the threshold β. Note that these inequations are challenging to express in the utility function. The NP-hard problem can be converted to the product of system throughput and selection function $\epsilon\left(a_i, \boldsymbol{a}_{-i}\right)$, which can distinguish feasible users who meet the SINR requirement; i.e., only qualified users can be eligible to select the best positions and maximize throughput; otherwise, they are ineligible. Thus, this conversion is reasonable. The

function $\epsilon\left(a_i, a_{-i}\right)$ approximates constraints of equation (3.17), which can be expressed as

$$\epsilon\left(a_i, \boldsymbol{a}_{-i}\right)=\begin{cases} 0, f_i\left(a_i, \boldsymbol{a}_{-i}\right)+g_i\left(a_i, \boldsymbol{a}_{-i}\right)>\frac{1}{\beta} \\ 1, f_i\left(a_i, \boldsymbol{a}_{-i}\right)+g_i\left(a_i, \boldsymbol{a}_{-i}\right) \leqslant \frac{1}{\beta} \end{cases} \tag{3.22}$$

Then, the utility function of system throughput $u1_i\left(a_i, \boldsymbol{a}_{-i}\right)$ can be rewritten by the utility function format as follows:

$$u1_i\left(a_i, \boldsymbol{a}_{-i}\right)=\left\{\frac{|\mathcal{S}|+|\mathcal{M}|+2}{\sum_{i \in \mathcal{M}}\left[\frac{1}{R_i\left(a_i, \boldsymbol{a}_{-i}\right)}+\frac{1}{R_j\left(a_i, \boldsymbol{a}_{-i}\right)}\right]}\right\} \epsilon\left(a_i, \boldsymbol{a}_{-i}\right) \tag{3.23}$$

where $R_i\left(a_i, \boldsymbol{a}_{-i}\right)$ and $R_j\left(a_i, \boldsymbol{a}_{-i}\right)$ denote the movable user i 's and the other user $j \in \{\mathcal{S} \cup\{Sor\} \cup\{Des\}\}$ transmission rate functions, respectively. Based on (3.12)-(3.15), the rate function $R_i\left(a_i, \boldsymbol{a}_{-i}\right)$ can also be rewritten as

$$\begin{aligned} R_i\left(a_i, \boldsymbol{a}_{-i}\right) &= \log_2\left[1+\frac{1}{f_i\left(a_i, \boldsymbol{a}_{-i}\right)+g_i\left(a_i, \boldsymbol{a}_{-i}\right)}\right] \\ &\cong \log_2\left[\frac{1}{f_i\left(a_i, \boldsymbol{a}_{-i}\right)+g_i\left(a_i, \boldsymbol{a}_{-i}\right)}\right] \end{aligned} \tag{3.24}$$

To analyze the utility function easily, we define the other function $u2_i\left(a_i, \boldsymbol{a}_{-i}\right)$ as follows:

$$\begin{aligned} u2_i\left(a_i, \boldsymbol{a}_{-i}\right) &\triangleq -\frac{|\mathcal{S}|+|\mathcal{M}|+2}{u1_i\left(a_i, \boldsymbol{a}_{-i}\right)} \\ &= \frac{1}{\epsilon\left(a_i, \boldsymbol{a}_{-i}\right)} \sum_{i \in \mathcal{M}}\left[-\frac{1}{R_i\left(a_i, \boldsymbol{a}_{-i}\right)}-\frac{1}{R_j\left(a_i, \boldsymbol{a}_{-i}\right)}\right] \end{aligned} \tag{3.25}$$

Then, $-\frac{1}{R_i\left(a_i, \boldsymbol{a}_{-i}\right)}$ can be expressed as

$$\begin{aligned} -\frac{1}{R_i\left(a_i, \boldsymbol{a}_{-i}\right)} &= \frac{1}{\log_2\left[f_i\left(a_i, a_j\right)+g_i\left(a_i, a_j, a_k\right)\right]} \\ &= \frac{1}{\log_2\left[N_0 \frac{\left\|a_j-a_i\right\|^\alpha}{gP}+\sum_{i \neq j, j \neq k}\left(\frac{\left\|a_j-a_i\right\|}{\left\|a_i-a_k\right\|}\right)^\alpha\right]} \end{aligned} \tag{3.26}$$

For other users' (except for movable users) transmission rates, the function $R_j\left(a_i, \boldsymbol{a}_{\mathcal{M}_i}\right)$ is managed only by the distance between the movable and fixed users. Therefore, we define a function $\Upsilon\left(a_i, \boldsymbol{a}_{\mathcal{M}_i}\right)$, which is dominated by variable strategy a_i and can be given by

$$\begin{aligned} \Upsilon\left(a_i, \boldsymbol{a}_{-i}\right) &\triangleq -\frac{1}{R_j\left(a_i, \boldsymbol{a}_{-i}\right)} \\ &= \frac{1}{\log_2\left[N_0 \frac{\left\|\tilde{d}_w-a_i\right\|^\alpha}{gP}+\sum_{\omega \neq \upsilon}\left(\frac{\left\|\tilde{d}_w-a_i\right\|}{\left\|a_i-\tilde{d}_\upsilon\right\|}\right)^\alpha\right]} \end{aligned} \tag{3.27}$$

where $\tilde{d}_w$ and $\tilde{d}_\upsilon$ are known constants and denote different fixed locations. Based on (3.26)

and (3.27), we can derive and rewrite the utility function $u2_i\left(a_i, \boldsymbol{a}_{-i}\right)$ as

$$u2_i\left(a_i, \boldsymbol{a}_{-i}\right) := \frac{1}{\epsilon\left(a_i, \boldsymbol{a}_{-i}\right)} \sum_{i \in \mathcal{M}} \frac{1}{\log_2\left[N_0 \frac{\|a_j - a_i\|^\alpha}{gP} + \sum_{i \neq j, j \neq k} \left(\frac{\|a_j - a_i\|}{\|a_i - a_k\|}\right)^\alpha\right]} + \frac{1}{\epsilon\left(a_i, \boldsymbol{a}_{-i}\right)} \sum_{i \in \mathcal{M}} \Upsilon\left(a_i, \boldsymbol{a}_{-i}\right) \tag{3.28}$$

Definition 4 (Bilateral Symmetric Interaction (BSI) game [74]): A strategic form game $\mathcal{G} := \left(\mathcal{M}, \left(\mathcal{A}_i\right)_{i \in \mathcal{M}}, \left(u_i\right)_{i \in \mathcal{M}}\right)$ is called a BSI game if there exist functions $\zeta_{i,j}\left(a_i, a_j\right) : \mathcal{A}_i \times \mathcal{A}_j \rightarrow \mathbb{R}$ and $\psi_i\left(a_i\right) : \mathcal{A}_i \rightarrow \mathbb{R}$ such that

$$u_i\left(a_i, \boldsymbol{a}_{-i}\right) := \left(\sum_{i \neq j} \zeta_{ij}\left(a_i, a_j\right)\right) + \psi_i\left(a_i\right) \tag{3.29}$$

where $i \neq j$ and $\zeta_{ij}\left(a_i, a_j\right) = \zeta_{ji}\left(a_i, a_j\right)$ for every $\left(a_i, a_j\right) \in \mathcal{A}_i \times \mathcal{A}_j$. □

The definition of an exact potential game exploits a potential function (3.19). However, we sometimes do not know whether a given game is an exact potential game, because it is difficult to determine it directly based on the potential function. In this case, we can convert the IPG game to a BSI game, knowing that it is an exact potential game. If we can prove that the IPG game is a BSI game, then the IPG game is an exact potential game.

Theorem 1: A BSI Game $\mathcal{G} := \left(\mathcal{M}, \left(\mathcal{A}_i\right)_{i \in \mathcal{M}}, \left(u_i\right)_{i \in \mathcal{M}}\right)$ is an exact potential game with a potential function such that

$$\begin{aligned} \phi\left(a_i, \boldsymbol{a}_{-i}\right) &= \frac{1}{2} \sum_i \sum_{j \neq i} \zeta_{ij}\left(a_i, a_j\right) + \sum_i \psi_i\left(a_i\right) \\ &= \sum_{i<j} \zeta_{ij}\left(a_i, a_j\right) + \sum_i \psi_i\left(a_i\right) \end{aligned} \tag{3.30}$$

Proof. The proof procedure can be referred to in Section 2 in [73]. □

Theorem 2: Game $\mathcal{G} := \left(\mathcal{M}, \left(\mathcal{A}_i\right)_{i \in \mathcal{M}}, \left(u2_i\right)_{i \in \mathcal{M}}\right)$ is an exact potential game, where the potential function can be expressed as

$$\phi 2\left(a_i, \boldsymbol{a}_{-i}\right) = \sum_{i<j} \zeta 2_{ij}\left(a_i, a_j\right) + \sum_i \psi 2_i\left(a_i\right) \tag{3.31}$$

where $\zeta 2_{i,j}\left(a_i, a_j\right)$ and $\psi 2_i\left(a_i\right)$ can be given by

$$\begin{aligned} \zeta 2_{i,j}\left(a_i, a_j\right) &= \frac{1}{\epsilon\left(a_i, \boldsymbol{a}_{-i}\right)} \left\{\frac{1}{\log_2\left[f_i\left(a_i, a_j\right) + g_i\left(a_i, a_j, a_k\right)\right]}\right\} \\ &= \frac{1}{\epsilon\left(a_i, \boldsymbol{a}_{-i}\right)} \left\{\frac{1}{\log_2\left[N_0 \frac{\|a_j - a_i\|^\alpha}{gP} + \sum_{i \neq j, j \neq k} \left(\frac{\|a_j - a_i\|}{\|a_i - a_k\|}\right)^\alpha\right]}\right\} \end{aligned} \tag{3.32}$$

$$\psi 2_i\left(a_i\right) = \frac{\Upsilon\left(a_i, \boldsymbol{a}_{-i}\right)}{\epsilon\left(a_i, \boldsymbol{a}_{-i}\right)} \tag{3.33}$$

Proof. It is evident that $u2_i\left(a_i, \boldsymbol{a}_{-i}\right)$ can be divided into two parts, $\zeta 2_{i,j}\left(a_i, a_j\right)$ and $\psi 2_i\left(a_i\right)$. For $g_i\left(a_i, a_j, a_k\right)$, since a_j and a_k denote other strategies except for a_i and $a_j, a_k \in \mathcal{M}_i, j \neq k$. Thus, even though $g_i\left(a_i, a_j, a_k\right)$ has three variables, the summation of $f_i\left(a_i, a_j\right)$ and $g_i\left(a_i, a_j, a_k\right)$ also varies only by a_i, a_j. Each user satisfies the symmetry condition $\zeta 2_{i,j}\left(a_i, a_j\right) = \zeta 2_{j,i}\left(a_j, a_i\right)$ due to interactive interference. Finally, according to **Definition 4**, **Theorem 1**, and **Theorem 2**, we can prove that this game is a BSI game as well as an exact potential game. □

Theorem 3: The maximum of the potential function $\phi 2\left(a_i, \boldsymbol{a}_{-i}\right)$ in this game $u2_i\left(a_i, a_j\right)$ is proportional to the maximum system throughput potential function $\phi 1\left(a_i, \boldsymbol{a}_{-i}\right)$ of game $u1_i\left(a_i, a_j\right)$; i.e., the result strategies of game $u2_i\left(a_i, a_j\right)$ can be considered the best strategies for maximum system throughput.

Proof. In (3.25), we know that the relationship between utility function $u2_i\left(a_i, a_j\right)$ and $u1_i\left(a_i, a_j\right)$ is

$$u2_i\left(a_i, \boldsymbol{a}_{-i}\right) = -\frac{|\mathcal{S}| + |\mathcal{M}| + 2}{u1_i\left(a_i, \boldsymbol{a}_{-i}\right)} \tag{3.34}$$

It is known that the utility function $u1_i\left(a_i, \boldsymbol{a}_{-i}\right)$ can be expressed by $\zeta 1_{ij}\left(a_i, a_j\right)$ and $\psi 1_i\left(a_i\right)$ as

$$u1_i\left(a_i, \boldsymbol{a}_{-i}\right) = \sum_{i \neq j} \zeta 1_{ij}\left(a_i, a_j\right) + \psi 1_i\left(a_i\right) \tag{3.35}$$

where $\zeta 1_{ij}\left(a_i, a_j\right)$ and $\psi 1_i\left(a_i\right)$ can be given by

$$\zeta 1_{ij}\left(a_i, a_j\right) = -\frac{\left(|\mathcal{S}| + |\mathcal{M}| + 2\right) \frac{\sum_{i<j} \zeta 2_{ij}\left(a_i, a_j\right)}{\sum_i \psi 2_i\left(a_i\right)}}{\left[\sum_{i<j} \zeta 2_{ij}\left(a_i, a_j\right) + \sum_i \psi 2_i\left(a_i\right)\right]} \tag{3.36}$$

$$\psi 1_i\left(a_i\right) = -\frac{\left(|\mathcal{S}| + |\mathcal{M}| + 2\right)}{\sum_i \psi 2_i\left(a_i\right)} \tag{3.37}$$

Then, the potential function $\phi 1\left(a_i, \boldsymbol{a}_{-i}\right)$ can be given by

$$\phi 1\left(a_i, \boldsymbol{a}_{-i}\right) = \sum_{i<j} \zeta 1_{ij}\left(a_i, a_j\right) + \sum_i \psi 1_i\left(a_i\right) \tag{3.38}$$

Finally, we can obtain that $\phi 1\left(a_i, \boldsymbol{a}_{-i}\right)$ is proportional to $\phi 2\left(a_i, \boldsymbol{a}_{-i}\right)$.

$$\phi 1\left(a_i, \boldsymbol{a}_{-i}\right) \propto \phi 2\left(a_i, \boldsymbol{a}_{-i}\right) \tag{3.39}$$

□

There are a variety of algorithms for facilitating and converging a pure Nash equilibrium point. However, spatial adaptive play (SAP) maximizes the potential function with a high probability of converging to optimal NE [75]. In SAP, each player is randomly assigned to

select a position profile within the square range at first. Then, in the kth step, player $i \in \mathcal{M}$ updates its selection and strategy with a probability $x_i(a_i)$ according to the Boltzmann-Gibbs distribution as

$$x_i\left(a_i \mid \boldsymbol{a}_{-i}[k]\right) = \frac{\exp\left\{\gamma u_i\left(a_i, \boldsymbol{a}_{-i}[k]\right)\right\}}{\sum_{a_i' \in \mathcal{A}_i} \exp\left[\gamma u_i\left(a_i', \boldsymbol{a}_{-i}[k]\right)\right]} \tag{3.40}$$

where this process denotes that player i changes strategy from $a_i[k]$ to a_i with probability $x_i(a_i)$, and γ $(0 < \gamma < \infty)$ is related to the inverse temperature in the statistical physics parameter. When the parameter $\gamma \to \infty$, the SAP approaches the best dynamical response. This SAP process can be executed iteratively as Algorithm 1 until a predefined iteration is reached.

Algorithm 1: Spatial adaptive play (SAP)

1: Initially, set $k = 0$ and let each movable user $i \in \mathcal{M}$ randomly select position $a_i \in \mathcal{A}_i$ within the limited square area with equal probability.
2: All of the movable users exchange and collect information about opponents' strategies.
3: A player is randomly selected, called user i, $i \in \mathcal{M}$.
4: User i calculates the utility function over all its available actions with strategies information received from opponents, i.e., $u2_i\left(a_i, \boldsymbol{a}_{-i}\right)$, $\forall a_i \in \mathcal{A}_i$.
5: User i updates its position strategies according to (41). During this interval, other movable users repeat selections.
6: These steps stop if the predefined iteration is reached; otherwise, go back to step 2.

For strategy information acquisition from other movable users, it is easy to collect messages by a broadcast method when they connect and constitute an ad hoc network system. Note that the parameter γ implies that movable users are more inclined to select a suboptimal or locally optimal strategy at a smaller value γ. In contrast, more significant factors make them prefer to choose the best response action, e.g., movable users decide on any action $a_i \in \mathcal{A}_i$ as $\gamma = 0$, while $\gamma \to \infty$ signifies that they tend to select a strategy from the set of best response actions. Equation (3.40) can be rewritten for approximate maximization as

$$\max_{a_i \in \mathcal{M}_i} u2\left(a_i, \boldsymbol{a}_{-i}\right) \approx \max \left[\sum_{a_i \in \mathcal{M}_i} x_i\left(a_i\right) u2\left(a_i, \boldsymbol{a}_{-i}\right) \; - \frac{1}{\gamma} \sum_{a_i \in \mathcal{M}_i} x_i\left(a_i\right) \log x_i\left(a_i\right) \right] \tag{3.41}$$

This derivation is referred to in [76]. From (3.41), it is evident that the SAP algorithm converges to a global optimum as the iteration increases and makes $\gamma \to \infty$. However, the iteration process may not satisfy convergence in practical implementation, which causes a deviation between the calculated value of this algorithm and the real optimal value. Therefore, we need to make a trade-off between iteration convergence and optimal value. The trade-off is determined by the circumstances in which the proposed system is used. In other words, it depends on the situation, such as the margin of calculation time and accuracy. To balance the trade-off between iteration convergence and the precision of results, we choose

$\gamma = k$ in our simulation, where k is the iteration step [49].

3.3.2 Simulated annealing algorithm

For the NP-hard problem, many heuristic algorithms can calculate and obtain approximate optimality or suboptimality, e.g., greedy algorithms, genetic algorithms, and simulated annealing (SA) algorithms. It is well known that the SA algorithm is an effective and general algorithm that is widely adopted to solve the NP-hard problem in engineering, which is a stochastic optimization algorithm based on the Monte-Carlo iterative solution strategy [77]. Thus, we consider it a comparison with the game theory method in performance.

The SA algorithm selects the similarity between the annealing process of solid matter in physics and the general combinatorial optimization problem as a starting point. The SA algorithm starts from a specific high initial temperature and is combined with the probability jump characteristic with the continuous decline in temperature parameters [78]. Then, the optimal global solution of the objective function can be randomly found in the solution space, i.e., the optimal local solution can jump out of the solution probability and eventually tend to the global optimality [79]. This algorithm process can be performed by Algorithm 2 to maximize system throughput.

Note that the SA algorithm has many advantages compared with a conventional greedy algorithm. This algorithm accepts a solution that is worse than the current solution based on a certain probability; thus, it can jump out of the local optimum to a certain extent, and the iterative search is efficient and parallelized. Additionally, the final solution is independent of the initial solution; therefore, it has robustness properties and asymptotic convergence.

Algorithm 2: Simulated annealing (SA) algorithm

1: Initially, let each movable user $i \in \mathcal{M}$ randomly select position $a_i \in \mathcal{A}_i$ as the initial status S, and then, set temperature $T_{\max} = 1000$, $T_{\min} = 1$ and the number of iterations at each T as $\xi = 100$.
2: Repeat from step 3 to step 6 for each iteration $l = 1,2,\cdots,\xi$.
3: Generate a new position $a_{new} = a_i + \Delta a$ and set it as a new status S_{new}, where Δa is the per unit step with four directions for movable users.
4: According to (3.18), calculate the system throughput increment $\Delta U = U(S_{new}) - U(S)$ as the decision function.
5: If $\Delta U > 0$, then, accept the new position a_{new} of status S_{new} as the current solution position, otherwise accept a_{new} as the new current solution position with the probability $\exp\left(\frac{\Delta U}{KT}\right)$, where K denotes the Boltzmann constant and T is the current temperature.
6: Define the termination condition as several consecutive new solutions are not accepted. Then, these steps stop if the termination condition is satisfied; otherwise, decrease the temperature, $T > T_{\min}$, and go back to step 2.

However, there are many problems to be considered in the SA algorithm. First, setting the initial temperature is the critical, influential factor in search performance. If the initial value is high, then it has a greater successful probability of obtaining the optimum at the cost

of computation time. Otherwise, it achieves a suboptimum. In the simulation, to maintain the accuracy, we set it to 1,000. For the number of iterations at each temperature T; i.e., the annealing speed and temperature management need to make a trade-off between the accuracy and computational cost. Thus, we set the number of iterations ξ as 100 to maintain the accuracy of the solution as well as the annealing temperature following the exponential descent function.

3.4 Simulation and numerical results analysis

To verify the effectiveness of the IPG proposed in this paper in multiple movable user ad hoc networks, we simulate and compare the proposed game theory method with the intuitive method, SA algorithm, and exhaustive global algorithm. The performance of the different methods by analyzing the system throughput and computational cost time is evaluated. Further, we compare the communication overhead between the SAP and SA algorithms. Finally, we analyze the effects of different SINR thresholds and a varied number of users. We use MATLAB and NS3 to simulate multiple user mobility in the ad hoc network.

3.4.1 Simulation scenario

In this ad hoc network scenario, all users (except the AP) are located at the $100 \times 100\text{m}^2$ square field without any obstacles, where the radius is 100 m. Every movable user has four directions, and the per-unit step is 1 m.

We define the mobility speed for each movable user as 1.5 m/s, which is the normal speed of ordinary pedestrians with reality. It indicates that the location information of each mobile user is updated 1.5 times per second. The different mobility speeds only change the convergence time to achieve optimal throughput performance, i.e., the time for mobile users to reach the optimal location, but they would not have impacts on the final throughput performance results. The AP sends data packages to the source user with an infinite stream to retransmit to the destination user. The topology always keeps chain-type and does not change to star or tree types, even though movable users move to a random position because social intimacy among users can guarantee the uniqueness of the transmission link.

In system throughput simulation, we only consider two movable users to facilitate analysis. The numerical results show locations change of two movable users, because it is too difficult to numerically show for three mobile users' scenarios, even though the system model and approaches apply for more than three movable users.

All of the uploading transmission links are saturated, and the capacity is nearly equal to the transmission rate. Thus, we can use the average harmonic value of all users to represent the system throughput. Due to the reflection and refraction of building and ground, the big transmission area, and the high wave frequency as 2.4 GHz, we set the path loss exponent as 4.00. We set the SINR threshold as 24.56 dB in system throughput simulation. To validate

the effect of different SINR thresholds, we set two different values, 24.56 dB and 10.79 dB. We employ IEEE 802.11g as the communication standard and user datagram protocol (UDP) in NS3 [108]. The other main parameters in our simulation are given in Table 3.3.

Table 3.4 Parameter values for simulation.

Parameters	**Value**
Area	100×100 m^2
Communication Standard	IEEE 802.11g
Transport Protocol	UDP
Length side of the square (L)	100 m
Path loss Exponent (α)	4.00
Reference Loss	40.045997
Mobility Speed	1.5 m/s
Tx Power	32 dBm
Tx Rate Source	54 Mbps (β=24.56 dB)
Tx Rate Source	18 Mbps (β=10.79 dB)
White Gaussian Noise	10^{-13} W
Bandwidth	125 kHz
Wave Frequency	2.4 GHz

3.4.2 Simulation results

Since fixed users locate random coordinates that cause different optimal position strategies for movable users, we need to consider a variety of circumstances about fixed users' locations; For simplicity, fixed users move unit step intervals; then, we can consider only three scenarios, which are described as follows to present different situations because these three scenarios present the changing location cases based on the above qualitative analysis and show the location of all possible state of affairs. Here, we set different positions of fixed users as the reference and compare the performance of different methods by two movable users' mobility when two fixed users change location coordinates. In the following throughput comparison figures, the X-axis denotes the distance between fixed users M and N, and the distance unit is one meter. The Y-axis denotes the system throughput values.

As shown in Fig. 3.4, fixed users M and N are located around and close to the destination user at the beginning, after which user N moves away by moving a unit step from user M and approaches the source user. This scenario denotes location coordinate cases that change status from case I to case IV, as shown in Table 3.1.

We analyze the system throughput performance of different methods as scenario I with an increment of the X-axis, which means the distance between user M and N. These methods include the intuitive method, SA algorithm, game theory SAP algorithm and exhaustive global search, as shown in Fig. 3.5. Exhaustive global search indicates that all of the possible

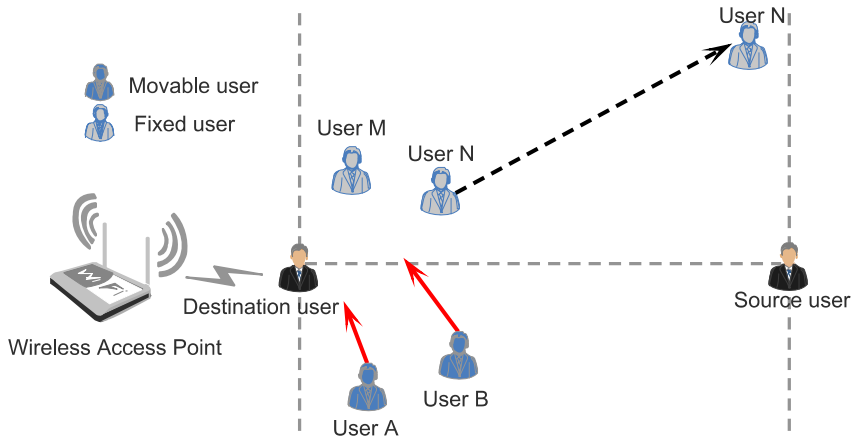

Fig. 3.4 Scenario I: Fixed users M and N are close to the destination user at first; after that, user N changes location coordinates and moves close to the edge of the area while user M is unchanged.

suitable position coordinates for movable users within a limited square range are traversed by the NS3 simulator, which implies the global optimum. It is shown that the system throughput curve increases with distance growth and remains stable after 28 m. The performance of the game theory SAP algorithm is approximate to the global optimum and sometimes obtains the optimum global value. The reasons are that i) the interference between the destination user and user N weakens, and the receiving signal power of the source user increases when user N remains far away from the destination user and close to the source user. Then, the average SINR increases, and the system throughput increases as a result; ii) the SINR remains steady when user N moves close to the edge of the limited space. Moreover, we can observe that compared with the intuitive method and conventional SA algorithm, the game theory SAP algorithm performs better than the former two methods and improves the maximum throughput ratio by 10.62% and 26.03% at a distance of 8 m. The reason is that the proposed IPG method makes users cooperate and attains the nearly global SINR optimum instead of the local optimum by the SA algorithm. The intuitive method is the worst performing method because it chooses the central location of each link as the movable users' moving position, but other methods measure the SINR by users' coordinate information to calculate interference and receiving power.

As shown in Fig. 3.6, fixed user M is far away from destination user, but user N is close to destination user at first. After that, user N changes location coordinates and moves far away from destination user and close to user M, while users M unchanged. This scenario denotes that location coordinate cases change status from case II to case III, as shown in Table 3.1.

The throughput comparison in scenario II is shown in Fig. 3.7. It is noted from the figure that only a small performance degradation of the optimum, i.e., exhaustive global search, is observed for the game theory SAP algorithm. The system throughput performance of the

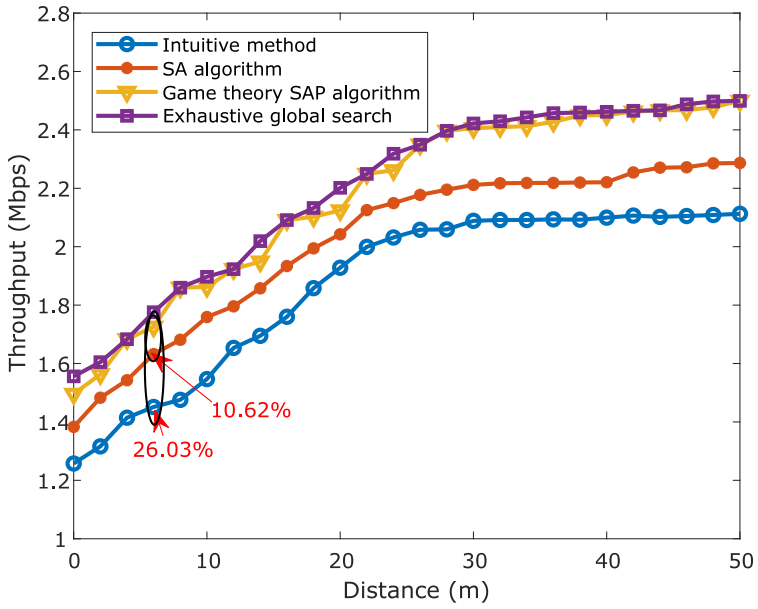

Fig. 3.5 System throughput comparison in the scenario I.

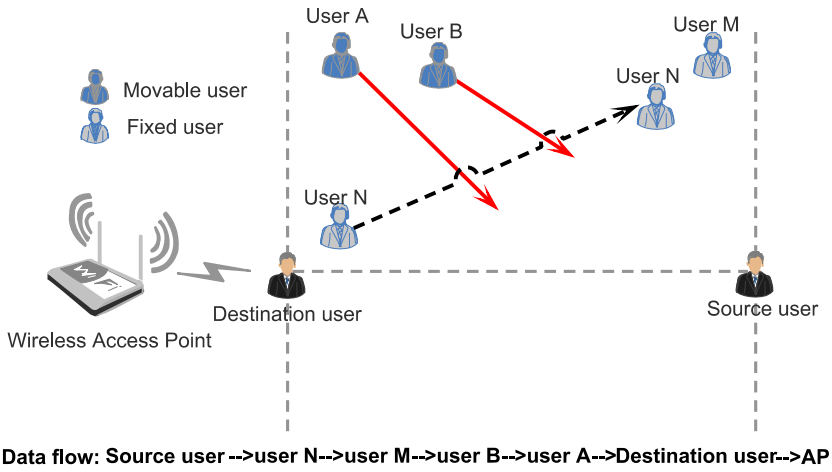

Fig. 3.6 Scenario II: Fixed user M is far away from destination user, but user N is close to destination user at first. After that, user N moves far away from destination user and close to user M, while users M unchanged.

SAP algorithm is better than that of the SA algorithm and intuitive method and sometimes is equal to that of the SA algorithm because they obtain the same local optimum value at the same time. The improvement of the maximum ratio of the SAP algorithm to the SA algorithm and intuitive method is 27.27% and 57.35% at 36 m, respectively. The reason is that the receiving power of user M and the source user degrade and interferences between user N and the destination user increase, which causes the average SINR to decline; then, the system throughput drops down consequently until user N is close to source user. Thus, the curve decreases with increasing distance. The intuitive method is also the worst performance method due to the least system SINR.

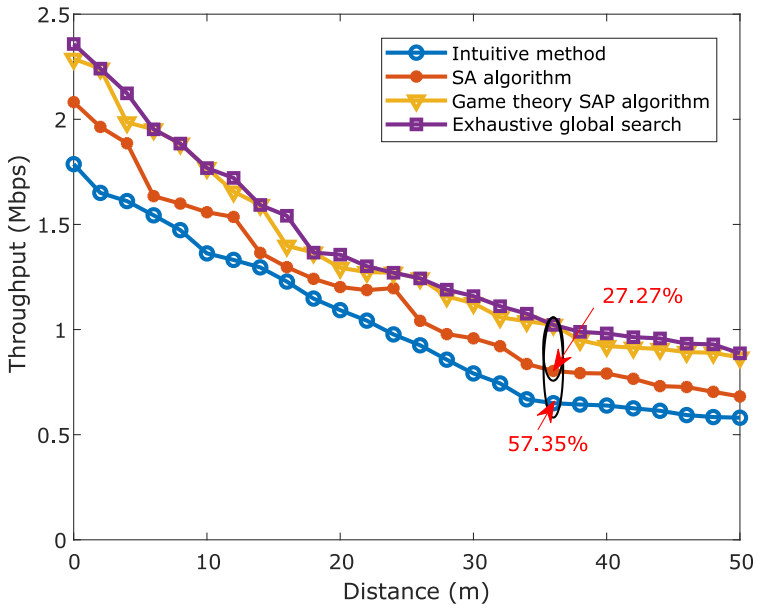

Fig. 3.7 System throughput comparison in the scenario II.

Finally, scenario III is shown in Fig. 3.8, where fixed users M and N are located far away from the destination user at first, then user N moves through the source user while user M remains unchanged. This scenario denotes that location coordinate cases change status from case II to case V, as shown in Table 3.1.

Fig. 3.9 depicts that the system throughput curve distance increases from 0 m to 30 m, then reaches the maximum at 30 m and descends until maximal distance. The system throughput performance of the game theory SAP algorithm is still better than that of the SA algorithm and intuitive method. The improvement of the maximum ratio of the IPG method to the former two methods is nearly 8.62% at 24 m and 17.89% at 46 m, respectively. In this scenario, as user N moves close to the source user, the receiving signal power of the source user increases; therefore, the system throughput increases. Whereas user N moves far away from the source user, the receiving signal power of user N and the source user decrease so that the average of SINR degrades; therefore, system throughput decreases as a result.

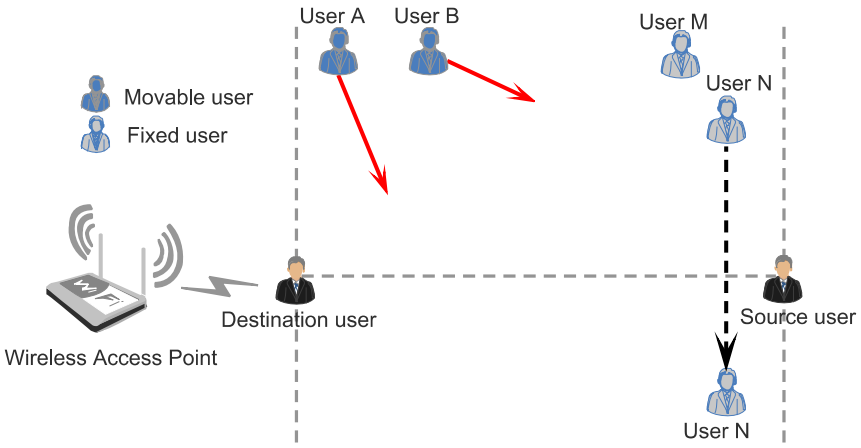

Fig. 3.8 Scenario III: Fixed user M and N are far away from the destination user at first. After that, user N moves through the source user while user M remains unchanged.

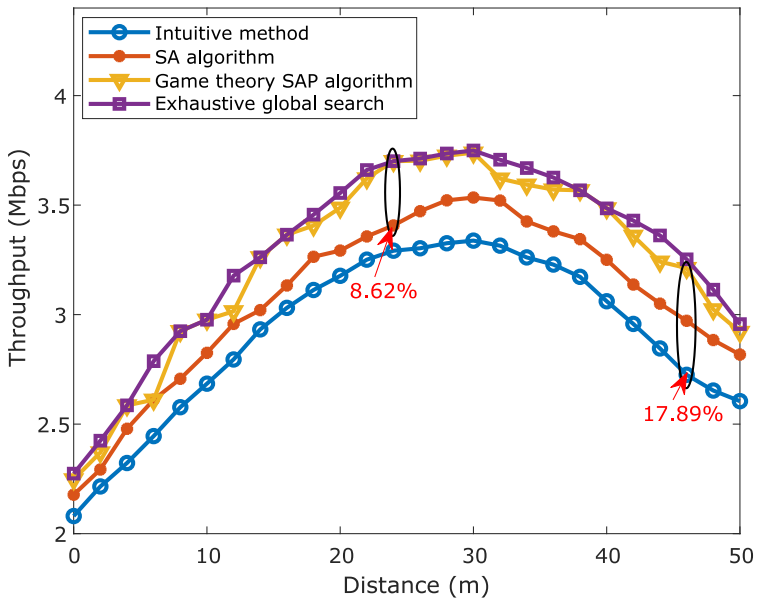

Fig. 3.9 System throughput comparison in the scenario III.

3.4.3 Computation cost and overhead

From the above throughput result analysis, we observe that exhaustive global search by NS3 accomplishes optimal performance, while the game theory SAP algorithm is inferior. In this section, we analyze the convergence behaviors with iteration numbers, computation cost and overhead of the SAP algorithm, SA algorithm, and exhaustive global search method.

The convergence behavior comparison is shown in Fig. 3.10. Here, we set 1) the transmission scenario in scenarios I, and 2) the distance between users M and N is 8 m, where it is more obvious to observe the comparison due to the maximum ratio of throughput improvement of 10.62%. It can be noted that the curve of convergence speed of SAP ascends significantly more than SA with the increment in the number of iterations. When the number of iterations is 30, the SAP algorithm catches up with a maximum system throughput of 1.86 Mbps, which is the global optimum by NS3. However, the maximum of the SA algorithm reaches 1.68 Mbps when the number of iterations is 84. Moreover, the SAP algorithm converges to the global optimum faster than SA. The reasons are that i) SAP calculates only the utility function and updates the position strategy other than the annealing temperature for many recycles of the SA algorithm, ii) the domain of SAP is smaller than SA; therefore, the curve of SAP is steeper before the convergence, and iii) SA always obtains a local optimum instead of the global optimum. This is because the iterations converging to the global optimums are random variables,which are determined by the stochastic nature or parameters of the learning algorithms. Thus, we compare the convergence speed toward the global optimum of SAP and SA from a statistical perspective.

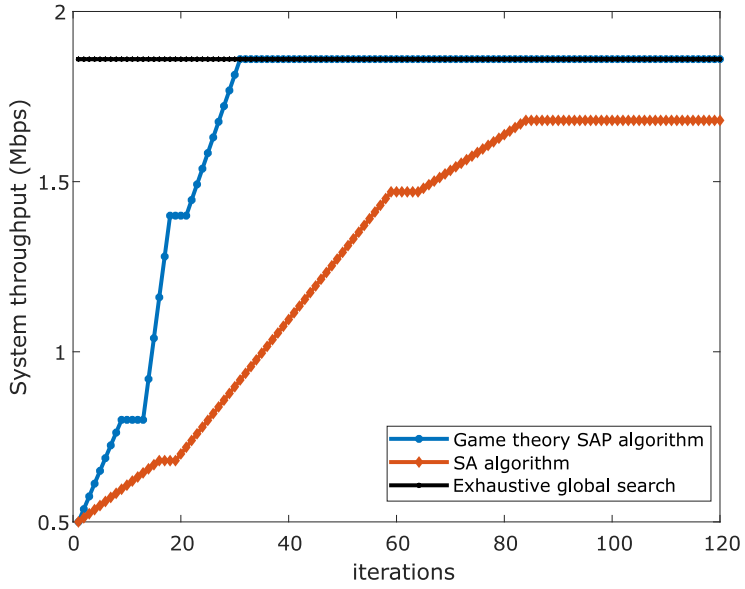

Fig. 3.10 Convergence behavior of SAP, SA, and global optimum (exhaustive global search by NS3) in the scenario I ($\hat{d}_{\mathrm{M,N}} = 8$m).

Specifically, the cumulative distribution function (CDF) of the iterations converging to

the global optimum is shown in Fig. 3.11. It is noted from the figure that the convergence of the SAP increases significantly, whereas SA increases slightly when the number of iterations increases. Furthermore, the convergence speed of SAP is faster than that of SA, as expected, and the convergence speed increases by 2.8 times. These results show the advantage of SAP over SA.

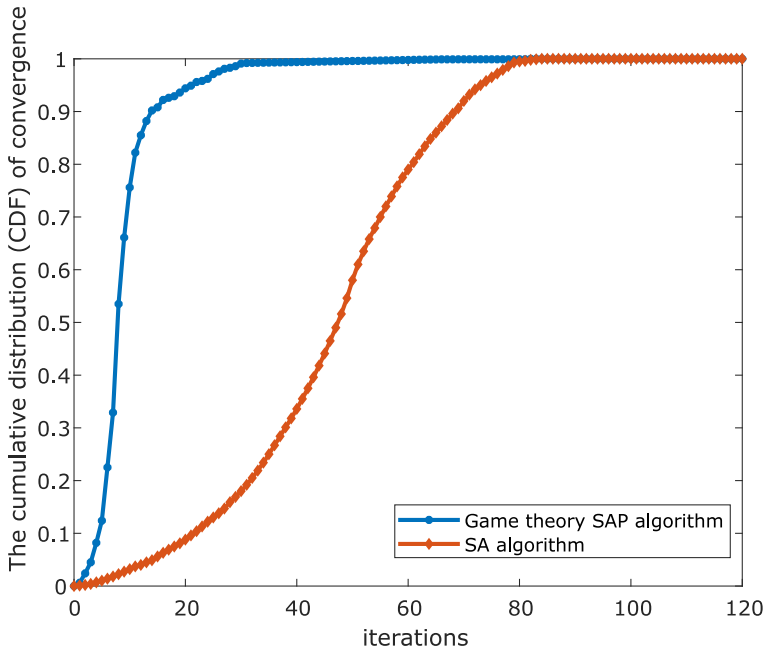

Fig. 3.11 Convergence speed of SAP and SA algorithm in the scenario I ($\hat{d}_{\mathrm{M,N}} = 8$m).

The computation complexity of SAP is $O\left(L^{|\mathcal{M}|} \cdot n\right)$, where $|\mathcal{M}|$ is the number of movable users in the network, L is the length side of the square, and n is the number of iterations. For the SA algorithm, the complexity is $O\left(L^{2|\mathcal{M}|}\left(T_{\max} - T_{\min}\right)^{\xi} \cdot n\right)$, where $T_{\max}$ and $T_{\min}$ denote the maximum and minimum of temperature, respectively, and ξ is the maximum number of iterations at each temperature. Here, consider high accuracy of the SA algorithm, we set the value of $\left(T_{\max} - T_{\min}\right)^{\xi}$ as 10^5. Then, the complexity of the SA algorithm is $O\left(10^5 \cdot L^{2|\mathcal{M}|} \cdot n\right)$. It is noted that the proposed game theoretical method (IPG) significantly reduces computation cost compared with the conventional SA algorithm.

The simulation computer configuration is an Intel(R) Core i7-8700 3.20 GHz. For comparison, we simulate the unit distance as 10 m and set the transmission scenario as scenario I. The completion time comparison of the three algorithms is shown in Fig. 3.12. It is noted that SAP remains absolutely stable as well as exhaustive global search by NS3. In contrast, SA increases slightly at first and then decreases after 30 m. Since the SAP algorithm considers all interference and SINR for users, the completion time is not related to distances and locations between fixed users by SAP. The exhaustive global search method should traverse all possible positions of movable users so that the completion time remains stable. The reason for the SA algorithm is that the initial temperature is not adaptive to distance; additionally, the annealing speed and temperature management are also random and arbitrary.

Table 3.5 Computational cost time comparison in scenario I ($\hat{d}_{\mathrm{M,N}} = 30$m).

Algorithm	**SAP**	**SA**	**Exhaustive global search**
Computation time (Sec)	20.85	52.64	121.21

Intending to calculate and observe the maximum improvement of computational cost time, Table 3.4 shows the computational cost comparison among SAP, SA, and exhaustive global search by NS3 at 30 m distance. This result shows that SAP reduces by 60.39% and 82.79% compared with the SA and exhaustive global search methods, respectively. It is noted that even though the exhaustive search can obtain the best throughput, it requires too many computations and does not meet the actual application. Our proposed game theory method achieves the highest throughput benefit at the lowest computational cost. Thus, it can be concluded that the proposed IPG method has the best performance in a comprehensive analysis.

In practical application, we also need to consider the communication overhead during algorithm execution besides throughput performance and computation cost. The comparison of communication overhead between the game theory SAP algorithm and the SA algorithm is shown in Fig. 3.13. In this figure, X-axis denotes the computation cost of the algorithms. Y-axis denotes the percentage of redundant data in total transmission data. Here, we set the percentage of redundant data in total data as the evaluation index of overhead. If this value is high, then the communication overhead of the algorithm costs large. The total transmission data contains redundant data and valid data information. The redundant data is defined as the command control information, the movable users' locations information, and the effective strategies information of movable users.

Fig. 3.13 depicts that the proportion of redundant information becomes smaller with the increase of algorithm computation cost. For the SAP algorithm, this is because the strategies and locations information required by the algorithm is decreasing until the Nash equilibrium is finally obtained with the iteration of the algorithm. Also, for the SAP algorithm, the required locations information continuously decreases until it reaches the global or local optimal. For the SA algorithm, the percentage of redundant data is lower than the SAP at first. As computation time goes on, the curve slowly decreases until the end of the algorithm. The SA algorithm only needs to obtain the location range of the movable users initially. With the execution of iterations, it iterates under the defined parameters and function. Thus, the overhead of the SA algorithm is lower than the SAP.

The performance of communication overhead is the sum of redundant communication data during the whole period of algorithm execution. In Fig. 3.13, communication overhead is the area around the curve and X axis. We calculate that the communication overhead of the SAP algorithm is 108.368, and the SA algorithm is 80.08. It can be noted that after two algorithms execution, the communication overhead of the SAP algorithm is 35.32%

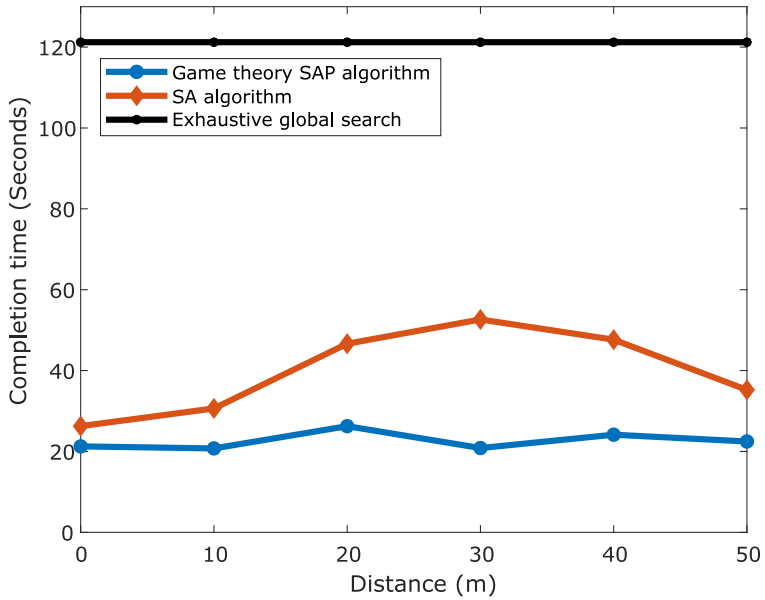

Fig. 3.12 Completion time comparison of SA algorithm, SAP algorithm, and exhaustive global search by NS3 in the scenario I.

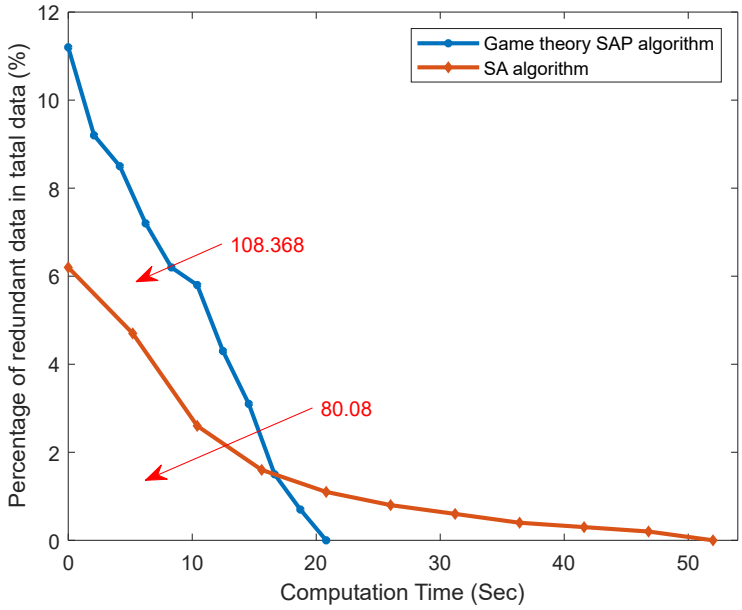

Fig. 3.13 Communication overhead comparison between the SAP and SA algorithm.

higher than the SA algorithm. The reason is that the SAP algorithm makes all movable users cooperate and satisfy with game-theoretic convergence condition. This indicates that during the iteration time, the transmission data should contain the other users' available strategies and action information, and then find Nash equilibrium. The SA algorithm only iterates under the defined temperature and the decision function. It is obvious that the SAP algorithm requires more redundant data than the SA algorithm and generates a larger communication overhead.

In summary, we can extrapolate the practical application places based on the advantages and shortages of these two algorithms. Firstly, for the throughput performance of improvement, the SAP algorithm is better than the SA algorithm. In addition, the computation time and complexity of the SAP algorithm are lower than the SA algorithm. However, for the communication overhead, the SAP algorithm costs higher than the latter. Therefore, in the real-world system, the SAP algorithm is suitable for communication environments with high throughput performance requirements, low feedback delay, and high communication overhead. For example, it is better to be implemented at high-traffic malls or office buildings with high data traffic demand. For the SA algorithm, it is better to be implemented at the environments with low throughput performance, loose delay, and low communication overhead, such as private gatherings or residence with low data traffic and low throughput improvement requirements.

3.4.4 Different SINR thresholds and a varied number of users

According to the above, we elaborate that if the actual SINR identified at the receiver is smaller than the SINR threshold β, then the transmission data package cannot be correctly decoded and is failed. Therefore, the value of the SINR threshold β plays a vital role in determining whether or not a transmission is successful. For studying the effects of different SINR thresholds β for system throughput, we refer to the IEEE 802.11a standard and set two different values as a comparison, $\beta = 24.56$ dB and $\beta = 10.79$ dB. In addition, a varied number of movable and fixed users also has an impact on throughput performance. From above, $|\mathcal{S}|$ and $|\mathcal{M}|$ denote the number of fixed and movable users, respectively. Here, we set the varied number as 2 and 10, respectively. Then it contains four combinations, i) $|\mathcal{S}| = 2$, $|\mathcal{M}| = 2$, ii) $|\mathcal{S}| = 2$, $|\mathcal{M}| = 10$, iii) $|\mathcal{S}| = 10$, $|\mathcal{M}| = 2$, and iv) $|\mathcal{S}| = 10$, $|\mathcal{M}| = 10$. We simulate to comprehensively analyze the effects of different SINR thresholds and a varied number of users.

For simplicity, we regard the scenario I as an application scene and compare the throughput between the SAP and SA algorithm. As shown in Fig. 3.14, we present the throughput comparison under different SINR thresholds with four combinations of different numbers of users. Here, for Fig. 3.14 (c) and (d), the number of fixed users is 10. In order to simplify the transmission model and correspond to the scenario I, we assume that the user close to the source user is regarded as user M, and the other nodes are aggregated into a group as virtual

user N. X-axis also denotes the distance between user M (close to the source user) and user N (the group users).

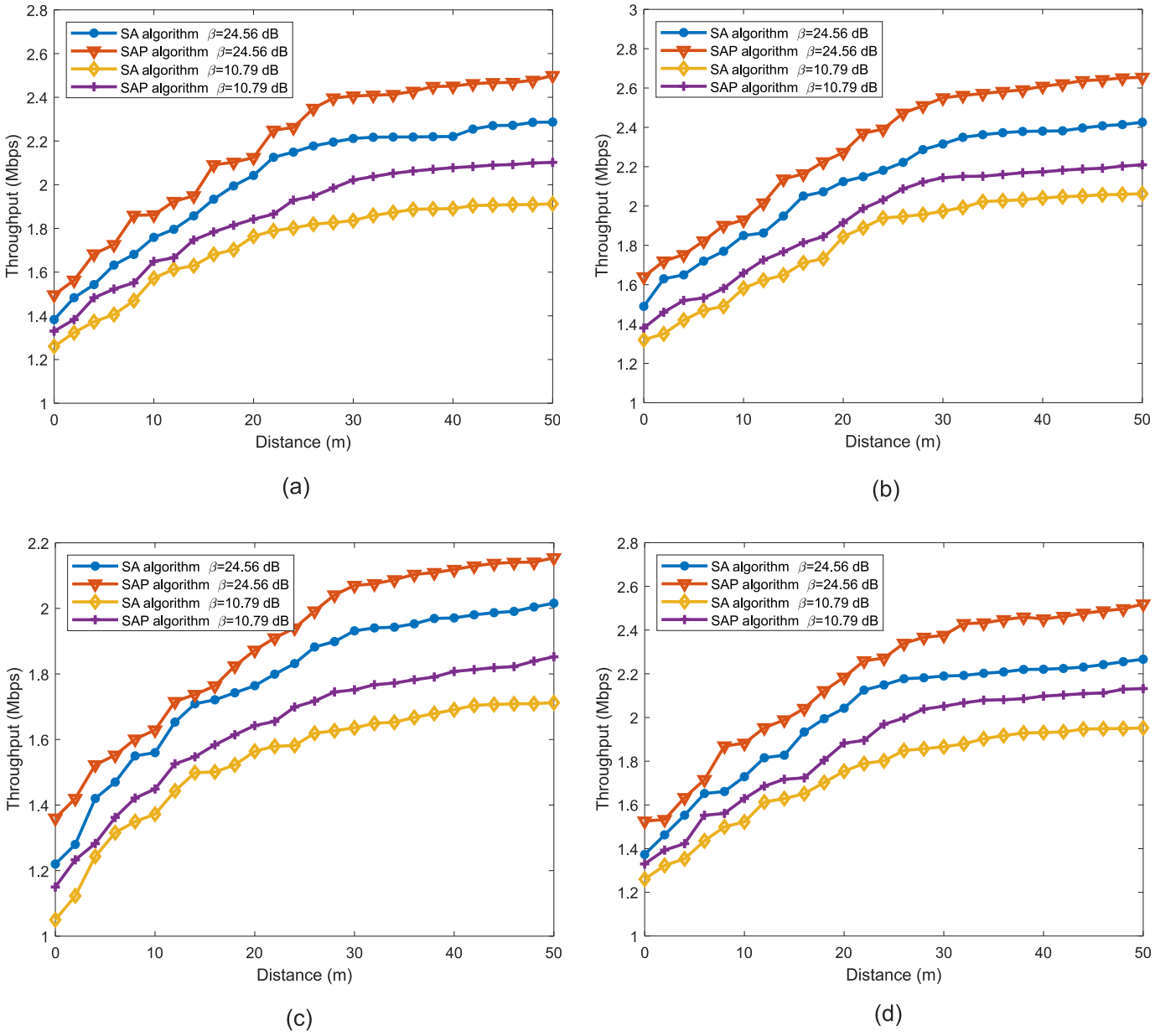

Fig. 3.14 The throughput comparison under different SINR thresholds, and the number of users satisfy: (a) $|\mathcal{S}| = 2$, $|\mathcal{M}| = 2$, (b) $|\mathcal{S}| = 2$, $|\mathcal{M}| = 10$, (c) $|\mathcal{S}| = 10$, $|\mathcal{M}| = 2$, and (d) $|\mathcal{S}| = 10$, $|\mathcal{M}| = 10$.

The curve shapes of throughput in these four figures are also consistent with the previous, i.e., rising first and then stabilizing as the fixed user distance increases. Despite changes in the number of users, since the locations information of fixed users refers to scenario I, the analysis of user-to-user interference remains unchanged. For the analysis of different SINR thresholds, it can be noted that the throughput of β as 24.56 dB, is larger than that of β as 10.79 dB. It is because the SINR perceived at the receiver has to exceed the threshold β for

successful transmission. Then, if the decision standard of SINR is improved, the link can sustain the higher transmission rate. Therefore, the transmission rate of β as 24.56 dB is greater than that of β as 10.79 dB. Finally, the throughput of the higher SINR threshold is more than that of the lower SINR threshold.

The effect of a varied number of movable and fixed users for the throughput is shown in Fig. 3.15. Here, we set the execution algorithm as the SAP algorithm and SINR threshold value as 24.56 dB. It shows that the case of $|\mathcal{S}| = 2$, $|\mathcal{M}| = 10$ has the best performance and obtain the highest throughput, while the case of $|\mathcal{S}| = 10$, $|\mathcal{M}| = 2$ is the worst. Meanwhile, both the cases of $|\mathcal{S}| = 2$, $|\mathcal{M}| = 2$ and $|\mathcal{S}| = 10$, $|\mathcal{M}| = 10$ have comparable performance.

The reasons are that i) more movable users mean more effective strategies, available actions, and higher throughput benefits through cooperative mobility, ii) on the contrary, more fixed users reduce the proportion of effective strategies and opportunities by movable users, then the benefits of throughput are not high, and iii) the harmonic value of system throughput ensures that the benefits through multiple user cooperative mobility are unchanged. It illustrates that the higher the proportion of movable users in the total number of users, the higher the throughput gains. Of course, this is also in line with the universal values of society: the more cooperation, the more benefits. However, in practical application, we also need to take into account of computation cost and overhead of algorithms.

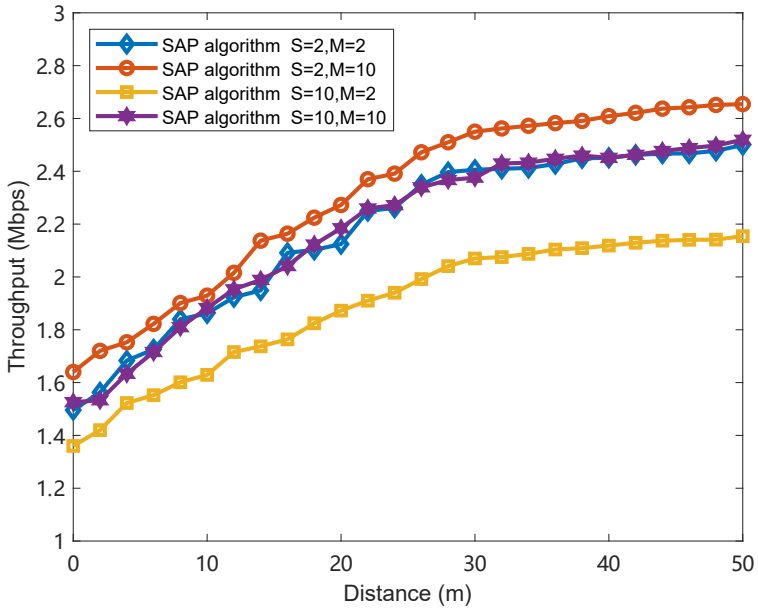

Fig. 3.15 The throughput comparison of a varied number of users under the SAP algorithm and SINR threshold β is 24.56 dB.

3.5 Summary

In this chapter, we model the multiple user cooperative mobility transmission system and address the optimization of the NP-hard problem for system throughput, jointly considering different geographical places and distances among all of the users. Then, an interaction position game is proposed for the global optimization of the problem. We prove that this game is an exact potential game and that optimal Nash equilibrium (NE) points exist. Moreover, we investigate SAP algorithm to obtain NE points and introduce the simulated annealing algorithm as a comparison. Specifically, compared with the intuitive method and SA algorithm in different position cases, the maximum ratio throughput at the NE points increased by 57.35% and 27.27%, respectively. Additionally, the computational cost of this game is reduced by 82.79% compared with the exhaustive global method. Moreover, we validate that the higher the proportion of movable users in the total number of users becomes the larger the system throughput improves.

Chapter 4

An Optimal Location Allocation for High Throughput and Low Algorithmic Complexity

4.1 Related work

A significant work in using graph theory to solve wireless network problems is reported in [53], S. Ramanathan *et al.* proved that directed graph can be used for near-optimal scheduling and can be extended to any network. The summary of related work for improving throughput by graph theory methodology is shown in Table 2.3. The length of the scheduling is proportional to the graph thickness multiplied by the optimal color number. Kamal Jain *et al.* [54] first proposed using a conflict graph to determine the optimal throughput boundaries for a given network and workload. Lijun Chen *et al.* [55] presented using contention graph and contention matrix to formulate resource allocation in the network with joint congestion control and media access control.

Table 4.1 Summary of related work for improving throughput by graph theory methodology

High throughput	Low complexity	Multiuser cooperative mobility	Ad hoc network	Related work
✓	×	×	×	[54]-[55]
✓	×	×	✓	[56]
×	✓	×	✓	[57]
✓	✓	✓	✓	**Our work**

For the conflict perspective, based on [54], Shaohe Lv *et al.* [56] introduced a conflict set graph to characterize the interference and define interference degree to measure a link's interference. Jun Luo *et al.* [57] employed a practical interference model based on SINR, which is used to make the link transmission coordinate without conflict. In [57], a graph network model, and the SINR calculation algorithm for spatial reuse time division, multiple access link scheduling is proposed. Unlike the previous time-scheduling concept, we split the feasible location partitions into mobile nodes by using cooperative behavior to maximize throughput performance.

In summary, few research papers have jointly considered the issue of interference in ad hoc networks in multi-user cooperative mobility. Further, a suitable algorithm has not yet been proposed and adopted for a multi-user cooperative mobility system, i.e., to maximize throughput while ensuring low complexity.

4.2 System model and problem formulation

In this subchapter, we demonstrate a detailed system modeling of multiple user cooperative mobility. Besides, we formulate the maximizing system throughput as a mixed-integer with a non-linear and non-convex problem.

4.2.1 System model

We model an ad hoc network as a set $\mathcal{H}$ of nodes h_i, which consists of a set $\mathcal{F}$ of fixed nodes f_i, a set $\mathcal{M}$ of movable nodes m_i, with $\mathcal{H} = \mathcal{F} \cup \mathcal{M}$. The number of fixed and movable nodes are $|F|$ and $|M|$, respectively. Each node $h_i \in \mathcal{H}$ is associated with a geographical location, whereas each movable node $m_i \in \mathcal{M}$ could move within a limited two-dimensional circle C, radius R_c. The multiple user cooperative mobility system is shown in Fig. 4.1, where transceivers pairs form communication links by Device-to-Device technique.

We hypothesize the following:

1) Each node is equipped with a single-antenna and cannot send and receive packets simultaneously.

2) All nodes have the same transmission power due to the same antenna performance and a slight convergence radius change, both of which generate data traffic, and all of the links are saturated.

3) The topology of the data flow remains a multi-hop chain. It does not change to star or tree type with node mobility because stable relationships between nodes, such as friends and collaborators, ensure that the transmission path remains unchanged.

The application scenario of the cooperative mobility communication system, which is depicted in Fig. 4.1. Initially, these fixed and movable nodes are randomly located in a limited circular space. Several nodes are far away from AP, and they ask other movable helpers or partners to become intermediaries and relay the data traffic. We assume that a virtual central controller is deployed in the AP, such as Google Maps Navigation, which can run the proposed algorithm and arrange each movable node's location. The AP sends control messages through the control channel at the physical layer to arrange each movable node's geographic location. The frame header of data traffic contains the control information, so two-hop or multi-hop nodes can also receive it. This method of sending a control message is similar to "beacon."

During the transmission period, these collaborators transmit by the User Datagram Protocol (UDP) service. To facilitate analysis system throughput, we calculate the uplink data generated from all users to the AP while all links are saturated. Based on this consideration, system throughput is defined as the amount of data per unit time received by the AP, i.e., the average harmonic of all users' transmission rates [80].

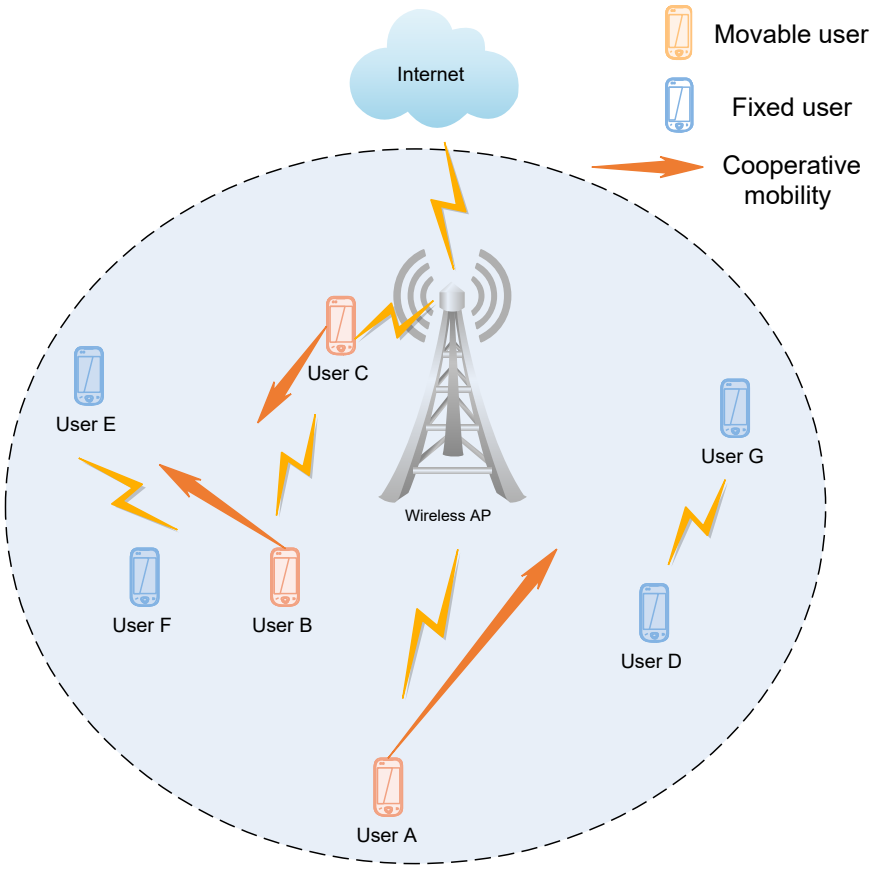

Fig. 4.1 Multiple user cooperative mobility transmission system.

This work aims to assign each movable node a suitable location within the limited circle space while assuring the system throughput performance as better as possible. Specifically, the best strategy for maximizing system throughput is to attain the best position for them deliberating mutual interference. The best geographical positions maintain the maximum throughput keeping desirable SINR.

However, it is a combinatorial optimization problem of exorbitant complexity considering mobility user locations' diversity and inter-user interference. Solving this optimization problem will result in a tradeoff between the accuracy of the best throughput performance and the allowed computation cost [34]. We deduce and propose an effective algorithm by analyzing the relationship between SINR, the location of movable nodes, and system throughput. The virtual control center executes the algorithm to efficiently allocate the best location to the movable nodes, which improves the overall throughput of the system. Before the problem formulation, we present the location model's definition and the location distribution function of fixed nodes.

We deploy polar coordinates to define the positions and the distance between two nodes. Let the position coordinate of node $h_i \in \mathcal{H}$ be expressed as $h_i\left(\rho_i, \Theta_i\right)$, where ρ_i is the polar diameter, $\rho_i \leqslant R_c$, and Θ_i is called as the polar angel. Then, we define the set of nodes $\mathcal{H}$ positions as $\boldsymbol{H}\left(\boldsymbol{\rho},\ \boldsymbol{\Theta}\right)$, $\boldsymbol{H}\left(\boldsymbol{\rho}, \boldsymbol{\Theta}\right) = \{h_i\left(\rho_i, \Theta_i\right) | h_i \in \mathcal{H}\ , \rho_i \in \boldsymbol{\rho}, \Theta_i \in \boldsymbol{\Theta}\}$, $|\boldsymbol{\rho}| \leqslant R_c$,

$0 \leqslant |\boldsymbol{\Theta}| \leqslant \pi$ where $\boldsymbol{\rho}$ and $\boldsymbol{\Theta}$ denote the set of polar diameter and angel, respectively. Correspondingly, for fixed and movable nodes $f_i \in \mathcal{F}$, $m_i \in \mathcal{M}$, the position sets can be expressed as $\boldsymbol{F}\left(\boldsymbol{\rho}_f,\ \boldsymbol{\Theta}_f\right) = \left\{f_i\left(\rho_i, \Theta_i\right) | f_i \in \mathcal{F}\ , f_i \in \boldsymbol{\rho}_f, f_i \in \boldsymbol{\Theta}_f\right\}$, $\boldsymbol{M}\left(\boldsymbol{\rho}_m,\ \boldsymbol{\Theta}_m\right) = \left\{m_i\left(\rho_i, \Theta_i\right) | m_i \in \mathcal{M}\ , \rho_i \in \boldsymbol{\rho}_m, \Theta_i \in \boldsymbol{\Theta}_m\right\}$. The polar coordinate unit is defined as $\mathbf{1}$. As for arbitrary two nodes $h_1\left(\rho_1, \Theta_1\right)$ and $h_2\left(\rho_2, \Theta_2\right)$, the distance d_{h_1,h_2} can be given by

$$\begin{aligned} d_{h_1,h_2} &= \left\|h_1\left(\rho_1, \Theta_1\right) - h_2\left(\rho_2, \Theta_2\right)\right\| \\ &= \begin{cases} \left|\rho_1 - \rho_2\right|, \Theta_1 = \Theta_2, \Theta_1 \neq 0, \Theta_2 \neq 0 \\ \sqrt{\rho_1^2 + \rho_2^2 - 2\rho_1\rho_2\cos\left(\Theta_1 - \Theta_2\right)}, \Theta_1 \neq \Theta_2 \end{cases} \end{aligned} \tag{4.1}$$

Here, we define that all of the nodes should not locate at the same line, i.e., $\Theta_i \neq 0$. This is because that the best position for movable users is at the bisection position if $\Theta_i = 0$, which makes no sense to calculate. In order to better fit the practice and simulate fixed nodes, we utilize the Poisson point process (PPP) [81] to present the property of positions. In the limited circle $C : r\left(\Theta_i\right) = R_c$, the positions of these fixed nodes $f_1\left(\rho_1, \Theta_1\right)$, $f_2\left(\rho_2, \Theta_2\right), \ldots,$ $f_F\left(\rho_F, \Theta_F\right)$ are independent of each other.

Definition 1: Fixed nodes set $\mathcal{F}$ is located in the region spaces set $\boldsymbol{\chi}$, $f_i\ \rightarrow \chi_i, f_i \in \mathcal{F}, \chi_i \subseteq \boldsymbol{\chi}$, which is a space homogeneous Poisson point process, the following two conditions are satisfied.

1. For a random regions χ_i that lies in the space of the restricted circle $C : r\left(\theta\right) = R_c$, $\chi_i \subseteq \boldsymbol{\chi} \subseteq C$, $X = \delta\left(\chi_i\right)$ obeys Poisson distribution with mean value of $\lambda\nu_r\left(\chi_i\right)$, which can be expressed as

$$P\left[\delta\left(\chi_i\right) = k\right] = \left[\lambda\nu_r\left(\chi_i\right)\right]^k \exp\left[\frac{\left(-\lambda\nu_r\left(\chi_i\right)\right)}{m!}\right] \tag{4.2}$$

   where $\delta\left(\chi_i\right)$ is the number of points in the bounded region χ_i, λ is a constant, which is denoted as the average number of points per unit area, and $\nu_r\left(\chi_i\right)$ is an area of the bounded region χ_i.

2. Random bounded regions $\chi_1, \chi_2, ..., \chi_F$ do not intersect with each other, then $\delta\left(\chi_1\right), \delta\left(\chi_2\right), ..., \delta\left(\chi_F\right)$ are independent of each other.

Accordingly, the fixed nodes in space are completely random, and the expectation of the number of points $\delta\left(\chi_i\right)$ per unit area is constant λ, which is unchanged with the area and the position of the limited circle space C. In that case, random variable of the distance between any two fixed nodes, $\boldsymbol{l}_{f_i,f_j}$, is independent and identically distributed, which can be subject to exponential distribution with λ. The probability that no fixed nodes exists in the bounded region χ_i is $P\left[\delta\left(\chi_i\right) = 0\right] = e^{-\lambda\nu_r(\chi_i)}$. Then, the cumulative distribution function $F\left(\boldsymbol{l}_{f_i,f_j}\right)$

can be derived as

$$\begin{aligned} F\left(\boldsymbol{l}_{f_i,f_j};\lambda\right) &= F\left(\boldsymbol{l}_{f_i,f_j} \leqslant r\right) \\ &= 1 - P\left[\delta\left(\chi_i\right) = 0\right] \\ &= 1 - e^{-\lambda\pi r^2} \end{aligned} \tag{4.3}$$

where $F\left(\boldsymbol{l}_{f_i,f_j} \leqslant r\right)$ denotes the probability that the distance between fixed node f_i and f_j is at most r. Therefore, the expectation of $\boldsymbol{l}_{f_i,f_j}$, $E\left[\boldsymbol{l}_{f_i,f_j}\right]$, we have

$$\begin{aligned} E\left[\boldsymbol{l}_{f_i,f_j}\right] &= \int_0^{R_c} 2\pi r^2 \exp\left(-\lambda\pi r^2\right) dr \\ &= \frac{erfi\left(R_c\sqrt{\lambda}\sqrt{\pi}\right)}{2\sqrt{\lambda}} - R_c \exp\left(-\lambda\pi R_c^2\right), \\ erfi\left(x\right) &= \frac{2}{\sqrt{\pi}}\int_0^x e^{t^2} dt \end{aligned} \tag{4.4}$$

In this model, we analyze the inter-signal interference between users at the physical layer, rather than analyzing the specific frame slot scheduling and multiple packet processing conflicts at the link-layer MAC frame's perspective. There are packet frame conflicts in the actual transmission. Still, since we assume that the data stream is saturated, i.e., the performance degradation due to data frame conflicts on each link has less impact on our results.

4.2.2 Problem formulation

As shown in Fig. 4.2(a), fixed location users satisfy the Poisson space point process and are distributed around the AP. Considering that the practical application is in a large square or park, we set the propagation model as the non-line-of-sight (NLOS), and the obstacles might distort the radio waves. In addition, multi-path signals are superimposed, and the strength of the attenuation coefficient approximately obeys the Rayleigh distribution. The notation used for problem formulations is shown in Table 4.1.

Under Decode-and-Forward (DF) [83], the cooperative relay node m_i decodes the received signal from node f_i, and reencodes it before forwarding it to the destination node f_{i+1}, which could maximize the utilization of spatial diversity. Thus, we make use of the DF with diversity combining [84] between nodes transmission to expound the system throughput and extrapolate the best position, which is presented in Fig. 4.2(b). Assume fixed node f_i sends data packets to f_{i+1} relaying by movable node m_i, the received power P_{m_i} of movable node m_i can be given by

$$P_{m_i} = P_{tx} K \left(\frac{l_{f_i,m_i}}{d_0}\right)^{-\alpha} \tag{4.5}$$

where P_{tx} is the transmission power of fixed node f_i, l_{f_i,m_i} is the distance between node f_i and m_i, d_0 is the reference distance, K is a constant related to the antenna gain and average

Table 4.2 Notation used for problem formulations.

Parameters	Description
$\mathcal{F}$	Set of fixed nodes
$\mathcal{M}$	Set of movable nodes
$\|F\|$	Number of fixed nodes
$\|M\|$	Number of movable nodes
R_c	Radius of circle space
P_{tx}	Transmission power
$\boldsymbol{F}\left(\boldsymbol{\rho}_f,\ \boldsymbol{\Theta}_f\right)$	Set of fixed nodes positions
$f_i\left(\rho_i, \Theta_i\right)$	Fixed node f_i position
$\varphi\left(\boldsymbol{l}_{f_i,f_j}\right)$	Distance function between fixed nodes
d_0	Reference distance
K	Constant, which is related to the antenna gain and average channel attenuation
α	Path loss exponent
β	SINR threshold
$\boldsymbol{M}\left(\boldsymbol{\rho}_m,\ \boldsymbol{\Theta}_m\right)$	Set of movable nodes positions
$\Phi 1\left[f_i\left(\rho_i, \Theta_i\right), m_i\left(\rho_i, \Theta_i\right)\right]$	Distance function between fixed node f_i and movable node m_i
$\Phi 2\left[f_{i+1}\left(\rho_{i+1}, \Theta_{i+1}\right), m_i\left(\rho_i, \Theta_i\right)\right]$	Distance function between fixed node f_{i+1} and movable node m_i
$\Phi 3\left[m_i\left(\rho_i, \Theta_i\right), m_j\left(\rho_j, \Theta_j\right)\right]$	Distance function between movable nodes m_i and m_j
$\Gamma 1\left[\Phi 1\left(x\right), \Phi 2\left(x\right)\right]$	Angel function between fixed node f_i and movable node m_i
$\Gamma 2\left[\Phi 1\left(x\right), \Phi 2\left(x\right)\right]$	Angel function between fixed node f_{i+1} and movable node m_i
$\gamma_{f_i,f_{i+1}}$	SINR of link $f_i \rightarrow f_{i+1}$ for receiver f_{i+1}
$\gamma_{m_i,f_{i+1}}$	SINR of link $m_i \rightarrow f_{i+1}$ for receiver f_{i+1}
γ_{f_i,m_i}	SINR of link $f_i \rightarrow m_i$ for receiver m_i
$R_{DF,i}$	Maximum combining transmission rate of link $f_i \rightarrow f_{i+1}$ and $f_i \rightarrow m_i \rightarrow f_{i+1}$
$\varepsilon 1\left[m_i\left(\rho_i, \Theta_i\right)\right]$	SINR function of link $f_i \rightarrow f_{i+1}$
$\varepsilon 2\left[m_i\left(\rho_i, \Theta_i\right)\right]$	Combining SINR function of link $f_i \rightarrow m_i \rightarrow f_{i+1}$

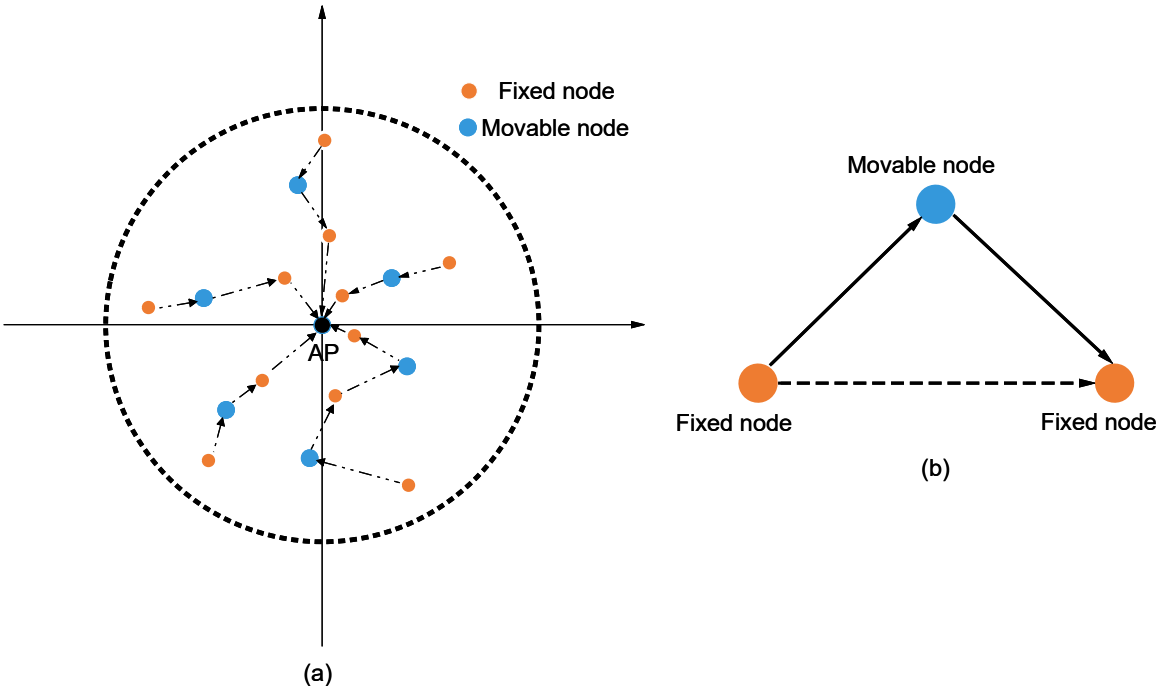

Fig. 4.2 Mathematical model. (a) Transmission of data flow between nodes; (b) Fixed and movable nodes transfer via Decode-and-Forward.

channel attenuation, and α is the path-loss exponent. The constant K can be calculated by the empirical average of the received power at the distance d_0. The reference distance d_0 varies from 10 to 100 meters at outdoor space, here, we set it as 20 [82]. The value of path loss exponent α, which depends on the propagation, usually ranges from 2 and 4. Consider the outdoor or urban shadowed space, $\alpha = 4$ [85]. Then, (4.5) can be simplified as $P_{m_i} = P_{tx} K \left(\frac{l_{f_i,m_i}}{20}\right)^{-4}$.

To jointly consider the path loss and shadowing effects, the relationship between P_{m_i} and P_{tx} is measured in dB, which can be presented as follows [86],

$$\left(\frac{P_{m_i}}{P_{tx}}\right)_{\text{dB}} = 10\log_{10} K - 40\alpha \log_{10}\left(\frac{d}{20}\right) + \Delta \tag{4.6}$$

where Δ is a Gaussian random variable with zero mean and standard deviation σ. At the urban microcells, the value of σ is from 4 to 12. This implies that the constant K can be calculated by (4.6).

In the DF relay transmission, fixed node f_{i+1} not only receive the signal from node f_i but also combine with the signal sent by relay node m_i, i.e., it makes f_{i+1} receive two copies of the signal due to the diversity combining. Let the receive power for node f_{i+1} from m_i and f_i, denote as P_{f_{i+1},m_i} and P_{f_{i+1},f_i}, respectively. Similarly, we can obtain $P_{f_{i+1},m_i} = P_{tx} K \left(\frac{l_{f_{i+1},m_i}}{20}\right)^{-4}$ and $P_{f_{i+1},f_i} = P_{tx} K \left(\frac{L_{f_i,f_{i+1}}}{20}\right)^{-4}$, where l_{f_{i+1},m_i} and $L_{f_i,f_{i+1}}$ denote the distance between node f_{i+1} and nodes m_i, f_i, respectively. $L_{f_i,f_{i+1}}$ can be considered as a known quantity due to fixed nodes location information, $L_{f_i,f_{i+1}} = \|f_i(\rho_i, \Theta_i) - f_i(\rho_{i+1}, \Theta_{i+1})\| \triangleq \varphi\left(\boldsymbol{l}_{f_i,f_j}\right)$, where $\varphi(x)$ is the distance function between fixed nodes, $E[\varphi(x)] = E\left[\boldsymbol{l}_{f_i,f_j}\right]$. The distance l_{f_i,m_i} and l_{f_{i+1},m_i} are derived as follows,

$$\begin{aligned} l_{f_i,m_i} &= \|f_i(\rho_i, \Theta_i) - m_i(\rho_i, \Theta_i)\| \\ &= \varphi\left(\boldsymbol{l}_{f_i,f_j}\right) \frac{\sin\left(\tilde{\theta}_{f_{i+1}}\right)}{\sin\left(\tilde{\theta}_{f_i} + \tilde{\theta}_{f_{i+1}}\right)} \\ &\overset{\text{def}}{=} \Phi 1\left[f_i(\rho_i, \Theta_i), m_i(\rho_i, \Theta_i)\right] \end{aligned} \tag{4.7}$$

$$\begin{aligned} l_{f_{i+1},m_i} &= \|f_{i+1}(\rho_{i+1}, \Theta_{i+1}) - m_i(\rho_i, \Theta_i)\| \\ &= \varphi\left(\boldsymbol{l}_{f_i,f_j}\right) \frac{\sin\left(\tilde{\theta}_{f_i}\right)}{\sin\left(\tilde{\theta}_{f_i} + \tilde{\theta}_{f_{i+1}}\right)} \\ &\overset{\text{def}}{=} \Phi 2\left[f_{i+1}(\rho_{i+1}, \Theta_{i+1}), m_i(\rho_i, \Theta_i)\right] \end{aligned} \tag{4.8}$$

where $0 < \tilde{\theta}_{f_i} < \pi$, $0 < \tilde{\theta}_{f_{i+1}} < \pi - \tilde{\theta}_{f_i}$. $\Phi 1(x)$ and $\Phi 2(x)$ represent the distance between fixed nodes f_i, f_{i+1} and movable node m_i, which are functions of location in-

formation $f_i(\rho_i, \Theta_i)$, $f_{i+1}(\rho_{i+1}, \Theta_{i+1})$ and $m_i(\rho_i, \Theta_i)$, with $f_i(\rho_i, \Theta_i), f_{i+1}(\rho_{i+1}, \Theta_{i+1}) \in \boldsymbol{F}(\boldsymbol{\rho}_m, \boldsymbol{\Theta}_m)$, $m_i(\rho_i, \Theta_i) \in \boldsymbol{M}(\boldsymbol{\rho}_m, \boldsymbol{\Theta}_m)$. If $\Phi 1(x)$ and $\Phi 2(x)$ can be determined, then the angles of the movable nodes can also be confirmed, i.e., the coordinate positions can be established as a result. Here, we use $\tilde{\theta}_{f_i}$ and $\tilde{\theta}_{f_{i+1}}$ to denote the angle functions. Similarly, the distance between movable nodes $m_i(\rho_i, \Theta_i)$ and $m_j(\rho_j, \Theta_j)$ can be defined as $\Phi 3[m_i(\rho_i, \Theta_i), m_j(\rho_j, \Theta_j)]$. We abbreviate these distance functions to $\Phi 1(f_i, m_i)$, $\Phi 2(f_{i+1}, m_i)$ and $\Phi 3(m_i, m_j)$ in the following content, respectively. The SINR at receiver f_{i+1} is given by

$$\begin{aligned}
\text{SINR}_{f_{i+1}} &= \gamma_{f_i,f_{i+1}} + \gamma_{m_i,f_{i+1}} \\
\gamma_{f_i,f_{i+1}} &= \frac{1}{\frac{N_0}{P_{tx}K}\left(\frac{\varphi(\boldsymbol{l}_{f_i,f_{i+1}})}{20}\right)^4 + \sum_{k=1,k\neq i}^{|F|-2}\left(\frac{\varphi(\boldsymbol{l}_{f_i,f_{i+1}})}{\varphi(\boldsymbol{l}_{f_k,f_{i+1}})}\right)^4 + \sum_{k=1}^{|M|}\left(\frac{\varphi(\boldsymbol{l}_{f_i,f_{i+1}})}{\Phi 2(f_{i+1},m_k)}\right)^4} \\
\gamma_{m_i,f_{i+1}} &= \frac{1}{\frac{N_0}{P_{tx}K}\left(\frac{\Phi 2(f_{i+1},m_i)}{20}\right)^4 + \sum_{k=1}^{|F|-1}\left(\frac{\Phi 2(f_{i+1},m_i)}{\varphi(\boldsymbol{l}_{f_k,f_{i+1}})}\right)^4 + \sum_{j=1,j\neq i}^{|M|-1}\left(\frac{\Phi 2(f_{i+1},m_i)}{\Phi 2(f_{i+1},m_j)}\right)^4}
\end{aligned} \tag{4.9}$$

where $\gamma_{f_i,f_{i+1}}$ and $\gamma_{m_i,f_{i+1}}$ denote the SINR of link $f_i \to f_{i+1}$ and link $m_i \to f_{i+1}$ at receiver f_{i+1}, respectively. Similarly, the SINR at receiver m_i can be expressed as

$$\text{SINR}_{m_i} = \gamma_{f_i,m_i} = \frac{1}{\frac{N_0}{P_{tx}K}\left(\frac{\Phi 1(f_i,m_i)}{20}\right)^4 + \sum_{k=1,\,k\neq i}^{|F|-1}\left(\frac{\Phi 1(f_i,m_i)}{\Phi 1(f_k,m_i)}\right)^4 + \sum_{j=1,\,j\neq i}^{|M|-1}\left(\frac{\Phi 1(f_i,m_i)}{\Phi 3(m_i,m_j)}\right)^4} \tag{4.10}$$

According to the physical interference protocol, the packet is successfully received and correctly decoded for receiver f_{i+1} and m_i if and only if the SINR is greater than or equal to a certain threshold β, i.e., $\text{SINR}_{m_i} \geqslant \beta$ and $\text{SINR}_{f_{i+1}} \geqslant \beta$. Here, we set the SINR threshold β of each node to be equal, considering the same Radio Frequency (RF) circuit performance. From the above, the system capacity is approximately equal to the link transmission rate due to stable chain topology and saturated links. According to [82], the capacity $C_{DF,i}$ for DF under the one-relay structure is given by

$$C_{DF,i} = R_{DF,i} \leqslant \frac{1}{2} W \min\left\{\log_2(1+\text{SINR}_{m_i}), \log_2\left(1+\gamma_{f_i,f_{i+1}}+\gamma_{m_i,f_{i+1}}\right)\right\} \tag{4.11}$$

where $R_{DF,i}$ is the maximum total transmission rate of for link $f_i \to f_{i+1}$, W is physical channel bandwidth, which can be normalized as $\mathbf{1}$. Substituting (4.7), (4.8), (4.9) and (4.10)

into (4.11), the transmission rate $R_{DF,i}$ can be rewritten as

$$
\begin{aligned}
&\left(R_{DF,i}\right)_{\max}=\frac{1}{2}\min\left\{\varepsilon 1\left[m_i\left(\rho_i,\Theta_i\right)\right],\varepsilon 2\left[m_i\left(\rho_i,\Theta_i\right)\right]\right\}\\
&\varepsilon 1\left[m_i\left(\rho_i,\Theta_i\right)\right]\triangleq\log_2\left(1+\frac{1}{\frac{N_0}{P_{tx}K}\left(\frac{\Phi 1(f_i,m_i)}{20}\right)^4+\sum_{k=1,\,k\neq i}^{|F|-1}\left(\frac{\Phi 1(f_i,m_i)}{\Phi 1(f_k,m_i)}\right)^4+\sum_{j=1,\,j\neq i}^{|M|-1}\left(\frac{\Phi 1(f_i,m_i)}{\Phi 3(m_i,m_j)}\right)^4}\right)\\
&\varepsilon 2\left[m_i\left(\rho_i,\Theta_i\right)\right]\triangleq\log_2\left(\begin{array}{l}1+\frac{1}{\frac{N_0}{P_{tx}K}\left(\frac{\varphi\left(\boldsymbol{l}_{f_i,f_{i+1}}\right)}{20}\right)^4+\sum_{k=1,\,k\neq i}^{|F|-2}\left(\frac{\varphi\left(\boldsymbol{l}_{f_i,f_{i+1}}\right)}{\varphi\left(\boldsymbol{l}_{f_k,f_{i+1}}\right)}\right)^4+\sum_{k=1}^{|M|}\left(\frac{\varphi\left(\boldsymbol{l}_{f_i,f_{i+1}}\right)}{\Phi 2\left(f_{i+1},m_k\right)}\right)^4}\\+\frac{1}{\frac{N_0}{P_{tx}K}\left(\frac{\Phi 2\left(f_{i+1},m_i\right)}{20}\right)^4+\sum_{k=1}^{|F|-1}\left(\frac{\Phi 2\left(f_{i+1},m_i\right)}{\varphi\left(\boldsymbol{l}_{f_k,f_{i+1}}\right)}\right)^4+\sum_{j=1,\,j\neq i}^{|M|-1}\left(\frac{\Phi 2\left(f_{i+1},m_i\right)}{\Phi 2\left(f_{i+1},m_j\right)}\right)^4}\end{array}\right)
\end{aligned}
\tag{4.12}
$$

We can find that the transmission rate $R_{DF,i}$ is a function of the node m_i's position variable $m_i\left(\rho_i,\Theta_i\right)$, $m_i\left(\rho_i,\Theta_i\right)\in\boldsymbol{M}\left(\boldsymbol{\rho}_m,\ \boldsymbol{\Theta}_m\right)$. For all links in this ad hoc network, the system throughput Th_{sys} is defined as the reciprocal of the sum of harmonic means of each node [80],

$$
Th_{sys}=\frac{\frac{1}{2}\left|M\right|}{\sum_{i=1}^{|M|}\frac{1}{R_{DF,i}}} \tag{4.13}
$$

Then, the maximizing system throughput Th_{sys} problem can be converted to minimize $\sum_{i=1}^{|M|}\frac{1}{R_{DF,i}}$. The global objective is to find the optimal movable nodes position to maximize network throughput. Summarizing from (4.7) to (4.12) into (4.13), the throughput optimization problem is as follows,

$$
\begin{aligned}
\min_{\boldsymbol{M}(\boldsymbol{\rho}_m,\,\boldsymbol{\Theta}_m)}\ &\sum_{m\in\mathcal{M}}^{|M|}\frac{1}{\min\left\{\varepsilon 1,\varepsilon 2\right\}}\\
s.t.\qquad &0<\left|\boldsymbol{\rho}_m\right|\leqslant R_c\\
&0\leqslant\left|\boldsymbol{\Theta}_m\right|\leqslant\pi\\
&\gamma_{f_i,f_{i+1}}\geqslant\beta\\
&\gamma_{f_i,m_i}\geqslant\beta\\
&\gamma_{m_i,f_{i+1}}\geqslant\beta\\
&E\left[\varphi\left(\boldsymbol{l}_{f_i,f_{i+1}}\right)\right]=E\left[\boldsymbol{l}_{f_i,f_j}\right]
\end{aligned}
\tag{4.14}
$$

where $E\left[\varphi\left(\boldsymbol{l}_{f_i,f_{i+1}}\right)\right]$ is a constant, and $\varphi\left(\boldsymbol{l}_{f_i,f_{i+1}}\right)$ can be calculated by known location information f_i. Note that $\boldsymbol{M}\left(\boldsymbol{\rho}_m,\ \boldsymbol{\Theta}_m\right)$ is the optimization variable to determine the mobility-optimal scheduling. In particular, the objective function is mixed-integer with non-linear and non-convex constraints variable functions $\Phi 1\left(f_i,m_i\right)$, $\Phi 2\left(f_{i+1},m_i\right)$ and $\Phi 3\left(m_i,m_j\right)$. This causes this problem to be a Mixed-Integer with Non-Linear and Non-Convex Problem (MINLNCP), which is NP-hard generally. This problem can be solved by using exhaustive

search, but has intractable and prohibitive complexity $O\left(C_{|M|}^{\lfloor \pi R_c^2 \rfloor}\right)$, where $\lfloor \pi R_c^2 \rfloor$ denotes the number of selection position profiles (number of nodes per unit area is 1). Conventional heuristic methods are alternative approaches, like simulated annealing, game theory method, etc. However, they cannot guarantee that the optimal solutions can be obtained. High computation complexity and low accuracy of solutions are also significant constraints to these heuristic algorithms' practical application.

In the following subchapters, we introduce the concept of domain and then illuminate the search region of movable nodes, including upper and lower bounds. The original exhaustive problem is decomposed into a two-step problem, namely deducing the domain of upper and lower bound by conflict graph method and location allocation for movable nodes considering interference. Moreover, we design the Maximum Throughput algorithm for Optimal Position (MTOP) based on the derived domain. Finally, we compare MTOP with conventional heuristic methods and obtain analytical results.

4.3 Location domain of movable nodes

This subchapter presents the domain concept, which is a certain search region for movable nodes considering the interference. And then, we prove the upper and lower bounds invoked by the conflict graph. In addition, we provide algorithms for obtaining these two bound values.

4.3.1 Concept of domain

Notice that general heuristic algorithms cannot obtain the resolution of MINLNCP. Our idea is to explore a small enough domain and contain the optimal position assembles to reduce redundant computation and improve search accuracy. Please refer to Table 4.2 for a summary of additional notation pertaining to the Definitions and Propositions to follow.

Table 4.3 Notation used for definitions and propositions.

Parameters	Description
$\mathcal{G}$	Domain, which represents the range of $\boldsymbol{M}^*\left(\boldsymbol{\rho}_m,\ \boldsymbol{\Theta}_m\right)$
$\mathcal{G}_{Upper}$	Upper bound of the domain
$\mathcal{G}_{Lower}$	Lower bound of the domain
D_U	Determination of upper bound range
D_L	Determination of lower bound range
Ω	All profiles of movable nodes locations
$G_p\left(V, E\right)$	Communication graph
$\mathscr{G}\left(\mathcal{V}, \mathcal{E}\right)$	Conflict graph
$\mathcal{U}$	Set of satisfying the upper bound
$\mathcal{I}$	Set of satisfying the lower bound

Conforming to (14), the optimization problem is related to the variable $\boldsymbol{M}\left(\boldsymbol{\rho}_m,\ \boldsymbol{\Theta}_m\right)$, which can be expressed in terms of distance functions l_{f_i,m_i} and l_{f_{i+1},m_i}. We define a domain $\mathcal{G}$ as the desirable range of $\boldsymbol{M}^*\left(\boldsymbol{\rho}_m,\ \boldsymbol{\Theta}_m\right)$ which is the optimal locations, given by

$$\begin{aligned}
\mathcal{G} &= \left\{ \boldsymbol{M}\left(\boldsymbol{\rho}_m,\ \boldsymbol{\Theta}_m\right) \in \bigcup_{i=1}^{|M|} \mathcal{Q}_i \,|\mathcal{Q}_i = \mathcal{O}1 \cap \mathcal{O}2, \Phi 3\left(m_i, m_j\right) \leqslant R_c \right\} \\
\mathcal{O}1 &\triangleq \left\{ m_i\left(\rho_i, \Theta_i\right) \left| \rho_{m_i}^2 - 2\rho_{m_i}\rho_{f_i}\left(\theta_{m_i} - \theta_{f_i}\right) + \rho_{f_i}^2 \leqslant l_{f_i,m_i}^2, \Phi 1\left(f_i, m_i\right) \leqslant R_c \right.\right\} \\
\mathcal{O}2 &\triangleq \left\{ m_i\left(\rho_i, \Theta_i\right) \left| \rho_{m_i}^2 - 2\rho_{m_i}\rho_{f_{i+1}}\left(\theta_{m_i} - \theta_{f_{i+1}}\right) + \rho_{f_{i+1}}^2 \leqslant l_{f_{i+1},m_i}^2, \Phi 2\left(f_{i+1}, m_i\right) \leqslant R_c \right.\right\}
\end{aligned} \tag{4.15}$$

$\mathcal{O}1$ and $\mathcal{O}2$ denote circular regions with fixed nodes f_i and f_{i+1} as centers, respectively. $\mathcal{Q}_i$ is the intersection of regions both $\mathcal{O}1$ and $\mathcal{O}2$, i.e., the movable range for m_i on each link $f_i \rightarrow f_{i+1}$. If the range of $\mathcal{G}$ can be determined, then it is easier to attain the approximate optimal solution of (4.16) by using iterative approaches. However, $\mathcal{G}$ cannot be directly resolved because of interfering interactions and the randomness of mobility. Hence, we further define upper and lower bounds to obtain an interval to estimate the fetch space of $\mathcal{G}$, defined as follows.

Definition 2: In a limited two-dimensional circle C with radius R_c, arbitrary fixed nodes f_i and f_{i+1} transfer data packets by DF with diversity combining, then the set of all movable nodes $m_i \in \mathcal{M}$ exist boundaries in the domain space, called as upper bound and lower bound.

Upper bound:

$$\begin{aligned}
\mathcal{G}_{Upper} &= \left\{ \boldsymbol{M}\left(\boldsymbol{\rho}_m,\ \boldsymbol{\Theta}_m\right) \in \bigcup_{i=1}^{|M|} \mathcal{Q}_i \,\middle|\, \mathcal{Q}_i = \left\{\mathcal{O}1 \cap \mathcal{O}2 \cap D_U\right\}, D_U \leqslant R_c \right\} \\
D_U &= \arg\max\left\{\Phi 1\left(f_i, m_i\right), \Phi 2\left(f_{i+1}, m_i\right), \Phi 3\left(m_i, m_j\right)\right\}
\end{aligned} \tag{4.16}$$

Lower bound:

$$\begin{aligned}
\mathcal{G}_{Lower} &= \left\{ \boldsymbol{M}\left(\boldsymbol{\rho}_m,\ \boldsymbol{\Theta}_m\right) \in \bigcup_{i=1}^{|M|} \mathcal{Q}_i \,\middle|\, \mathcal{Q}_i = \left\{\mathcal{O}1 \cap \mathcal{O}2 \cap D_L\right\}, D_L \leqslant R_c \right\} \\
D_L &= \arg\min\left\{\Phi 1\left(f_i, m_i\right), \Phi 2\left(f_{i+1}, m_i\right), \Phi 3\left(m_i, m_j\right)\right\}
\end{aligned} \tag{4.17}$$

Fig. 4.3 depicts the domain definition of movable nodes (blue area). It indicates that for each mobile node m_i, its active region $\mathcal{Q}_i$ is the intersection of the feasible domains $\mathcal{O}1$ and $\mathcal{O}2$ generated by the two fixed nodes as circles. The blue area is the concatenation of all active domains $\mathcal{Q}_i$. We analyze the successful reception of packets for the receiving node at the dimension, physical interference model. For the physical model, the receiving SINR should be greater than or equal to the threshold β. We will evaluate the upper and lower

bounds based on meeting this model. The outline for the rest of this section is as follows:

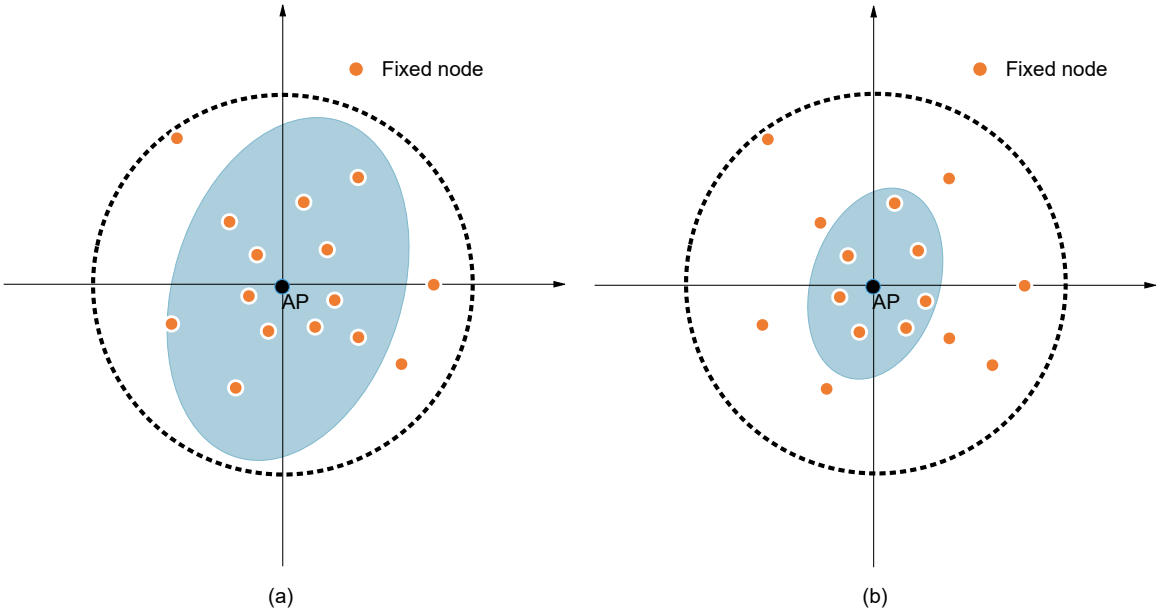

Fig. 4.3 Domain of movable nodes. (a) Upper bound; (b) Lower bound.

- Define the conflict graph based on meeting transmission mode, such that it guarantees feasible communication under the physical and protocol interference models. This conflict graph is more effective than the traditional graph to analyze the DF and ideal transmission conditions in the extreme case.
- Develop propositions and algorithms that can achieve upper and lower bounds but only require geographical information of fixed nodes. In the propositions, we derive and prove the key properties of D_U and D_L find the algorithm' borders.

4.3.2 Lower bound

To characterize the interference at different positions for movable nodes and simultaneous conflict-free operation of links, we define a conflict set of locations graph (CSLG) model. Note that a conflicting concept for the edge-based physical interference model is first introduced in [28]. The author focused on the weighted degree of the directed graph to indicate the interference and noise intensity. However, this model is only from the perspective of the linear programming approach, i.e., two adjacent edges cannot share the same endpoint.

Further, [87] proposed the conflict set graph concept to characterize and measure the interference degree. The fundamental difference between our CSLG and the conflict graph of [87] is that our CSLG model schedules the locations to the movable nodes, while [87] concentrated on allocating the number of slot times to each link. Compared with [54], [87], CSLG considers the conflict condition based on SINR according to different locations. Hence, in order to incorporate interference and obtain the bound range, we define the conflict graph as follows:

Definition 3 (Conflict set of locations graph (CSLG)): Within the limited circle space C, we define the accessible profiles of locations for movable nodes $\boldsymbol{M}\left(\boldsymbol{\rho}_m,\ \boldsymbol{\Theta}_m\right)$ as $\Omega = \left\{\tau_1, \tau_2, \tau_3, ..., \tau_{\lfloor \pi R_c^2 \rfloor}\right\}$, then $m_i\left(\tau_i\right)$ denotes that node m_i is at location τ_i. Movable nodes by assigning locations with fixed nodes together form a communication graph as $G_p = (V, E)$, where V is the set of movable nodes, $m_i\left(\tau_i\right) \in V$, and edge E denote the existence of a communication link between two vertices.

- A conflict set of positions graph (CSLG) $\mathscr{G}\left(\mathcal{V}, \mathcal{E}\right)$, where the set of vertices $\mathcal{V}$ denotes the links in the communication graph G_p, and the edge $\mathcal{E}$ means that if two vertices conflict with each other, then they can be connected by an edge. Concerning the edge $\mathcal{E}$, the conflict property is present.

- Conflict: Let $\xi \subset \mathcal{V}$ denote a set of vertices, given a vertex l such that $l \notin \xi$, ξ is a conflict set of vertex l if and only if $\mathcal{C}_l = \{\xi \,|\text{SINR}_l\left(\xi \cup \{l\}\right) < \beta\ , \text{SINR}_l\left(\xi\right) \geqslant \beta\}$, where $\mathcal{C}_l$ is the collection of conflict sets at one of location assembles Ω.

Revisiting MINLNCP's limitation in (4.16), we can assert that the ideal situation for movable nodes is that there exists no location conflict that makes each node's SINR less than the threshold. In other words, it could make $\underset{\boldsymbol{M}(\boldsymbol{\rho}_m,\, \boldsymbol{\Theta}_m)\to\boldsymbol{M}^*(\boldsymbol{\rho}_m,\, \boldsymbol{\Theta}_m)}{P_r\left\{\gamma_{f_i,f_{i+1}} \geqslant \beta\right\}} \equiv 1$, $\underset{\boldsymbol{M}(\boldsymbol{\rho}_m,\, \boldsymbol{\Theta}_m)\to\boldsymbol{M}^*(\boldsymbol{\rho}_m,\, \boldsymbol{\Theta}_m)}{P_r\left\{\gamma_{f_i,m_i} \geqslant \beta\right\}} \equiv 1$ and $\underset{\boldsymbol{M}(\boldsymbol{\rho}_m,\, \boldsymbol{\Theta}_m)\to\boldsymbol{M}^*(\boldsymbol{\rho}_m,\, \boldsymbol{\Theta}_m)}{P_r\left\{\gamma_{m_i,f_{i+1}} \geqslant \beta\right\}} \equiv 1$ valid in this case. Therefore, the concept is transferred to the conflict graph corresponding to the proposition that there are no occurring edges for each vertex in CSLG. The domain of lower bound can be defined as follows.

Proposition 1: An allocation composed of assembles of locations is feasible for the lower bound if and only if the following condition is satisfied:

- There's no link between arbitrary two vertices for the set of positions assigned to movable nodes, i.e., no edges exist in $\mathscr{G}\left(\mathcal{V}, \mathcal{E}\right)$. For $\forall v_1 \subset \mathcal{V}$, $\forall v_2 \subset \mathcal{V}$,

$$\mathcal{I} = \{v_1, v_2 \,|\text{SINR}\left(v_1, v_2\right) \geqslant \beta, v_1 \nrightarrow v_2\} \tag{4.18}$$

Proof. The lower bound can be obtained by searching all of the feasible locations for movable nodes satisfying the SINR larger than threshold β. Mapping to the CSLG means that the in-degree and out-degree of vertices in the CSLG are both zero. Then, there's no link, and edges exist in $\mathscr{G}\left(\mathcal{V}, \mathcal{E}\right)$. □

Proposition 2: The range for D_L satisfies the following inequality,

$$\begin{aligned} D_L &< \left(D_L\right)_{\max} \\ \left(D_L\right)_{\max} &= \frac{\varphi\left(\boldsymbol{l}_{f_i,f_{i+1}}\right)\beta^{\frac{1}{4}}}{|M|\left(|M|-1\right)-\beta^{\frac{1}{4}}} \end{aligned} \tag{4.19}$$

Proof. For the node m_i, the interference-to-signal ratio (ISR) can be expressed as

$$\begin{aligned} \text{ISR} &= \frac{\sum_{k=1}^{|F|-1} P_{tx} K \left(\frac{l_{f_k,f_{i+1}}}{20}\right)^{-4} + \sum_{j=1,\, j\neq i}^{|M|-1} P_{tx} K \left(\frac{\Phi 3(m_i,m_j)}{20}\right)^{-4}}{P_{tx} K \left(\frac{\Phi 1(f_i,m_i)}{20}\right)^{-4}} \\ &\leqslant \left[\frac{\sum_{k=1}^{|F|-1} \Phi 2\left(f_k, m_i\right) + \sum_{j=1,\, j\neq i}^{|M|-1} \Phi 3\left(m_i, m_j\right)}{\Phi 1\left(f_i, m_i\right)}\right]^{-4} \end{aligned} \tag{4.20}$$

In order to ensure that transmit without conflict, ISR $> \frac{1}{\beta}$, then we have

$$\sum_{j=1,\, j\neq i}^{|M|-1} \Phi 3\left(m_i, m_j\right) < \Phi 1\left(f_i, m_i\right) \beta^{\frac{1}{4}} - \sum_{k=1}^{|F|-1} \Phi 2\left(f_k, m_i\right) \tag{4.21}$$

$$\frac{|M|\left(|M|-1\right)}{2} \arg\min\left\{\Phi 3\left(m_i, m_j\right)\right\} \leqslant \sum_{j=1,\, j\neq i}^{|M|-1} \Phi 3\left(m_i, m_j\right) \tag{4.22}$$

Due to $\Phi 1\left(f_i, m_i\right) - \Phi 2\left(f_i, m_i\right) < \varphi\left(\boldsymbol{l}_{f_i,f_{i+1}}\right)$, then the equality implies

$$\sum_{k=1}^{|F|-1} \left[\Phi 1\left(f_i, m_i\right) - \Phi 2\left(f_i, m_i\right)\right] < \sum_{k=1,\, k\neq i}^{|F|-2} \varphi\left(\boldsymbol{l}_{f_i,f_{i+1}}\right) \tag{4.23}$$

Since $\Phi 1\left(f_i, m_i\right) - \Phi 2\left(f_i, m_i\right) < \varphi\left(\boldsymbol{l}_{f_i,f_{i+1}}\right)$ and $D_L \leqslant \arg\min\left\{\Phi 2\left(f_i, m_i\right)\right\}$, D_L can be derived as

$$D_L < \frac{\varphi\left(\boldsymbol{l}_{f_i,f_{i+1}}\right) \beta^{\frac{1}{4}}}{|M|\left(|M|-1\right) - \beta^{\frac{1}{4}}} \tag{4.24}$$

□

Remark 4.3.1. *The lower bound comes from the necessary condition: even though there exist interferences among nodes in the communication graph, the optimal location in the lower bound can guarantee SINR for each node larger than the threshold, i.e., no edges in CSLG. For allocation locations to movable nodes, the domain can be repeated search from 0 to* $\left(D_L\right)_{\max}$ *until any two vertices have no edges in CSLG. The lower bound calculation can be executed iteratively as Algorithm 3.*

4.3.3 Upper bound

Under extreme scenarios, we sometimes cannot discover the optimal location in the lower bound due to the limitations of moving conditions or noise influence; that is, an outage can occur. Then, we characterize this status that there exist location conflicts that make SINR of someone less than the threshold, i.e., the edges can be allowed in CSLG. It implies that the prerequisite of finding the optimal location for maximum throughput is to ensure two

Algorithm 3: Lower bound calculation

input: Communication graph $G_p = (V, E)$, Geographical information of fixed nodes $\varphi\left(\boldsymbol{l}_{f_i,f_{i+1}}\right)$, $(D_L)_{\max}$.
output: $\mathcal{G}_{Lower}$.
for $D_L = 0$ to $(D_L)_{\max}$ **do**
$\mathcal{G} \leftarrow G_p$ generates the domain of movable nodes locations.
$\mathscr{G} \leftarrow G_p$integrates each link as a dot.
    for arbitrary two vertices in $\mathscr{G}$, $v_1 \subset \mathcal{V}$, $v_2 \subset \mathcal{V}$ **do**
    $\mathcal{I} = \{v_1, v_2 \,|\text{SINR}\,(v_1, v_2) < \beta, v_1 \to v_2\}$
        if $\mathcal{I} = \oslash$
            then $\mathcal{G}_{Lower} \leftarrow \mathcal{G}$
        else
        $D_L = D_L + \Delta D_L$, $\Delta D_L = \frac{(D_L)_{\max}}{|M|}$
        end if
    end for
end for
return $\mathcal{G}_{Lower}$

aspects. On one hand, it is necessary to ensure the normal transmission of each DF link. On the other hand, we also need to minimize the number of conflicting nodes in the conflict graph. The domain of the upper bound could be designated as follows.

Proposition 3: An allocation composed of assembles of locations $\Omega = \left\{\tau_1, \tau_2, \tau_3, ..., \tau_{\lfloor \pi R_c^2 \rfloor}\right\}$ is feasible for the upper bound if and only if the following condition is satisfied:

- For the set of positions assigned to movable nodes, the upstream and downstream links that contain the public nodes cannot influence each other in the communication graph G_p. Assume the three connection nodes in the DF link, $\forall v_1 \subset V$, $\forall v_2 \subset V$, $\forall v_3 \subset V$ in $G_p = (V, E)$, the vertices can be denoted as $v_1v_2 \in \mathcal{V}$, $v_1v_3 \in \mathcal{V}$, and $v_2v_3 \in \mathcal{V}$ in $\mathscr{G}$ respectively. Then, there's no vertices $v_i \subset V$ that make v_1v_i, v_2v_i and v_3v_i such that

$$\begin{aligned}
\mathcal{U} &= \{v_1v_i, v_2v_i, v_3v_i \,|\boldsymbol{U} \neq \oslash\} \\
\boldsymbol{U} &= \{u1 < \beta\} \ \wedge \{u2 < \beta\} \wedge \ \{u3 < \beta\} \\
u1 &= \text{SINR}\,(v_1v_2, v_1v_i) \\
u2 &= \text{SINR}\,(v_2v_3, v_2v_i) \\
u3 &= \text{SINR}\,(v_1v_3, v_3v_i)
\end{aligned} \tag{4.25}$$

Proof. According to the DF protocol, the premise for smooth transmission is that the DF upstream and downstream communications do not conflict with each other; that is, they can be transmitted simultaneously. Because if they are conflicting, it will produce data congestion, resulting in a sharp decrease in throughput. Hence, note that the upper bound means that there exist edges in CSLG $\mathscr{G}$, but should ensure that DF transmits smoothly. Indeed, the principle of obtaining an optimal location in the upper bound is that the less conflict, the

better. The reason is that the more conflicting edges, the stronger the interference. Hence, we should minimize the number of vertices that are not included in the adjacent DF links. □

Proposition 4: The range for D_U satisfies

$$\begin{aligned}
&(D_U)_{\min} \leqslant D_U \leqslant (D_U)_{\max} \\
&(D_U)_{\max} = \frac{\sqrt{2}}{\sqrt{2\left|M\right|+1}-1} R_c \\
&(D_U)_{\min} = \arg\max \left\{ 20\left[\frac{P_{tx}K}{N_0}\left(\frac{1}{\beta}-20\right)\right]^{-\frac{1}{4}}, \varrho 1 \right\}
\end{aligned} \tag{4.26}$$

Proof. Consider the fixed and movable nodes connect to form a large lattice, which is located in the limited circle. Let each side of lattice has n nodes, $(n+1)^2 \geqslant 2\left|M\right|+1$, which means the lattice contains all the nodes sets. The maximal side length of this lattice is $\sqrt{2}R_c$, then $nD_U \leqslant \sqrt{2}R_c$. We can derive that $D_U \leqslant \sqrt{2}\frac{R_c}{n} \leqslant R_c \frac{\sqrt{2}}{\sqrt{2|M|+1}-1}$.

It should guarantee that the SINR for DF transmission both $\gamma_{f_i,f_{i+1}}$ and $\gamma_{m_i,f_{i+1}}$ are larger than the threshold, then we can obtain

$$\frac{N_0}{P_{tx}K}\left(\frac{\varphi\left(\boldsymbol{l}_{f_i,f_{i+1}}\right)}{20}\right)^4 + \sum_{k=i-1,\,k\neq i}^{i+1}\left(\frac{\varphi\left(\boldsymbol{l}_{f_i,f_{i+1}}\right)}{\varphi\left(\boldsymbol{l}_{f_k,f_{i+1}}\right)}\right)^4 + \sum_{k=i-1,\,k\neq i}^{i+1}\left(\frac{\varphi\left(\boldsymbol{l}_{f_i,f_{i+1}}\right)}{\Phi 2\left(f_{i+1},m_k\right)}\right)^4 \leqslant \frac{1}{\beta} \tag{4.27}$$

$$\frac{N_0}{P_{tx}K}\left(\frac{\Phi 2\left(f_{i+1},m_i\right)}{20}\right)^4 + \sum_{k=i-1,\,k\neq i}^{i+1}\left(\frac{\Phi 2\left(f_{i+1},m_i\right)}{\varphi\left(\boldsymbol{l}_{f_k,f_{i+1}}\right)}\right)^4 + \sum_{j=i-1,\,j\neq i}^{i+1}\left(\frac{\Phi 2\left(f_{i+1},m_i\right)}{\Phi 2\left(f_{i+1},m_j\right)}\right)^4 \leqslant \frac{1}{\beta} \tag{4.28}$$

Since $\Phi 2\left(f_{i+1},m_k\right) \leqslant \arg\max\left\{\Phi 2\left(f_{i+1},m_k\right)\right\}$, we simplify (4.27) and (4.28) to derive as

$$\begin{aligned}
&\varrho 1 \leqslant \arg\max\left\{\Phi 2\left(f_{i+1},m_k\right)\right\} \leqslant \varrho 2, \\
&\varrho 1 \triangleq \varphi\left(\boldsymbol{l}_{f_i,f_{i+1}}\right)\left\{\frac{1}{2}\left[\frac{1}{\beta}-\left(\frac{N_0}{P_{tx}K}\left(\frac{\varphi\left(\boldsymbol{l}_{f_i,f_{i+1}}\right)}{20}\right)^4+\left(\frac{\varphi\left(\boldsymbol{l}_{f_i,f_{i+1}}\right)}{\varphi\left(\boldsymbol{l}_{f_{i-1},f_{i+1}}\right)}\right)^4+\left(\frac{\varphi\left(\boldsymbol{l}_{f_i,f_{i+1}}\right)}{\varphi\left(\boldsymbol{l}_{f_{i+1},f_{i+1}}\right)}\right)^4\right)\right]\right\}^{-\frac{1}{4}} \\
&\varrho 2 \triangleq \left(\frac{1}{\beta}-2\right)\left[\frac{N_0}{P_{tx}K}\left(\frac{1}{20}\right)^4+\frac{2}{\varphi\left(\boldsymbol{l}_{f_i,f_{i+1}}\right)^4}\right]^{-\frac{1}{4}}
\end{aligned} \tag{4.29}$$

Consider γ_{f_i,m_i} also satisfies the above rule, it can be derived as follows,

$$\frac{N_0}{P_{tx}K}\left(\frac{\Phi 1\left(f_i,m_i\right)}{20}\right)^4 + \sum_{k=i-1,\,k\neq i}^{i+1}\left(\frac{\Phi 1\left(f_i,m_i\right)}{\Phi 1\left(f_k,m_i\right)}\right)^4 + \sum_{j=i+1,\,j\neq i}^{i-1}\left(\frac{\Phi 1\left(f_i,m_i\right)}{\Phi 3\left(m_i,m_j\right)}\right)^4 \leqslant \frac{1}{\beta} \tag{4.30}$$

then we obtain

$$20\left[\frac{P_{tx}K}{N_0}\left(\frac{1}{\beta}-20\right)\right]^{-\frac{1}{4}} \leqslant \arg\max\left\{\ \Phi 1\left(f_i,m_i\right),\Phi 3\left(m_i,m_j\right)\ \right\} \tag{4.31}$$

Due to $D_U \geqslant \arg\max\left\{\Phi 2\left(f_{i+1},m_k\right)\right\}$ and $D_U \geqslant \arg\max\left\{\Phi 1\left(f_i,m_i\right),\Phi 3\left(m_i,m_j\right)\right\}$, hence, D_U can be derived as

$$D_U \geqslant \arg\max\left\{\ 20\left[\frac{P_{tx}K}{N_0}\left(\frac{1}{\beta}-20\right)\right]^{-\frac{1}{4}},\varrho 1\right\} \tag{4.32}$$

□

Remark 4.3.2. *As for the upper bound, it must be ensured that adjacent DF links cannot conflict, i.e., there are no edges between each adjacent DF vertices in CSLG. In addition, we update $\mathcal{G}$ by minimizing the number of conflict vertices that are not comprised in the neighboring DF links. As illustrated in Algorithm 4, the upper bound calculation can be executed iteratively.*

Algorithm 4: Upper bound calculation

input: Communication graph $G_p=(V,E)$, Geographical information of fixed nodes $\varphi\left(\boldsymbol{l}_{f_i,f_{i+1}}\right)$, $\left(D_U\right)_{\min}$ and $\left(D_U\right)_{\max}$.
output: $\mathcal{G}_{Upper}$.
for $D_U=\left(D_U\right)_{\min}$ to $\left(D_U\right)_{\max}$ **do**
$\mathcal{G} \leftarrow G_p$ generates the domain of movable nodes locations.
$\mathscr{G} \leftarrow G_p$integrates each link as a dot.
    for $\forall v_1 \subset V, \forall v_2 \subset V, \forall v_3 \subset V$ in a DF link at G_p **do**
    Generate vertices in $\mathscr{G}$, $v_1v_2 \in \mathcal{V}$, $v_1v_3 \in \mathcal{V}$ and $v_2v_3 \in \mathcal{V}$
        if $\exists v_i \subset V$ make v_1v_i, v_2v_i and v_3v_i such that
        $\{u1<\beta\}\ \wedge\{u2<\beta\}\wedge\ \{u3<\beta\} \neq \oslash$
            then
            $D_U = D_U + \Delta D_U$,
            $\Delta D_U = \frac{\left(D_U\right)_{\max}-\left(D_U\right)_{\min}}{|M|}$,
            $\min\left\{\sum_{v_i} i\right\}$
        else $\mathcal{G}_{Upper} \leftarrow \mathcal{G}$
        end if
    end for
end for
return $\mathcal{G}_{Upper}$

In summary, we present the upper and lower bound range and calculation algorithm. It is convenient to estimate and search the optimal locations of movable nodes for best throughput. In the next section, we propose a new algorithm, the Maximum Throughput algorithm for Optimal Position (MTOP), based on the upper and lower bounds to determine the optimal

locations. Besides, we also introduce several conventional algorithms or proposed methods as a comparison.

4.4 MTOP algorithm and conventional method

4.4.1 Maximum throughput algorithm for optimal position

Proposition 5: The optimal locations $\boldsymbol{M}^*(\boldsymbol{\rho}_m,\ \boldsymbol{\Theta}_m)$ of movable nodes $m_i \in \mathcal{M}$ for the best throughput Th^*_{sys} must be located at the scope of the upper bound $\mathcal{G}_{Upper}$ and lower bound $\mathcal{G}_{Lower}$ areas.

Proof. As stated in (4.16), the limitation factors indicate that the range of domain $\mathcal{G}$ should guarantee the transmission protocol regular operation. From the physical interference perspective, the SINR for fixed and movable nodes should be larger than the threshold β. If the link can transfer without conflict, i.e., there are no edges in CSLG, it must satisfy the requirement of SINR. On the other hand, from the protocol interference viewpoint, Euclidean distance between transceivers should be no less than the interference range and be no more than the communication range. If the upstream and downstream links that contain the public nodes cannot influence each other, then transmission data by the DF link is satisfied. All in all, the upper bound $\mathcal{G}_{Upper}$ meets the slight restrictions of (4.16). Moreover, the lower bound $\mathcal{G}_{Lower}$ satisfies the severe restrictions. Thus, the optimal locations for system throughput must be located at a range of the upper bound $\mathcal{G}_{Upper}$ and lower bound $\mathcal{G}_{Lower}$ areas. □

Remark 4.4.3. *The optimal locations for movable nodes within the range of $\mathcal{G}_{Upper}$ and $\mathcal{G}_{Lower}$ can significantly reduce the search coverage. From this, we propose a new heuristic algorithm based on the upper and lower bounds, called Maximum Throughput algorithm for Optimal Position (MTOP), which is clarified in Algorithm 5.*

We describe the MTOP algorithm for constructing a feasible location-allocation as below. In phase 1 (line 3-6), it initializes system throughput and optimal location. Specifically, the MTOP performs proposing algorithms to calculate the upper and lower bound values. In phase 2 (line 7-26), it generates initial locations by randomly selected in the $\mathcal{G}$, and then refer to simulated annealing algorithm [89] to determine the optimal locations $\boldsymbol{M}_{\mathcal{G}}$ for each $\mathcal{G}$. Here, we set the initial temperature T_{int} as 1000 to maintain accuracy, and configure the number of iterations κ as 100 considering the computation cost.

Finally, in phase 3 (line 25-38), with the search area slowly expanding, it compares old and new throughput values that are newly generated from optimal locations. If the new throughput is larger than the old value, it updates the optimal throughput and continues to expand the search range $\mathcal{G}$, where we define $\Delta\mathcal{G}$ as a per expansion area. Otherwise, it is out of the loop and no longer enlarges $\mathcal{G}$. There are two reasons as follows: i) considering the expansion of the search range and computing costs rising sharply, we make a trade-off

Algorithm 5: Maximum Throughput algorithm for Optimal Position

input: Geographical information of fixed nodes $\varphi\left(\boldsymbol{l}_{f_i,f_{i+1}}\right)$
output: Optimal locations $\boldsymbol{M}^*$, Maximal throughput Th^*_{sys}
$\mathcal{G}_{Lower} \leftarrow \varphi\left(\boldsymbol{l}_{f_i,f_{i+1}}\right)$ execute **Algorithm 3**.
$\mathcal{G}_{Upper} \leftarrow \varphi\left(\boldsymbol{l}_{f_i,f_{i+1}}\right)$ execute **Algorithm 4**.
Initialize throughput solution $Th_{sys} = 0$.
Initialize optimal location $\boldsymbol{M}^* = \oslash$.
for $\mathcal{G} = \mathcal{G}_{Lower}$ to $\mathcal{G}_{Upper}$ **do**
$\boldsymbol{M}_{\mathcal{G}} \leftarrow \boldsymbol{M}$ Generate initial locations by movable nodes randomly selecting in $\mathcal{G}$.
Set initial status S, temperature $T_{int} = 1000$, $T_{\min} = 1$.
    for $T = T_{int}$ to $T_{\min}$ **do**
        for $\kappa = 1$ to 100 **do**
Generate a new position allocation $\boldsymbol{M}_{new} = \boldsymbol{M} + \Delta\boldsymbol{M}$, where $\Delta\boldsymbol{M}$ is the new location $\mathcal{G}$.
            $\Delta Th_{sys} = Th_{sys}\left(\boldsymbol{M}_{new}\right) - Th_{sys}\left(\boldsymbol{M}\right)$
Compute acceptance probability $\Upsilon = \exp\left(\frac{\Delta Th_{sys}}{T}\right)$.
            Draw a random value $\psi \in [0,1]$.
                if $\psi < \Upsilon$ **then** $\boldsymbol{M} \leftarrow \boldsymbol{M}_{new}$, $\kappa = \kappa + 1$
                    else
                Update $\boldsymbol{M} \leftarrow \boldsymbol{M}$.
    Update temperature parameter $T \leftarrow T - 0.001 \times T$.
                end if
                if $Th_{sys}\left(\boldsymbol{M}_{\mathcal{G}}\right) < Th_{sys}\left(\boldsymbol{M}\right)$ **then**
                  Update $\boldsymbol{M}_{\mathcal{G}} \leftarrow \boldsymbol{M}$.
                end if
            end for
    end for
return $\boldsymbol{M}_{\mathcal{G}}$
    if $Th_{sys}\left(\boldsymbol{M}_{\mathcal{G}}\right) > Th_{sys}\left(\boldsymbol{M}^*\right)$ **then**
      $\Delta D = \frac{D_{\max} - D_{\min}}{|M|}$
      $\Delta\mathcal{G} \leftarrow \Delta D$
      $\mathcal{G} = \mathcal{G} + \Delta\mathcal{G}$
      $\boldsymbol{M}^* \leftarrow \boldsymbol{M}_{\mathcal{G}}$
      $Th_{sys} \leftarrow Th_{sys}\left(\boldsymbol{M}_{\mathcal{G}}\right)$
    else break;
    end if
end for
return $\boldsymbol{M}^*\left(\boldsymbol{\rho}_m,\ \boldsymbol{\Theta}_m\right)$
Construct locations allocation: allocate the optimal locations for all movable nodes $m_i \in \mathcal{M}$ according to $\boldsymbol{M}^*\left(\boldsymbol{\rho}_m,\ \boldsymbol{\Theta}_m\right)$.
return Th^*_{sys}

to ensure lowest complexity and highest accuracy; ii) the lower bound we derived could guarantee that the optimal value with a high probability locate within its range. In that case, the worst case is that the search area is expanded until it reaches $\mathcal{G}_{Upper}$. Obviously, compared with searching directly in the upper bound range, MTOP ensures the accuracy with the lowest computational cost.

If there are no movable nodes between fixed nodes, our proposed algorithm (MTOP) will not be executed. In addition, we do not specify node types because there are already many predefined fixed and movable nodes in this model, i.e., we do not need to select and assign which nodes are fixed or movable. In this research, we care about moving these movable nodes at the given PPP distribution case of nodes. If there are more than one movable nodes in the same location, then the selection strategy is based on social routing with the MTOP. If several users are satisfied according to social routing, then choosing one of them will not affect the result. Because according to the harmonic mean method, the best result can be achieved by selecting one of the users as the relay.

4.4.2 Conventional method

Many conventional heuristic algorithms estimate and attain approximate optimum or suboptimum for dealing with NP-hard problems. Specifically, simulated annealing (SA) is an effective and general algorithm for solving NP-hard problems, widely applied in engineering optimization problems. The SA algorithm starts from a specific high initial temperature. It continues to iterate with the continuous decline in temperature parameters until the optimal solution is found by setting termination conditions [88]. During each cooling iteration, the Metropolis criterion is used to determine whether or not to accept the new solution as the optimal solution. However, the SA algorithm obtains the optimal solution concerning the Metropolis criterion [89].

In many cases, the optimal solution is unstable. In other words, a suboptimal solution is often found out as a result. Essentially, SA is a stochastic optimization algorithm based on the Monte Carlo iteration strategy to be treated as a comparison with the performance of our proposed MTOP.

In our previous work [34], we proposed an interaction position game (IPG) and investigated the Spatial Adaptive Play (SAP) algorithm to work out the optimum. In this game, we employ cooperative behavior among movable nodes instead of assuming selfishness as the traditional game model. Compared with the SA algorithm, this game theory method could achieve lower computation cost and higher throughput performance. Nevertheless, the SAP algorithm costs excessive communication overhead. In practical application, the SAP's overhead and computation costs are not in line with actual current traffic and do not meet users' requirements. Some researchers proposed an intuitive method to be close to engineering applications: the helper node moves to the middle position between the transmitter and receiver in a link. It has been verified in [91], [33], to be capable of improving through-

put in one movable node system. However, the throughput performance of this method is insufficient in the multi-user mobility communication system. Thus, we compare the SAP algorithm and intuitive method with MTOP to interpret the performance variance.

Overall, in the next simulation results section, we compare the performance of the following algorithms:

(1) Intuitive Method (IM) [91], [33].

(2) Simulated Annealing (SA) [89].

(3) SAP algorithm of IPG (SAP) [34].

(4) Maximum Throughput algorithm for Optimal Position (MTOP).

(5) Exhaustive global search (ESG).

4.5 Simulation and numerical results

4.5.1 Simulation scenario

In our simulation experiments, we set the radius R_c of limited circle space as 150m for matching with real-life scenarios, such as high-traffic malls, parks, or squares. Each movable node has four directions (east, west, south, and north) to move, and the per-unit step is 1m. We define the mobility speed as 1.5 m/s, which is the ordinary pedestrians' average speed without generality loss. Our approach aims to find the best locations by the MTOP algorithm for movable nodes to maximize system throughput. Thus, different mobility speeds alter no more than the convergence time to achieve the optimum. In other words, mobility speed only changes the time for movable nodes to reach the optimal location, but it does not influence the throughput performance results.

λ, which is the average number of fixed nodes per unit area, i.e., a parameter for the degree of sparsity, impacts system throughput [81]. The number of fixed nodes $|F|$ is twice the number of movable nodes $|M|$, $|F| = 2\,|M|$. As $\lambda = 1.5 \times 10^{-4}$, $|F| = 10$, $|M| = 5$, and as $\lambda = 7 \times 10^{-4}$, $|F| = 50$, $|M| = 25$, respectively. We simulate the different values of $|F|$ and $|M|$ to evaluate these algorithms' performance.

Concerning the wireless communication configuration, we employ IEEE 802.11g as the communication standard and UDP as a transmission protocol in NS3. We set the path loss exponent as 4.00 due to the shadowing effect, and the wave frequency as 2.4 GHz. To verify the different performances of different SINR thresholds for these algorithms, thus we set two values, 24.56 dB and 10.79 dB [90]. The detailed parameter configuration is given in Table 4.3.

Table 4.4 Parameter values for simulation.

Parameters	Value
Radius of limited circle space, R_c	150 m
Communication Standard	IEEE 802.11g
Transport Protocol	UDP
Path loss Exponent (α)	4.00
Mobility Speed	1.5 m/s
Maximum transmission power	10 dBm
White Gaussian Noise (N_0)	-90 dBm
Wave Frequency	2.4 GHz
Bandwidth	2 MHz
SINR threshold (β)	24.56 dB, 10.79 dB
Number of fixed nodes ($\|F\|$)	10, 50
Number of movable nodes ($\|M\|$)	5, 25

4.5.2 System throughput

We first verify the distribution of positions of fixed nodes with different Poisson densities. Fig. 4.4(a) and Fig. 4.4(b) illustrate sparse distribution at the different number of fixed users, $|F| = 10$, $|F| = 50$. By comparing these two figures, we can see that the smaller the value of $|F|$, the sparser the distribution of fixed nodes. In addition, there are some fixed nodes around AP (red triangle), and the nodes far away from AP increase with the number of nodes. This indicates that our preset expectation function $E\left[\boldsymbol{l}_{f_i,f_j}\right]$ is fixed and computable in (4.4). From this, the geographical distance information of fixed nodes $\varphi\left(\boldsymbol{l}_{f_i,f_{i+1}}\right)$ also can be calculated.

In the following throughput comparison figures, the X-axis denotes the number of iterations, and the Y-axis denotes the system throughput values. We compare the throughput performance of five algorithms, which contains MTOP, SAP, SA, IM, and ESG, under different $|F|$ and $|M|$ in Fig. 4.5. It can be noted that the performance curves, both IM and ESG, are all straight lines. For IM, the positions of movable nodes are located at the middle position between each transceiver, so the number of iterations is just one. Regard to ESG, we only perform a global search once and do not care how it loops internally. Therefore, the throughput remains unchanged after one iteration.

We can note that the execution of MTOP can obtain the best throughput value that is close to that of exhaustive global search (ESG) in these two figures. The optimal obtained by MTOP is theoretically expected to be equal to the ESG value. However, since MTOP has numerical round-off errors during the iterations of the simulation, the figure shows the approximation to the ESG value. By analyzing the throughput value, the highest throughput by execution MTOP is 2.51 Mbps that occurred in Fig. 4.5(a) as $|M| = 5$, $|F| = 10$. The reasons are as follows: i) lower throughput benefits would be attained through cooperative

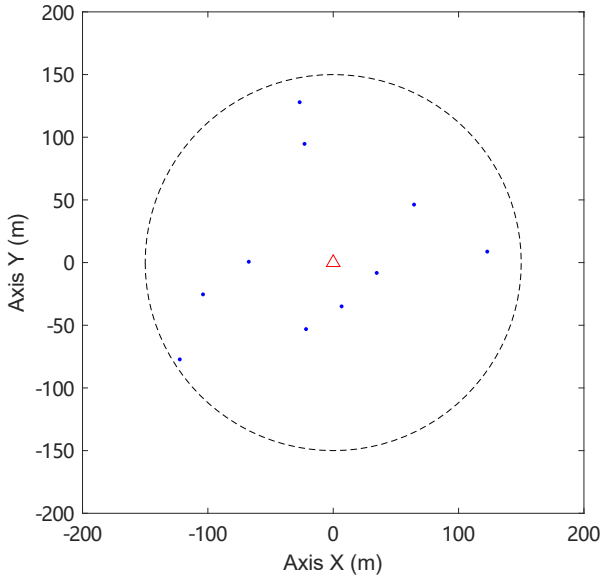

(a)

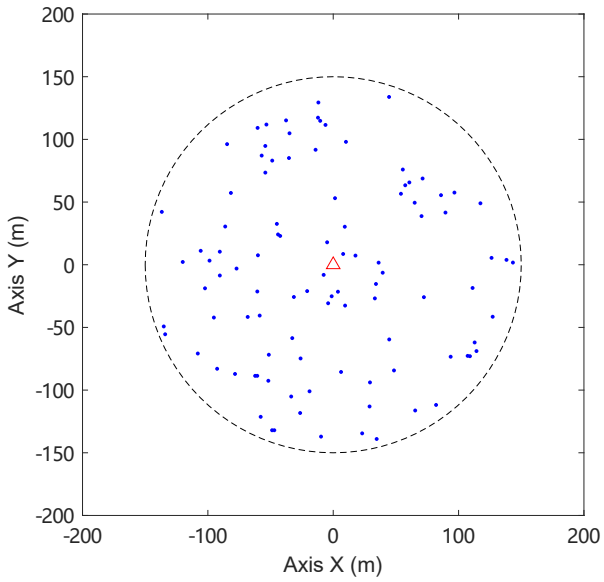

(b)

Fig. 4.4 The positions of fixed nodes obey a Poisson point process (PPP) in the circle with different $|F|$ values: (a) $|F| = 10$; (b) $|F| = 50$.

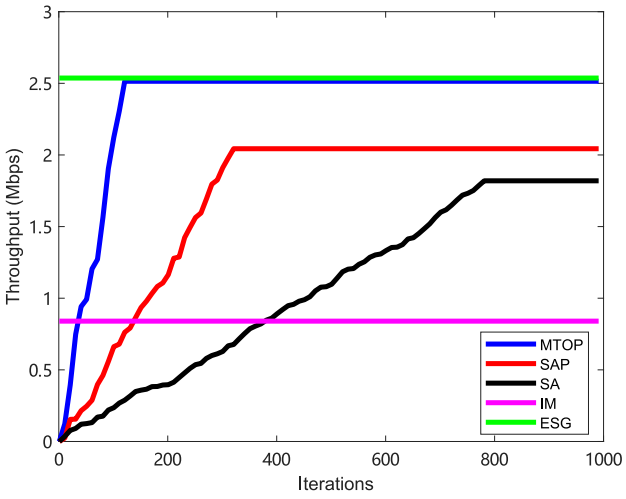

(a)

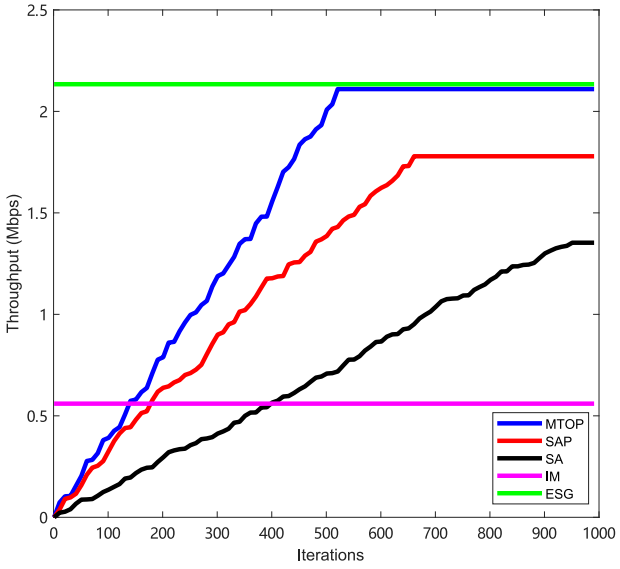

(b)

Fig. 4.5 MTOP, SAP, SA, IM, and ESG under different $|M|$ and $|F|$ with β=24.56 dB: (a) $|M| = 5$, $|F| = 10$; (b) $|M| = 25$, $|F| = 50$.

mobility due to larger multi-hops and interference, which are caused by larger number of nodes; ii) the harmonic value of system throughput ensures that the benefits are stable when the proportion between fixed and movable nodes unchanged. We also note that the performance of SAP is lower than that of MTOP. The reason is that MTOP limits the range of the optimal solution to the upper and lower bounds of the derivation by partitioning, and then iterates over each small block to obtain the optimal solution. Compared with the game method of SAP, MTOP has the characteristics of fast search speed and greater accuracy in large-scale user scenarios, so its performance is better. Compared with IM, SA, and SAP, MTOP performs better than the former three algorithms and improves the maximum throughput ratio by 298.81%, 37.91%, and 23.04% in Fig. 4.5(a).

Moreover, the number of iterations MTOP is the smallest among these three algorithms (SA, SAP and MTOP). The number of iterations for all algorithms rise up as $|M|$ increases, because it should calculate more location options for movable nodes, and loops boost in MTOP algorithm operation. The minimum of number of iterations for MTOP is 120, and the minimum ratio of MTOP to SA and SAP is respectively, 37.5% and 15.38% in Fig. 4.5(a). Specifically, these two figures are summarized two key statements: i) the performance of MTOP is much better than SA and SAP in terms of throughput and iteration times; ii) the larger number of nodes would decrease the throughput and increase iteration times.

With the purpose of illuminating the effect of SINR, the throughput comparison of the MTOP algorithm under different $|F|$, $|M|$ and SINR is shown in Fig. 4.6. We simulate four cases to clarify the relationship between number of nodes and SINR threshold. This figure depicts that the best throughput performance is 2.51 Mbps as $|M| = 5$, $|F| = 10$, and $\beta = 24.56$ dB. The performance on throughput can be divided into four levels. The first and second level is as $|M| = 5$ and $|F| = 10$, because the small number of nodes and multi hops, the throughput attenuation and interference caused by performance anomaly are reduced, which makes the throughput larger.

As far as different SINR thresholds are concerned, it can be noted that the throughput of β as 24.56 dB is larger than that of β as 10.79 dB. Because the SINR sensed by the receiver must exceed the threshold β to transmit successfully; otherwise, it causes an outage. Then, if the SINR determination criterion is raised, the link can maintain a higher transmission rate. Therefore, the transmission rate with $\beta = 24.56$ dB is higher than that with $\beta = 10.79$ dB. The ratio of iteration numbers maximum to a minimum is 5.72. The larger of $|M|$ and $|F|$, the more iterations are required.

4.5.3 Computation cost

In this section, we evaluate the convergence behaviors with iteration numbers and computation cost in MTOP, SAP, and SA under different $|F|$ and $|M|$. The cumulative distribution function (CDF) of the iterations converging to the maximum is shown in Fig. 4.7. In this figure, X-axis denotes the number of iterations, and Y-axis denotes the CDF of convergence.

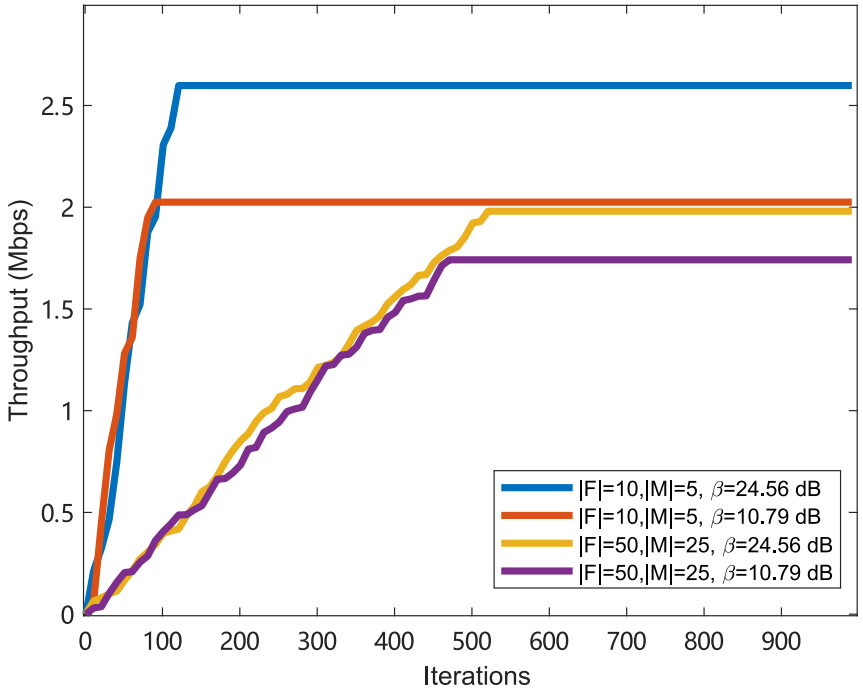

Fig. 4.6 The throughput comparison of MTOP algorithm under different $|F|$, $|M|$ and SINR.

Here, we set the SINR threshold for each receiver as 24.56 dB.

We can observe that the curve of convergence speed of MTOP ascends significantly more than the other two algorithms (SA and SAP) with the increment in the number of iterations. Notably, as the increment of $|F|$ and $|M|$, more iterations are needed to achieve convergence. The reason is that larger number of nodes would enlarge the computation of $\mathcal{G}_{Upper}$ and $\mathcal{G}_{Lower}$ for the MTOP algorithm with the number of fixed nodes increasing. In Fig. 4.7, compared with SAP and SA, the maximum convergence rate ratio of MTOP is increased by 2.63 and 4.80 times. With the growth of $|M|$, the gain of convergence rate from the MTOP algorithm is more noticeable. The detailed proof can be referred to as Lemma 2 in the analytical result section.

Turning to computation cost, the histogram Fig. 4.8 illustrates the comparison of completion time for MTOP, SAP, and SA under different $|F|$ and $|M|$. The CPU configuration of the simulation computer is Intel (R) core i7-8700 3.20 GHz. It is noted that MTOP costs the minimum completion time in these four cases compared with SAP and SA. The time complexity analysis and proof can be referred to as Lemma 1. The minimum completion time of MTOP is only 3.75 seconds and 7.838 seconds. For SAP, the completion time is 6.875 seconds and 18.38 seconds according to the X-axis order. Similarly, the completion time of SA is 11.88 seconds and 26.49 seconds respectively.

We can especially find that as the values of $|F|$ and $|M|$ scale up, the completion time ratio of SA and SAP to MTOP becomes increasingly higher. It means that the performance

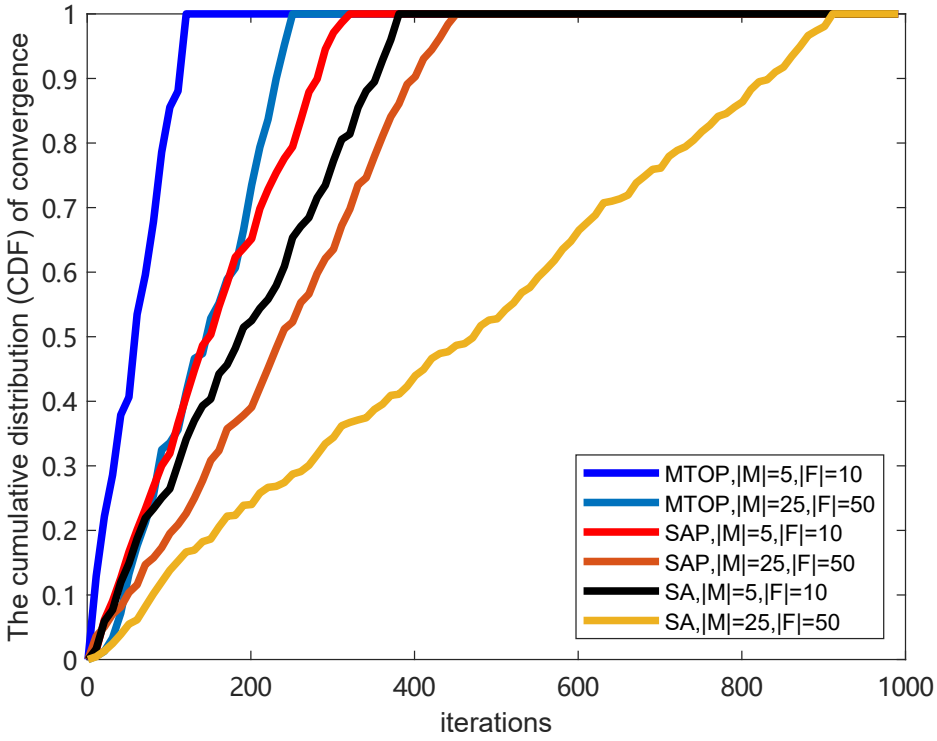

Fig. 4.7 Convergence speed of three algorithms (MTOP, SAP, SA) under different $|F|$ and $|M|$.

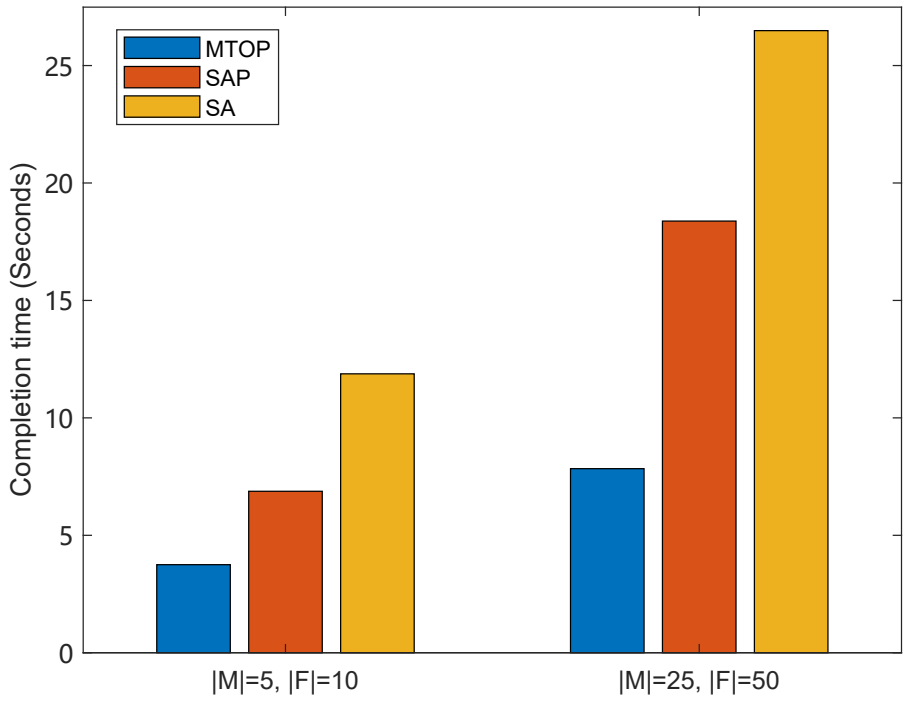

Fig. 4.8 The comparison of computation cost for three algorithms (MTOP, SAP, SA) under different $|F|$ and $|M|$.

benefit from the MTOP algorithm is more significant with the raising in the number of movable nodes $|M|$. According to the qualitative perspective analysis, this is because the search domain of valid and feasible locations diminishes after we execute lower and upper bounds. For the quantitative proof, please refer to Lemma 2. The result shows that compared with SAP and SA, MTOP algorithm reduces the most computation time by 44.12% and 237.97%, respectively, as $|M| = 25$, $|F| = 50$.

4.5.4 Overhead

In addition to deliberating the throughput performance and computation cost in the existing communication system, we also need to calculate the communication cost, i.e., communication overhead, in the process of algorithm execution. The comparison of communication overhead among MTOP, SAP, and SA is depicted in Fig. 4.9. In this figure, X-axis denotes the computation cost of the algorithms. Y-axis denotes the percentage of redundant data in total transmission data. We define the percentage of redundant data in total data as the evaluation index of overhead. In general, each packet contains redundant and valid data information. Redundant data refers to the center's control information, mobile users' location information, and mobile users' adequate policy information. The communication overhead is the sum of the redundant communication data during the entire algorithm execution. If the percentage is higher, the algorithm will consume more overhead. Hence, this value reflects the algorithm costs during the control center, executing algorithms.

Fig. 4.9 illuminates that the proportion of redundant information becomes smaller and smaller to zero during completion. For MTOP, the reason is that the strategies and locations information required by the algorithm is decreasing until $\mathcal{G}_{Upper}$ and $\mathcal{G}_{Lower}$ are finally calculated. Similarly, for SAP and SA, the required locations information continuously drops off until they achieve the global or local optimum.

In Fig. 4.9, we can detect that communication overhead represents the area around the curve and X-axis, which is the integration of curves. The communication overhead of MTOP, SAP, and SA is 18.916, 69.956, and 30.291. Then, it can be obtained that after three algorithms execution, the communication overhead of MTOP is 72.96% lower than SAP, and is 37.55% lower than SA. The reasons are following: i) MTOP reduces the search domain based on the upper and lower bounds, then the transmission data only contains slight geographical location information of fixed nodes; ii) for SAP, it should cover the opponent's available strategies and action information, and then meet Nash equilibrium; iii) for SA, it iterates under the defined temperature and the decision function. Therefore, MTOP only requires less redundant data than SAP and SA, resulting in less communication overhead to achieve optimal throughput performance.

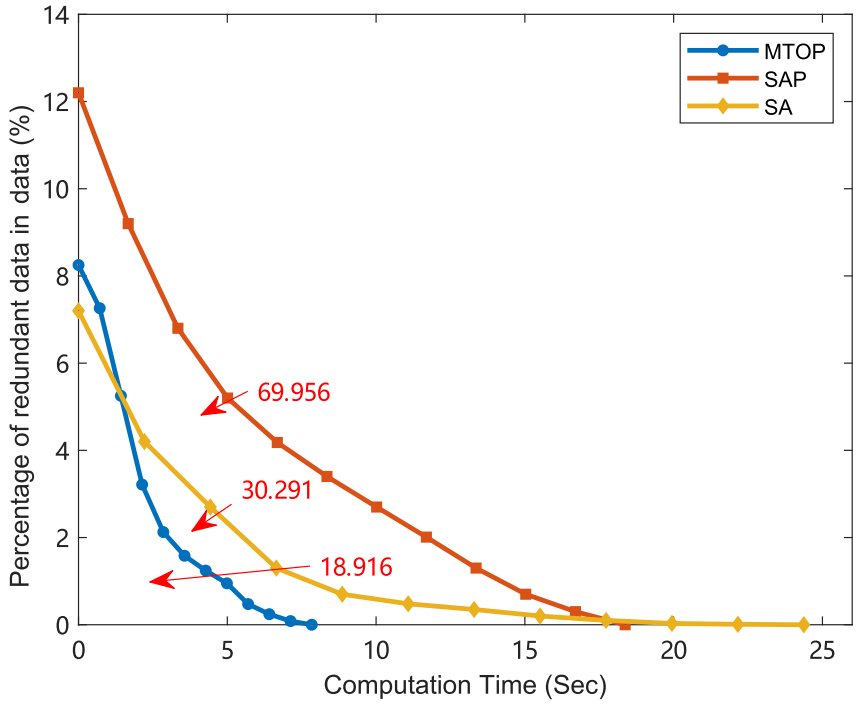

Fig. 4.9 The comparison of communication overhead among MTOP, SAP and SA with $|M| = 25$ and $|F| = 50$.

4.6 Analytical results

In this section, we quantitatively demonstrate the running time of SAP, SA, and MTOP through mathematical analysis. We derive and prove the following lemmas to verify and validate the correctness of the complexity simulation results.

Lemma 1: In terms of complexity, the running time for SAP, SA and MTOP are as follows:

- SAP: $O\left[|M|^2\left(R_c^{|M|}+R_c^2\right)\right]$
- SA: $O\left(10^5 \cdot R_c^{2|M|}\right)$
- MTOP: $O\left[\frac{1}{2}|M|^2\left(D_U^2+D_L^2\right)+|M|^2 R'^{|M|}\right]$

where R' is length parameter of the final domain, $D_L < R'^{<} D_U$ and $D_L < D_U < R_c$.

Proof. Refer to [26], the SAP algorithm exchanges and collects information about opponents' strategies. Each node calculates the utility function overall its available actions with strategies information received from opponents until Nash aquarium and the predefined iteration is reached. The time complexity of the SAP algorithm consists of two components, one is the iteration of the choice within the circle radius $O\left(|M|^2 R_c^{|M|}\right)$, and the other is the iteration of the individual nodes according to the range of the circle area $O\left(|M|^2 R_c^2\right)$. Therefore, the running time for SAP is $O\left[|M|^2\left(R_c^{|M|}+R_c^2\right)\right]$. As for the SA algorithm,

the complexity is $O\left[R_c^{2|M|}\left(T_{\max}-T_{\min}\right)^5\right]$, where $T_{\min}$ and $T_{\max}$ denote the maximum and minimum temperature, respectively. In our simulation, in order to guarantee the accuracy, we set the value of $\left(T_{\max}-T_{\min}\right)^5$ as 10^5. Hence, the time complexity of the SA algorithm is $O\left(10^5 \cdot R_c^{2|M|}\right)$.

Consider MTOP can be divided into three phases. In the first phase, the complexity of upper and lower bounds calculation is $O\left(\frac{1}{2}\left|M\right|^2 D_U^2\right)$ and $O\left(\frac{1}{2}\left|M\right|^2 D_L^2\right)$. In the second and third phases, the total complexity is $O\left(\left|M\right|^2 R'^{|M|}\right)$, where R' is length value which is related to the final domain. So, the time complexity is $O\left[\left(\frac{1}{2}\left|M\right|^2\left(D_U^2+D_L^2\right)+\left|M\right|^2 R'^{|M|}\right)\right]$. □

Lemma 2: The descending order of algorithm complexity is that SA $>$ SAP $>$ MTOP. In addition, with the increase in the number of movable nodes $|M|$, the performance benefit from MTOP algorithm is more obvious.

Proof. If $|M|=1$, the time complexity for these three algorithms are respectively, $O\left[\left(R_c+R_c^2\right)\right]$, $O\left(10^5 \cdot R_c^2\right)$ and $O\left[\left(\frac{1}{2}\left(D_U^2+D_L^2\right)+R'\right)\right]$. Because $D_L < R' < D_U$ and $D_L < D_U < R_c$, it is noticeable that the time complexity of MTOP is smallest, and the algorithmic complexity of SAP is much less than that of SA.

If $|M| \geqslant 2$, we define the complexity ratio as follows,

$$\begin{aligned}
\eta_1 &= \frac{O\left[\left|M\right|^2\left(R_c^{|M|}+R_c^2\right)\right]}{O\left(10^5 \cdot R_c^{2|M|}\right)} \\
\eta_2 &= \frac{O\left[\left(\frac{1}{2}\left|M\right|^2\left(D_U^2+D_L^2\right)+\left|M\right|^2 R'^{|M|}\right)\right]}{O\left(10^5 \cdot R_c^{2|M|}\right)} \\
\eta_3 &= \frac{O\left[\left(\frac{1}{2}\left|M\right|^2\left(D_U^2+D_L^2\right)+\left|M\right|^2 R'^{|M|}\right)\right]}{O\left[\left|M\right|^2\left(R_c^{|M|}+R_c^2\right)\right]}
\end{aligned} \tag{4.33}$$

where η_1, η_2 and η_3 denote the complexity ratio of SAP to SA, MTOP to SA and MTOP to SAP. It can be noted that as $|M| \to \infty$, the time complexity of SA grows exponentially faster than that of SAP and MTOP, so $\lim\limits_{|M|\to\infty} \eta_1 = 0$ and $\lim\limits_{|M|\to\infty} \eta_2 = 0$. Due to $R' < R_c$, derive $\eta_3 < 1$ and $\lim\limits_{|M|\to\infty} \eta_3 = 0$. Obviously, the MTOP has the highest performance benefit as $|M| \to \infty$. □

4.7 Summary

In this chapter, we illustrate the multiple user cooperative mobility system in an ad hoc network. Firstly, we utilize the Poisson point process to present the features of fixed nodes positions. From this, we employ the DF transmission protocol to formulate a system throughput maximization problem, which is a mixed-integer with a non-linear and non-convex problem. After that, the lower and upper bounds are defined to delineate the domain scope.

Furthermore, CSLG is proposed to clarify and calculate the values of these two bounds. Specifically, we propose the MTOP algorithm to obtain the optimal locations for movable nodes. The simulation results show that compared with IM and SA, the throughput of MTOP is increased by 298.81%, 37.91%, respectively. Compared with SAP and SA, MTOP reduces the computation cost by 44.12% and 237.97%, respectively; Besides, the communication cost of MTOP is reduced by 72.96% and 37.55%. It demonstrates that MTOP is a practical algorithm for improving system throughput and reducing computational costs and overhead in practical applications.

Chapter 5

Effective Collaboration to Maximize Throughput in Social-Physical Ad hoc Networks

5.1 Related work

With the widespread popularity of various ubiquitous mobile and wearable devices in the IoT context, choosing such a device as temporary relay may lead to data integrity and privacy concerns. The peer-to-peer relay selection process is crucial for D2D-assisted IoT operations. At present, social attributes have also become a non-negligible factor in IoT design since IoT device users' behavior will significantly affect performance. As the underlying driver of the social attributes among users, intimacy is consequently becoming an essential measure of social networks' stability [58]. Therefore, it is important to construct network architectures that can simultaneously satisfy demands for high QoS, high intimacy, and strong link reliability in existing networks.

Traditional research has focused on increasing bandwidth, enhancing transmission power, or improving the efficiency of medium access control (MAC) layer communication protocols to increase system throughput [59]. Unfortunately, these schemes always require high consumption of infrastructure resources and rarely consider social attributes such as intimacy. To date, researchers have presented several mechanisms of relay selection with comprehensive consideration of both social demands and throughput. M. Zhang *et al.* [60] proposed a socially aware relay selection mechanism based on optimal stopping theory, which provides a significant throughput gain compared with the direct transmission method. Pan *et al.* [61] introduced a distance-based relay selection mechanism that considers only different relay locations within a certain proximity. In regard to social-trust and physical-based integration schemes, Fang *et al.* [62] demonstrated that a hybrid scheme outperformed the methods of [63] and [64] in most scenarios. Furthermore, He Zhang *et al.* [65] proposed a joint social-physical relay reselection mechanism based on [60] and proved that the proposed scheme achieves a trade-off between the selection time and sufficient data traffic. However, for most of the above methods, only time-division multiple access (TDMA) communication systems, with a high selection time and poor throughput performance have been analyzed. Currently, an effective collaboration scheme that can achieve both high throughput and a low relay selection cost in practice has not yet been proposed.

The differences between this thesis and related work are highlighted [60]-[65]. The related work on relay selection schemes are summarized in Table 2.4. The previous schemes can be classified into three categories. Category I corresponds to the intuitive method [63],

Table 5.1 Summary of work related to relay selection schemes.

Relay selection scheme	Category	High social intimacy	Good throughput performance	Ad hoc network	Low complexity
Intuitive method [63]	Category I	×	×	×	✓
Social-trust-based relay selection [60]	Category II	✓	×	×	✓
Physical-based relay selection [61]	Category II	×	✓	×	×
Hybrid social trust and physical relay selection [62], [64]	Category III	✓	✓	×	×
Social-physical relay reselection [65]	Category III	✓	✓	×	×
Our work	Category III	✓	✓	✓	✓

while category II contains schemes based on only social trust [60] or only physical considerations [61]. Category III comprises a hybrid scheme [62], [64] and a reselection approach [65] in the social-physical layers. In the following, we explain the distinctions among these related work.

In the intuitive method [63], a mobile relay moves to the midpoint location between the source and destination users for each link. This method can yield only a minor throughput gain, but it is widely applied in practice due to its low complexity. Social-trust-based relay selection [60] and physical-based relay selection [61], are extreme methods that consider either only social intimacy or only throughput for optimization. Consequently, their practicality is not high because of the excessive relay selection time. On the basis of [60] and [61], some researchers have comprehensively considered the interactions between social trust and user transmission distance to propose hybrid schemes [62], [64] and a relay reselection scheme [65]. Unfortunately, these methods are applicable only for cellular networks and the time cost of relay selection is prohibitive. In contrast to the existing works described above, our work focuses on social-physical ad hoc networks, aiming to achieve optimal throughput performance with high social intimacy and low complexity.

5.2 System model

In this subchapter, we construct a social-physical dual-layer model and then analyze the channel model and interference.

5.2.1 A social-physical dual-layer model based on multiuser cooperative mobility in an ad hoc network

As shown in Fig. 5.1, we consider a multiuser cooperative mobility setting consisting of two layers, social and physical, deployed in an ad hoc network. In the physical layer,

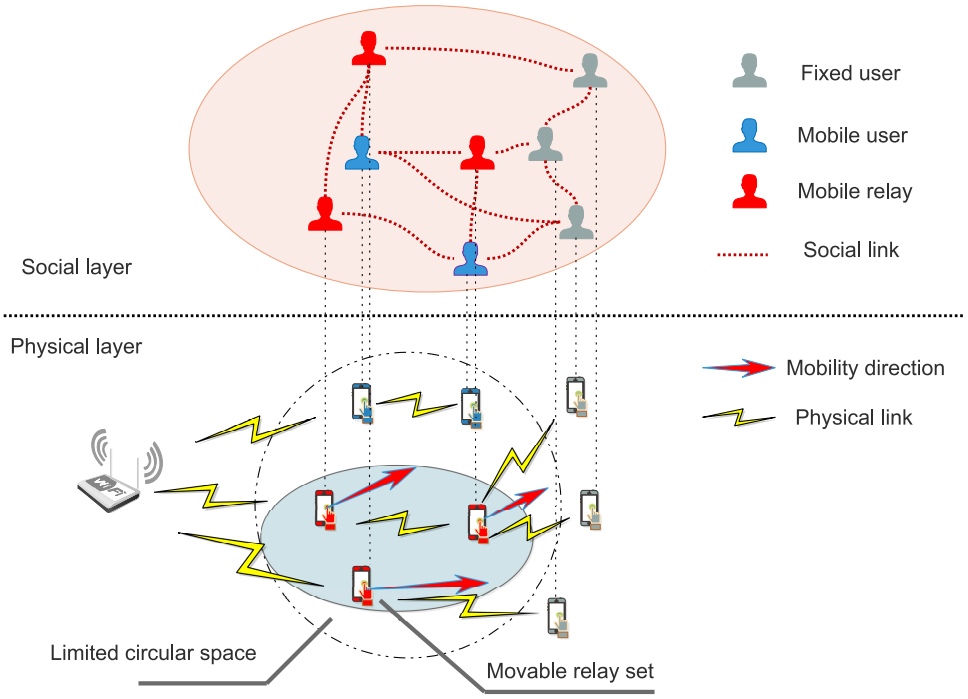

Fig. 5.1 A social-physical dual-layer model based on multiuser cooperative mobility in an ad hoc network.

the data flows between the AP and fixed user devices (FUDs) pass through relay user devices (RUDs) via D2D communication, for which the RUDs are selected from among the mobile user devices (MUDs). For ease of notation, we define $\mathcal{H} = \{1,2,...,|H|\}$ as the user set that comprises both the FUDs $\mathcal{F} = \{f_i \,|1 \leqslant i \leqslant |F|\,, i \in \mathbb{N}^+\}$ and the MUDs $\mathcal{M} = \{m_i \,|1 \leqslant i \leqslant |M|\,, i \in \mathbb{N}^+\}$, where $|F| + |M| = |H|$. Meanwhile, the MUDs include both RUDs and nonrelay user devices; the former are denoted by $\widehat{\mathcal{R}} = \left\{\widehat{r}_i \left| 0 \leqslant i \leqslant \left|\widehat{R}\right|, i \in \mathbb{N} \right.\right\}$ and the latter are represented by $\widetilde{\mathcal{R}} = \left\{\widetilde{r}_i \left| 0 \leqslant i \leqslant \left|\widetilde{R}\right|, i \in \mathbb{N} \right.\right\}$, where $\mathcal{M} = \widehat{\mathcal{R}} \cup \widetilde{\mathcal{R}}$ and $|M| = \left|\widehat{R}\right| + \left|\widetilde{R}\right|$. Given user privacy concerns, the number of relay nodes requested by fixed users should be as small as possible to ensure data integrity and prevent privacy disclosure. To this end, we assume D2D pairs consisting of only one RUD and one FUD, i.e., $|F| = \left|\widehat{R}\right|$. The mobility area of the MUDs is a limited circular area, with a maximum radius of L.

To facilitate the analysis of system throughput, we consider the uplink data sent by both the FUDs and MUDs to the AP while all links are saturated as the basis for the throughput calculation. Based on this consideration, the system throughput is defined as the data rate per unit time of the entire D2D communication system, i.e., the amount of data received by the AP per unit time is equal to the harmonic mean transmission rate of all users [34]. Therefore, the objective of optimal relay selection and multiuser cooperative mobility for enhancing throughput can be characterized as maximizing the effective transmission time and SINR by considering mutual interference.

Additionally, each device can be mapped from the physical and social layers and connected to form a social network through social links. In the actual social layer, people in-

teract through human habits, speech, and social ties. Here, the existence of each social link is determined on the basis of intimacy, which is an objective factor for judging the degree of likelihood of interaction between persons. We assume that this social intimacy information is known before transmission by using the system model. As for the measurement method, in real life, we can measure the intimacy according to the number of connections between users, the amount of data transmitted or the duration of connections. To represent the detailed information on the intimacy among users, we leverage a social graph, defined as $\boldsymbol{G}_s = \{\mathcal{H}, \mathcal{S}\}$, where $\mathcal{S}$ represents the intimacy values. Specifically, we introduce an intimacy matrix $\mathcal{S} = \left(\boldsymbol{S}_1^T, \boldsymbol{S}_2^T, ..., \boldsymbol{S}_{|H|}^T\right) \in \mathbb{R}^{|H|\times|H|}$, where each row vector has the form $\boldsymbol{S}_i = \left(s_{i,1}, s_{i,2}, ..., s_{i,|H|}\right) \in \mathbb{R}^{1\times|H|}$, $\forall i \in \{1,2,...,|H|\}$, with $s_{i,j}$ denoting the social trust value between user $i \in \mathcal{H}$ and another user $j \in \mathcal{H}\backslash\{i\}$. Here, $s_{i,j}$ is defined as

$$\begin{cases} s_{i,j} \in (0,1], \text{if } i \text{ and } j \text{ have social trust,} \\ s_{i,j} = 0, \text{otherwise.} \end{cases} \tag{5.1}$$

where $s_{i,i} \equiv 1$ represents that a user completely trusts him- or herself. In reality, a reliable social relationship can be established only if the intimacy reaches a certain value. In other words, if $s_{i,j}$ is larger than a predefined threshold $\overline{s}$, then a stable social connection link can be established between the two corresponding users.

The application scenario for this model is briefly described as follows. Due to the distance from the AP or poor channel conditions, the transmission performance of many FUDs may be low. Particularly, such lower-rate nodes can seriously affect the system throughput according to performance anomaly theory [92], making it challenging to meet users' typical QoS requirements. Meanwhile, for work or travel reasons, some MUDs may need to move closer to the locations of FUDs. Consequently, these FUDs can ask some of their friends, i.e., MUDs that are friendly to them, to act as relays to transfer data traffic via D2D technology. In line with a common trend in many previous system control mechanisms [93]-[95], to enable accessible analysis and exploration of the system performance limits while gaining useful insights, we hypothesize that there exists a virtual controller in the AP that can control the actions of the RUDs and track the location information of each user. This controller is capable of running the proposed relay selection scheme and mobility algorithms. In addition, a summary of the intimacy information between users will also be provided to this controller to support overall decision-making.

It is well known that the signal interference between users can seriously reduce throughput performance and channel utilization. A promising way out of this gridlock is successive interference cancellation (SIC) [96], which enables the decoding of collided or superposed signals due to interference. Specifically, in the SIC mechanism, the signal can be successfully decoded as long as the SINR of the receiving user is above a certain threshold. In our model, the SIC technique is deployed to combat conflicts arising in multipacket reception

among different users. Additionally, the instantaneous channel state information (CSI) of the users is unknown to each user, but we assume the statistics of the users' channel gains can be obtained [97]. Therefore, the channel gain can be calculated, and the CSI is assumed to be known at the D2D transmitter. Each of the user devices is equipped with a single omnidirectional antenna.

In general, consideration of dynamic elements, including locations and social states of users, is crucial for ensuring the reliability of such dual-layer network. Therefore, solutions that focus exclusively on network throughput are not always aligned with high reliability, which, as mentioned above, is critical for the robustness and operational stability of ad hoc networks. A reliability parameter is defined as being equal to the Cartesian product of the social intimacy and the probability of successful transmission. Specifically, we characterize the following features to formulate the optimization problem:

- **Relay selection scheme:** RUDs are selected from among MUDs on the basis of high social intimacy and a low selection time. In other words, the optimal relay requires the shortest time consumption for selection while guaranteeing the validity of the social link.
- **Multiuser cooperative mobility strategy:** The best throughput performance is achieved through the joint mobility of the mobile RUDs when the interference is minimized and the SINR is maximized.
- **Optimization constraints:** The optimization problem should be constrained in three dimensions, namely, the existence of a social link (high intimacy), the existence of a physical link (high SINR) and the link of reliability.

Since the data stream is saturated, frame conflicts have less impact on the results according to the definition of the harmonic mean throughput and the SIC decoding mechanism. From an operational standpoint, in this chapter, we are not concerned with the time assignment MAC frames or multipacket allocation; instead, we focus only on the selection and placement of the RUDs and on the interference among users. Additionally, this model considers only the dynamic changes in throughput before and after the relays' movement and ignores the data loss due to mobility, i.e., the time consumed is assumed to be short enough that the impact of mobility speed on the final throughput is negligible.

5.2.2 Channel model and interference analysis

Given that the application scenario of interest will mainly arise in a plaza, park or other large meeting place, the wireless model used is the independent Rayleigh fading model. Under the assumption that the instantaneous channel gain $\boldsymbol{H}$ includes the Rayleigh channel fading coefficient, the received signal can be expressed as

$$\boldsymbol{Y} = P_r \boldsymbol{H} \boldsymbol{X} + n_0 \tag{5.2}$$

where $\boldsymbol{X}$ is the transmitted signal, P_r is the received power, and n_0 is additive white Gaussian noise (AWGN) following a Gaussian distribution $\mathcal{N}(0, N_0)$. The received power P_r is given by

$$P_r = P_t K d_r^{-\alpha} \tag{5.3}$$

where P_t denotes the transmission power; K is the shadowing constant, which can be calculated from the CSI statistics; d_r denotes the distance between the transmitter and the receiver; and α represents the path-loss index.

In this case, the envelope of the received signal $\boldsymbol{Y}$ will be Rayleigh distributed with the following probability density function (PDF):

$$f(y) = \frac{2y}{\Omega} \exp\left(-\frac{y^2}{\Omega}\right), y \geqslant 0 \tag{5.4}$$

where Ω is the average received power determined by the path-loss and shadowing effects. Hence, the received power P_r will be exponentially distributed with mean Ω, where $\Omega = \mathbb{E}(P_r)$. According to (2)-(4), the signal received at RUD $\widehat{r}_i$, $\widehat{r}_i \in \widehat{\mathcal{R}}$, is then given by

$$y_{\widehat{r}_i} = H_{\mathrm{AP},\widehat{r}_i} \sqrt{P_{\mathrm{AP}} K d_{\mathrm{AP},\widehat{r}_i}^{-\alpha}} x_{\mathrm{AP}} + \quad H_{m_j,\widehat{r}_i} \sqrt{P_{m_j} K d_{m_j,\widehat{r}_i}^{-\alpha}} x_{m_j} + n_0 \tag{5.5}$$

where $H_{\mathrm{AP},\widehat{r}_i}$ denotes the channel fading coefficient from the AP to RUD $\widehat{r}_i$; P_{AP} is the transmission power of the AP; $d_{\mathrm{AP},\widehat{r}_i}$ is the Euclidean distance between the AP and RUD $\widehat{r}_i$; and x_{AP} is the signal from the AP with unit power. In particular, $H_{m_j,\widehat{r}_i} \sqrt{P_{m_j} K d_{m_j,\widehat{r}_i}^{-\alpha}} x_{m_j}$ represents the interference signal from m_j to $\widehat{r}_i$, where $m_j \in \widetilde{\mathcal{R}} \cup \widehat{\mathcal{R}} \backslash \{\widehat{r}_i\}$. Additionally, the received SINR at RUD $\widehat{r}_i$ can be expressed as

$$\gamma_{\mathrm{AP},\widehat{r}_i} = \frac{\left|H_{\mathrm{AP},\widehat{r}_i}\right|^2 P_{\mathrm{AP}} K d_{\mathrm{AP},\widehat{r}_i}^{-\alpha}}{\sum_{m_j \in \widetilde{\mathcal{R}} \cup \widehat{\mathcal{R}} \backslash \{\widehat{r}_i\}} \left|H_{m_j,\widehat{r}_i}\right|^2 P_{m_j} K d_{m_j,\widehat{r}_i}^{-\alpha} + n_0} \tag{5.6}$$

Similar to (5), the signal received at FUD f_i, $f_i \in \mathcal{F}$, is given by

$$y_{f_i} = H_{\widehat{r}_i,f_i} \sqrt{P_{\widehat{r}_i} K d_{\widehat{r}_i,f_i}^{-\alpha}} x_{\widehat{r}_i} + \quad H_{m_j,\widehat{r}_i} \sqrt{P_{m_j} K d_{m_j,\widehat{r}_i}^{-\alpha}} x_{m_j} + n_0 \tag{5.7}$$

Accordingly, for the received SINR at FUD f_i, we have

$$\gamma_{\widehat{r}_i,f_i} = \frac{\left|H_{\widehat{r}_i,f_i}\right|^2 P_{\widehat{r}_i} K d_{\widehat{r}_i,f_i}^{-\alpha}}{\sum_{m_j \in \widetilde{\mathcal{R}} \cup \widehat{\mathcal{R}} \backslash \{\widehat{r}_i\}} \left|H_{m_j,f_i}\right|^2 P_{m_j} K d_{m_j,f_i}^{-\alpha} + n_0} \tag{5.8}$$

In accordance with the SIC decoding mechanism, the SINR at any D2D receiver, including both RUD $\widehat{r}_i$ and FUD f_i, should be greater than $\overline{\gamma}$, which is the threshold for allowing the

signal to be decoded correctly. In the next section, we consider these constraints regarding the social trust, physical SINR, and reliability to formulate an optimization problem.

5.3 Relay selection with multiuser cooperative mobility for throughput maximization under link reliability

In this chapter, we formulate the problem of maximizing the effective system throughput based on an optimal relay selection scheme and an optimal multiuser cooperative mobility strategy.

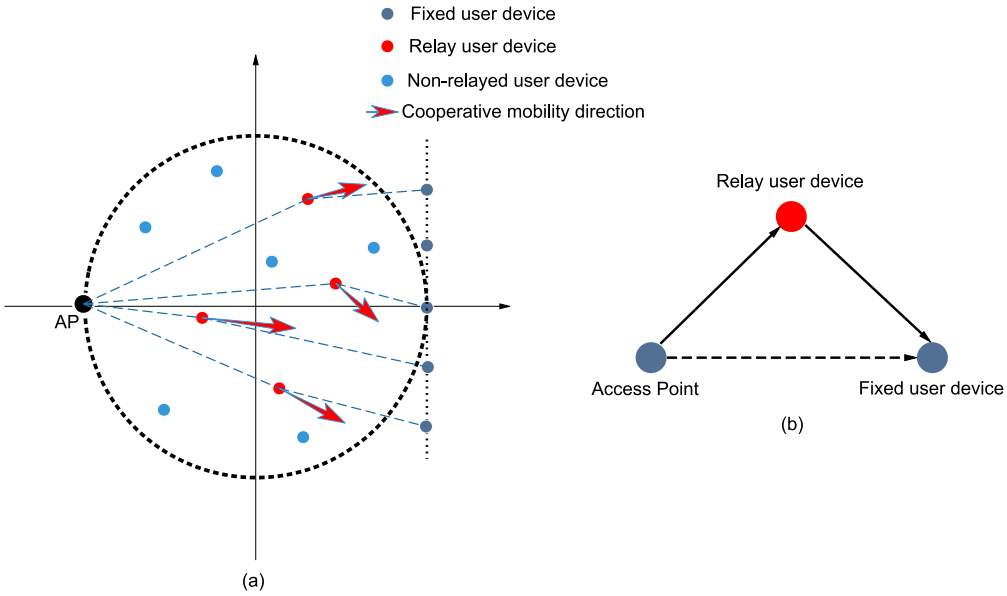

Fig. 5.2 Mathematical model. (a) Data transmission topology model; (b) Illustration of amplify-and-forward (AF) relaying mode.

Fig. 5.2 shows the mathematical model describing the transmission topology and the amplify-and-forward (AF) relaying mode. Let $u_{\widehat{r}_i}$ and u_{f_i} denote the position coordinates of an arbitrary RUD $\widehat{r}_i$ and FUD f_i, respectively, where $u_{\widehat{r}_i}$ is treated as a variable and u_{f_i} is a constant. The distance between $\widehat{r}_i$ and f_i is expressed as $D_{\widehat{r}_i,f_i} = \|u_{\widehat{r}_i} - u_{f_i}\|$, which can be treated as a function of the variable $u_{\widehat{r}_i} \in \boldsymbol{U}$, where $\boldsymbol{U}$ is the set of position coordinates of the RUDs. Furthermore, we define the set of the distances between the RUDs and other users as $\boldsymbol{D} \triangleq \left\{ \left(D_{\mathrm{AP},\widehat{r}_i}, D_{\widehat{r}_i,f_i}, D_{\widehat{r}_i,m_j} \right) \middle| \widehat{r}_i \in \widehat{\mathcal{R}}, f_i \in \mathcal{F}, m_j \in \widetilde{\mathcal{R}} \cup \widehat{\mathcal{R}} \backslash \{\widehat{r}_i\} \right\}$. Once the distance set $\boldsymbol{D}$ has been calculated, the set of RUD position coordinates $\boldsymbol{U}$ is also uniquely determined. Therefore, in the following analysis, we simply use the distance set $\boldsymbol{D}$ to represent the RUD position coordinates $\boldsymbol{U}$ for brevity. To better represent the selection of RUDs from among the MUDs, we introduce an indicator function $\omega\left(m_i\right) \in \boldsymbol{\Omega}$ defined on the set $\mathcal{M}$, $m_i \in \mathcal{M}$:

$$\omega\left(m_i\right) = \begin{cases} 1, \text{if } m_i \in \widehat{R} \ , \\ 0, \text{if } m_i \in \widetilde{R} \ . \end{cases} \tag{5.9}$$

where $\boldsymbol{\Omega}$ is the set of indicator function values. In addition, we give a detailed lists of the notations for the main sets and parameters in Table 5.1.

Table 5.2 List of main sets and parameters.

Notations	Descriptions
$\mathcal{F}$	The set of fixed user devices (FUDs)
$\mathcal{M}$	The set of mobile user devices (MUDs)
$\widehat{\mathcal{R}}$	The set of relay user devices (RUDs)
$\mathcal{S}$	The set of intimacy values between users
$\boldsymbol{U}$	The set of position coordinates of the RUDs
$\boldsymbol{D}$	The set of distances between the RUDs and other users
$\boldsymbol{\Omega}$	The set of indicator function values
$s_{i,j}$	The social trust value between user $i \in \mathcal{H}$ and $j \in \mathcal{H} \backslash \{i\}$
T	The random variable of contact durations
R_{eff}	The effective data transmission rate
T_{eff}	The effective transmission time
p_r	The probability of successful transmission within T_{eff}
p	The link reliability
Th_{sys}	The system throughput

According to [98], the AF relay mode has a greater array gain and a lower cost and complexity than the decode-and-forward (DF) mode for the same diversity gain. Here, to ensure high practicability, we adopt the AF mode to achieve cooperative diversity in our system model. Additionally, we assume that the transmission power P_{AP} from AP to each RUD is the same and that all nodes also have the same transmission power P_0 due to their identical antenna gain performance and use of the same transmission protocol, where $P_0 = P_{\widehat{r}_i} = P_{m_j}$. Hence, the achievable data rate pertaining to transmission from FUD $f_i \in \mathcal{F}$ in the AF mode is given by

$$\gamma_{\text{AP},f_i} = \frac{\gamma_{\text{AP},\widehat{r}_i}\gamma_{\widehat{r}_i,f_i}}{\gamma_{\text{AP},\widehat{r}_i} + \gamma_{\widehat{r}_i,f_i} + 1} \tag{5.10}$$

Then, the maximum achievable end-to-end rate can be derived as

$$R_{\text{AP},f_i} = \frac{1}{2}\mathscr{B}\log_2\left(1 + \frac{\gamma_{\text{AP},\widehat{r}_i}\gamma_{\widehat{r}_i,f_i}}{\gamma_{\text{AP},\widehat{r}_i} + \gamma_{\widehat{r}_i,f_i} + 1}\right) \tag{5.11}$$

where $\mathscr{B}$ is the normalized bandwidth. By substituting (5.6) and (5.8) into (5.11), R_{AP,f_i} can

be rewritten as

$$
\begin{aligned}
R_{\mathrm{AP},f_i}\left(\boldsymbol{D}\right) &= \frac{1}{2}\log_2\left(\frac{1+\frac{P_{\mathrm{AP}}}{P_0}G_{\mathrm{AP},\widehat{r}_i}G_{\widehat{r}_i,f_i}\left\{D_{\mathrm{AP},\widehat{r}_i}D_{\widehat{r}_i,f_i}\right\}^{-\alpha}}{\phi 1 G_{\widehat{r}_i,f_i}D_{\widehat{r}_i,f_i}^{-\alpha}+\phi 2\frac{P_{\mathrm{AP}}}{P_0}G_{\mathrm{AP},\widehat{r}_i}D_{\mathrm{AP},\widehat{r}_i}^{-\alpha}+\phi 1\phi 2}\right) \\
\phi 1 &\triangleq \sum_{m_j\in\widetilde{\mathcal{R}}\cup\widehat{\mathcal{R}}\backslash\{\widehat{r}_i\}} G_{m_j,\widehat{r}_i}D_{\widehat{r}_i,f_i}^{-\alpha}+\frac{n_0}{P_0} \\
\phi 2 &\triangleq \sum_{m_j\in\widetilde{\mathcal{R}}\cup\widehat{\mathcal{R}}\backslash\{\widehat{r}_i\}} G_{m_j,f_i}D_{m_j,f_i}^{-\alpha}+\frac{n_0}{P_0}
\end{aligned}
\tag{5.12}
$$

where $G_{\mathrm{AP},\widehat{r}_i}=K\left|H_{\mathrm{AP},\widehat{r}_i}\right|^2$, $G_{\widehat{r}_i,f_i}=K\left|H_{\widehat{r}_i,f_i}\right|^2$, $G_{m_j,\widehat{r}_i}=K\left|H_{m_j,\widehat{r}_i}\right|^2$ and $G_{m_j,f_i}=K\left|H_{m_j,f_i}\right|^2$ denote the channel gains among the AP, FUD f_i, RUD $\widehat{r}_i$ and MUD m_j. Here, the information on the relevant channel gain and CSI can be obtained from feedback on each link. Note that, the channel gains follow exponential distributions [99]. Specifically, $G_{\mathrm{AP},\widehat{r}_i}$ and $G_{m_j,\widehat{r}_i}$ obey exponential distributions with the same parameter $\frac{1}{\lambda}$, i.e., $G_{\mathrm{AP},\widehat{r}_i}\sim\mathrm{Exp}\left(\lambda\right)$, $G_{m_j,\widehat{r}_i}\sim\mathrm{Exp}\left(\lambda\right)$. Likewise, $G_{\widehat{r}_i,f_i}$ and G_{m_j,f_i} also follow exponential distributions with the same parameter $\frac{1}{\eta}$, i.e., $G_{\widehat{r}_i,f_i}\sim\mathrm{Exp}\left(\eta\right)$ and $G_{m_j,f_i}\sim\mathrm{Exp}\left(\eta\right)$. Therefore, the PDFs of these channel gains can be expressed as

$$
f_{G_{\mathrm{AP},\widehat{r}_i}}\left(x\right)=f_{G_{m_j,\widehat{r}_i}}\left(x\right)=\frac{1}{\lambda}e^{-\frac{x}{\lambda}} \tag{5.13}
$$

$$
f_{G_{\widehat{r}_i,f_i}}\left(x\right)=f_{G_{m_j,f_i}}\left(x\right)=\frac{1}{\eta}e^{-\frac{x}{\eta}} \tag{5.14}
$$

As mentioned in the section introducing the system model, the requirements in the relay selection process are to determine the cooperative gain and ensure the reliability of the social-physical dual-layer links. Let T denote the random variable representing the contact durations in a time slot, which follows a Gamma distribution [11], $T\sim Gamma\left(\mu,\rho\right)$. The PDF of T can be expressed as

$$
f\left(X_T\right)=\frac{x_T^{(\mu-1)}\exp^{\left(-\frac{x_T}{\rho}\right)}}{\Gamma\left(\mu\right)\rho^{\mu}} \tag{5.15}
$$

Considering the selection time, we have the following effective transmission time:

$$
\begin{aligned}
T_{eff}\left(\boldsymbol{\Omega}\right) &= T-\sum_{m_i\in\mathcal{M}}\tau_{m_i}\left(\boldsymbol{\Omega}\right) \\
\tau_{m_i}\left(\boldsymbol{\Omega}\right) &= \tau_{m_i}\boldsymbol{\Omega}\left(m_i\right)
\end{aligned}
\tag{5.16}
$$

where τ_{m_i} represents the time cost of relay selection, including both the detection time and the duration of algorithm execution. Specifically, τ_{m_i} follows the uniform distribution $\tau_{m_i}\sim U\left(0,T\right)$ [100]. Thus, we can obtain the cumulative distribution function (CDF) of

the effective transmission time T_{eff} as

$$F_{T_{eff}}(t, \boldsymbol{\Omega}) = \int_0^{+\infty} \int_{X_T - t}^{X_T} \frac{x_T^{(\mu-2)} \exp^{\left(-\frac{x_T}{\rho}\right)}}{\Gamma(\mu)\rho^{\mu}} d_{\tau_{m_i}} dX_T \tag{5.17}$$

Accordingly, we can obtain the PDF of T_{eff} as $f_{T_{eff}}(t) = F'_{T_{eff}}(t, \boldsymbol{\Omega})$. The expected effective transmission time can be calculated as $\mathbb{E}[T_{eff}] = \int_0^{+\infty} t f_{T_{eff}}(t)\, dt$. The effective data rate for transmission, R_{eff}, can be expressed as

$$\begin{aligned} R_{eff}(\boldsymbol{\Omega}, \boldsymbol{D}) &= R_{\mathrm{AP},f_i}(\boldsymbol{D}) \cdot T_{eff}(\boldsymbol{\Omega}) \\ &= R_{\mathrm{AP},f_i}(\boldsymbol{D}) \int_0^{+\infty} t F'_{T_{eff}}(t, \boldsymbol{\Omega})\, dt \end{aligned} \tag{5.18}$$

Notably, the throughput Th_{sys} is the reciprocal of the harmonic mean in the case that links are all saturated, which is given by

$$Th_{sys} = \frac{|F|}{\sum_{i=1}^{|F|} \frac{1}{R_{eff}(\boldsymbol{\Omega}, \boldsymbol{D})}} \tag{5.19}$$

Additionally, to guarantee reliability under social-physical dual-layer model, we assume that the packet size required to be transmitted is Z; then, the probability $p_r(\boldsymbol{\Omega}, \boldsymbol{D})$ of successful data transmission within T_{eff} is expressed as

$$\begin{aligned} p_r(\boldsymbol{\Omega}, \boldsymbol{D}) &= \Pr\left\{ R_{AP,f_i}(\boldsymbol{D}) \geqslant \frac{Z}{T_{eff}} \right\} \\ &= \Pr\left\{ \frac{\frac{P_{\mathrm{AP}} G_{\mathrm{AP},\widehat{r}_i} G_{\widehat{r}_i,f_i} \left\{ D_{\mathrm{AP},\widehat{r}_i} D_{\widehat{r}_i,f_i} \right\}^{-\alpha}}{\phi 1 \phi 2 P_0}}{\frac{P_{\mathrm{AP}} G_{\mathrm{AP},\widehat{r}_i} D_{\mathrm{AP},\widehat{r}_i}^{-\alpha}}{P_0 \phi 1} + \frac{G_{\widehat{r}_i,f_i} D_{\widehat{r}_i,f_i}^{-\alpha}}{\phi 2} + 1} \geqslant 2^{\frac{2Z}{WT_{eff}}} - 1 \right\} \end{aligned} \tag{5.20}$$

Evidently, the success probability $p_r(\boldsymbol{\Omega}, \boldsymbol{D})$ is related to the variables $G_{\mathrm{AP},\widehat{r}_i}$ and $G_{\widehat{r}_i,f_i}$. We introduce the following theorem to verify the properties of this probability and calculate $p_r(\boldsymbol{\Omega}, \boldsymbol{D})$ based on Eq. (5.13), Eq. (5.14), and Eq. (5.20).

Theorem 1: If the variables A and B both obey the independent exponential distribution with the parameters $\zeta_A = \lambda$ and $\zeta_B = \eta$, respectively, then the CDF of $Y = k_1 k_2 AB / (k_1 A + k_2 B + 1)$, with $k_1, k_2 > 0$, can be derived as

$$F_Y(y) = 1 - \frac{k_1 e^{-\frac{\lambda y}{k_1 k_2 - k_1 y}} (k_2 - y)}{k_1 k_2 \eta - k_1 \eta y + k_2 \lambda y} \tag{5.21}$$

Proof. Since A and B are continuous random variables and independently follow exponen-

tial distributions, we have

$$\begin{aligned} F_Y(y) &= P\{Y \leqslant y\} = P\{k_1k_2AB/(k_1A + k_2B + 1) \leqslant y\} \\ &= \int_0^{+\infty} \int_0^{\frac{y(k_2b+1)}{k_1k_2b-k_1y}} \lambda e^{-\lambda a} \eta e^{-\eta b} da db \\ &= 1 - \frac{k_1 e^{-\frac{\lambda y}{k_1k_2-k_1y}} (k_2 - y)}{k_1k_2\eta - k_1\eta y + k_2\lambda y} \end{aligned} \tag{5.22}$$

□

Let $k_1 = \frac{P_{\text{AP}} D_{\text{AP},\widehat{r}_i}^{-\alpha}}{P_0 \phi 1}$ and $k_2 = \frac{D_{\widehat{r}_i,f_i}^{-\alpha}}{\phi 2}$; then, the CDF of Y is given by

$$\begin{aligned} F_{R_{AP,f_i}(\boldsymbol{D})}\left(R_{AP,f_i}(\boldsymbol{D})\right) &= \Pr\left\{Y \leqslant 2^{2R_{AP,f_i}(\boldsymbol{D})} - 1\right\} \\ &= F_Y\left(2^{2R_{AP,f_i}(\boldsymbol{D})} - 1\right) \end{aligned} \tag{5.23}$$

Therefore, we have

$$\begin{aligned} p_r(\boldsymbol{\Omega}, \boldsymbol{D}) &= \Pr\left(R_{AP,f_i}(\boldsymbol{D}) \geqslant \frac{Z}{T - \sum_{i\in\mathcal{M}} \tau_i(\boldsymbol{\Omega})}\right) \\ &= 1 - F_{R_{AP,f_i}(\boldsymbol{D})}\left(\frac{Z}{T - \sum_{i\in\mathcal{M}} \tau_i(\boldsymbol{\Omega})}\right) \\ &= 1 - F_Y\left(2^{\frac{Z}{T-\sum_{i\in\mathcal{M}} \tau_i(\boldsymbol{V})}} - 1\right) \end{aligned} \tag{5.24}$$

Then, by substituting (5.24) into (5.21), the probability $p_r(\boldsymbol{\Omega}, \boldsymbol{D})$ of successful end-to-end data transmission can be calculated as

$$\begin{aligned} p_r(\boldsymbol{\Omega}, \boldsymbol{D}) = &\frac{k_1 \exp\left(-\frac{\lambda}{\frac{k_1k_2\left(T-\sum_{i\in\mathcal{M}} \tau_i(\boldsymbol{\Omega})\right)}{Z} - k_1}\right)}{k_1k_2\eta + (k_2\lambda - k_1\eta)\left(2^{\frac{Z}{T-\sum_{i\in\mathcal{M}} \tau_i(\boldsymbol{\Omega})}} - 1\right)} \\ &\times \left(k_2 - 2^{\frac{Z}{T-\sum_{i\in\mathcal{M}} \tau_i(\boldsymbol{\Omega})}} - 1\right), \\ k_1 \triangleq &\frac{P_{\text{AP}} D_{\text{AP},\widehat{r}_i}^{-\alpha}}{P_0 \phi 1}, \\ k_2 \triangleq &\frac{D_{\widehat{r}_i,f_i}^{-\alpha}}{\phi 2}. \end{aligned} \tag{5.25}$$

Consider that the RUDs are required not only to possess the intimacy and an SINR greater than given thresholds in the dual social-physical layers but also to ensure the reliability of the network; thus, the link reliability can be expressed as

$$p(\boldsymbol{\Omega}, \boldsymbol{D}) = p_r(\boldsymbol{\Omega}, \boldsymbol{D})\, s_{i,j}(\boldsymbol{\Omega}) \tag{5.26}$$

where $s_{i,j}(\boldsymbol{\Omega})$ is the social intimacy after relay selection.

We note that the reliability is the Cartesian product of the transmission success probability and the social intimacy. Consequently, by summarizing (5.9) to (5.26), the optimal relay selection and multiuser cooperative mobility strategy to maximize the system throughput can be formulated as follows:

$$
\begin{aligned}
\max_{\boldsymbol{\Omega},\boldsymbol{D}} \quad & \frac{|F|}{\sum_{i=1}^{|F|}\frac{1}{R_{eff,f_i}(\boldsymbol{\Omega},\boldsymbol{D})}} \\
\text{s.t.} \quad & s_{\widehat{r}_i,m_j}\left(\boldsymbol{\Omega}\right) \geqslant \overline{s}, \\
& s_{\widehat{r}_i,f_i}\left(\boldsymbol{\Omega}\right) \geqslant \overline{s}, \\
& p\left(\boldsymbol{\Omega},\boldsymbol{D}\right) \geqslant \overline{p}, \\
& \frac{\gamma_{\mathrm{AP},\widehat{r}_i}\gamma_{\widehat{r}_i,f_i}}{\gamma_{\mathrm{AP},\widehat{r}_i}+\gamma_{\widehat{r}_i,f_i}+1} \geqslant \overline{\gamma}, \\
& \gamma_{\widehat{r}_i,f_i} \geqslant \overline{\gamma}, \\
& \gamma_{\mathrm{AP},\widehat{r}_i} \geqslant \overline{\gamma}, \\
& D_{\widehat{r}_i,f_i} \leqslant 2L, \\
& D_{\widehat{r}_i,m_j} \leqslant 2L, \\
& \widehat{r}_i \in \widehat{\mathcal{R}}, f_i \in \mathcal{F}, m_j \in \widetilde{\mathcal{R}} \cup \widehat{\mathcal{R}} \backslash \left\{\widehat{r}_i\right\}.
\end{aligned}
\tag{5.27}
$$

where $\overline{p}$ is a reliability threshold that is predefined in accordance with the requirements of the real application scenario and satisfies $\overline{p} \in [0,1]$. Both the objective function and constraints are nonconvex and nonlinear; that is, the problem can be interpreted as a nonconvex and nonlinear (NCNL) problem, which is a typical NP-hard problem. Although this problem can be solved through exhaustive search, the complexity of doing so is prohibitive due to the properties of NCNL problems. In practical applications, the controller execution algorithm's latency plays an essential role in determining the overall performance, mostly the relay selection time and user experience. Therefore, we propose a new method to address this issue in the next section.

5.4 Relay Selection and Link Interference Degree Graph (RS-LIDG) algorithm

There are several available optimization packages, such as CVX for MATLAB and the Python Optimization Package, for solving convex optimization problems. However, an NCNL optimization problem cannot be solved to the global optimum with low computational complexity using traditional heuristic algorithms or optimization tools. Consequently, it is desirable to develop an effective and adaptable algorithm that can be deployed in actual ad hoc networks.

In this chapter, the optimization problem given in Eq. (5.27) is decomposed into two subproblems, and the RS-LIDG algorithm is proposed to solve this problem completely. The

proposed relay selection scheme based on the optimal stopping approach is proven to be efficient. Meanwhile, on the basis of a graph defined to represent the degrees of interference between physical links and Algorithm 1, it is demonstrated that the proposed multiuser cooperative mobility strategy can achieve the optimal throughput. The framework of our proposed RS-LIDG algorithm is shown in Figure 5.3.

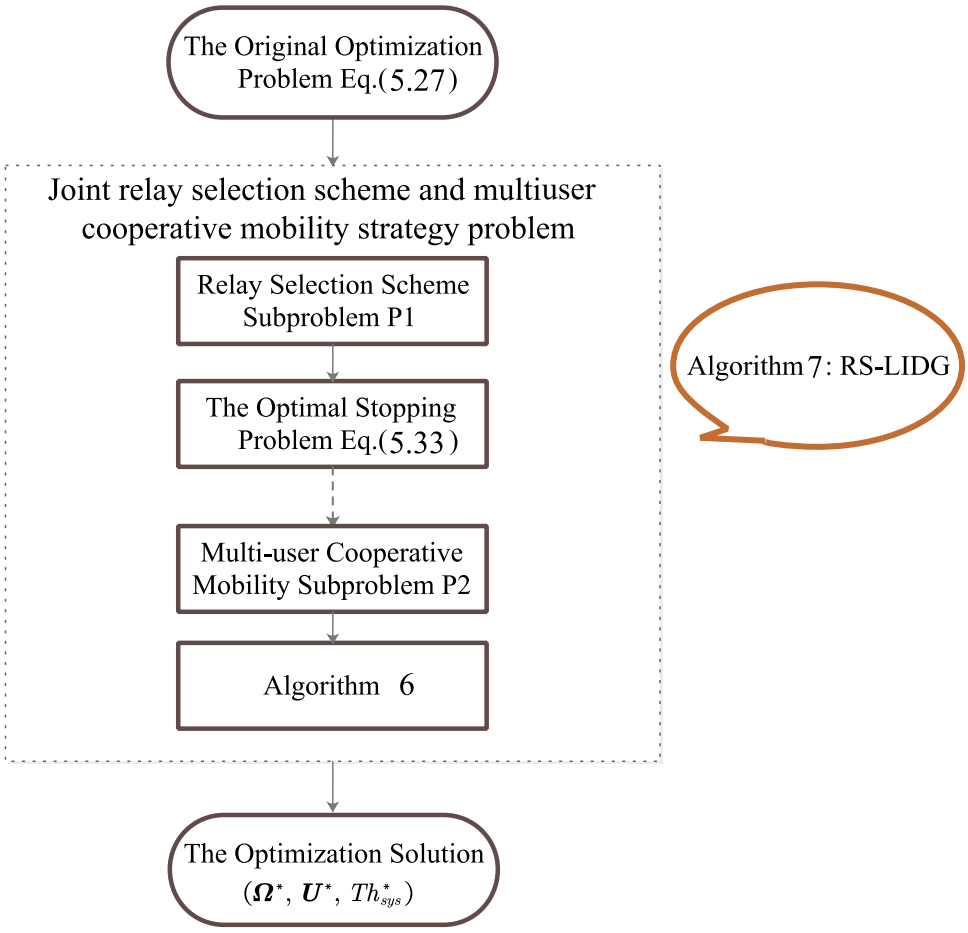

Fig. 5.3 The proposed framework for solving the optimization problem given in Eq. (5.27).

5.4.1 Relay selection scheme

Based on (5.16) and (5.27), the goal of relay selection is to choose a sequence of actions such that the system will achieve the optimal throughput performance in terms of the maximal effective transmission time (minimal selection cost time) and sufficiently large intimacy.

Accordingly, the relay selection subproblem can be expressed as

$$\begin{aligned}
(\mathbf{P1}): \quad & \max_{\boldsymbol{\Omega}} T_{eff}\left(\boldsymbol{\Omega}\right) \\
\text{s.t.} \quad & T_{eff}\left(\boldsymbol{\Omega}\right) = T - \sum_{m_i \in \mathcal{M}} \tau_{m_i} \boldsymbol{\Omega}\left(m_i\right), \\
& s_{\widehat{r}_i, m_j}\left(\boldsymbol{\Omega}\right) \geqslant \overline{s}, \\
& s_{\widehat{r}_i, f_i}\left(\boldsymbol{\Omega}\right) \geqslant \overline{s}, \\
& \widehat{r}_i \in \widehat{\mathcal{R}}, f_i \in \mathcal{F}, m_j \in \widetilde{\mathcal{R}} \cup \widehat{\mathcal{R}} \backslash \left\{\widehat{r}_i\right\}
\end{aligned} \tag{5.28}$$

Notably, for the selection of appropriate relays, it is required that the social intimacies between the RUDs, FUDs, and other MUDs (not relays) be greater than a predefined threshold, which depends on the specific scenario of interest. In this case, the optimal first step for the AP is to select viable relays to ensure stable social links, providing a solid foundation for effective and trustworthy peer-to-peer assistance in the multiuser cooperative mobility approach.

Then, the relay selection optimization problem defined in (5.28) can be cast as a finite-horizon optimal stopping problem, i.e., an optimal stopping policy can be set to maximize the expected reward by stopping in the optimal stopping phase. In fact, this scheme builds on the socially aware relay selection paradigm proposed in [6], in which the social tie structure is based on a cellular network and a time scheduling framework. Despite this similarity, we mainly focus on relay resource segmentation and minimizing the time cost of selection through the ad hoc network's social-physical layers.

Suppose that the virtual controller observes two random sequences, consisting of relay detection time costs $\tau_{m_{(1)}} \boldsymbol{\Omega}\left(m_{(1)}\right), \tau_{m_{(2)}} \boldsymbol{\Omega}\left(m_{(2)}\right), ...$ and communication durations $T_{(1)}, T_{(2)}, ...,$ through signal detection. Then, the controller must decide whether to stop after the detection of the k^{th} relay and achieve an effective transfer time T_{eff}^{k} or to continue to detect the next viable relay. It is possible that the controller might skip all potential MUDs without selecting any relays until all MUDs have been detected. In this case, direct communication would be established between the AP and the FUDs without any relays, for which $\tau_{m_{(0)}} \boldsymbol{\Omega}\left(m_{(0)}\right) = 0$ and $T_{eff}^{0} = T_{(0)}$. We first define the optimal stopping phase index as $k^* \in \mathcal{M}$, where $\sum_{k^* \in \mathcal{M}} |k^*| = |M|$ and $|k^*|$ denotes the number of stopping phase indices. The maximal effective transmission time, denoted by T_{eff}^{*}, satisfies the following:

$$\begin{aligned}
T_{eff}^{*} &\overset{\text{def}}{=} \sup_{k \in \mathcal{M}} \left[\mathbb{E}\left(T_{eff}^{k}\right)\right] \\
k^* &\overset{\text{def}}{=} \arg\max_{k \in \mathcal{M}} \left[\mathbb{E}\left(T_{eff}^{j}\right)\right]
\end{aligned} \tag{5.29}$$

According to optimal stopping theory [8], the effective transmission time T_{eff}^{k} can be defined as the instantaneous reward $T_{eff}^{k}\left[T, \tau_{m_{(k)}} \boldsymbol{\Omega}\left(m_{(k)}\right)\right]$ when the controller decides to

transmit after detecting the k^{th} relay. Therefore, we have

$$T_{eff}^{k}\left[T,\tau_{m_{(k)}}\boldsymbol{\Omega}\left(m_{(k)}\right)\right]=T-\sum_{m_k\in\mathcal{M}}\tau_{m_k}\boldsymbol{\Omega}\left(m_k\right) \tag{5.30}$$

Moreover, we use $\Phi_{eff}^{k}\left(T,\tau_{m_{(k)}}\boldsymbol{\Omega}\left(m_{(k)}\right)\right)$ to denote the expected achievable reward for the system upon detecting the k^{th} relay. Since T and $\tau_{m_{(k)}}$ are mutually independent and follow gamma and uniform distributions, respectively, with PDFs $f_T\left(x\right)\left(\cdot\right)$ and $f_{\tau_{m_{(k)}}}\left(x\right)\left(\cdot\right)$, which are related to the indicator function, the expected achievable reward is given by

$$\begin{aligned}&\Phi_{eff}^{k}\left(T,\tau_{m_{(k)}}\boldsymbol{\Omega}\left(m_{(k)}\right)\right)=\\&\max\left\{\begin{array}{c}T_{eff}^{k}\left[T,\tau_{m_{(k)}}\boldsymbol{\Omega}\left(m_{(k)}\right)\right],\\\mathbb{E}\left[\Phi_{eff}^{k+1}\left(T,\tau_{m_{(k+1)}}\boldsymbol{\Omega}\left(m_{(k+1)}\right)\right)\right]\end{array}\right\}\end{aligned} \tag{5.31}$$

where $\mathbb{E}\left[\Phi_{eff}^{k+1}\left(T,\tau_{m_{(k+1)}}\boldsymbol{\Omega}\left(m_{(k+1)}\right)\right)\right]$ denotes the expected effective transmission time in the $(k+1)^{th}$ detection phase. This means that $\mathbb{E}\left[\Phi_{eff}^{k+1}\left(T,\tau_{m_{(k+1)}}\boldsymbol{\Omega}\left(m_{(k+1)}\right)\right)\right]$ serves as the threshold for the controller to make its decision. Specifically, the AP compares these two values to determine whether to proceed beyond the k^{th} detection phase. If the instantaneous reward $T_{eff}^{k}\left[T,\tau_{m_{(k)}}\boldsymbol{\Omega}\left(m_{(k)}\right)\right]$ is larger than this threshold, then the controller stops detecting and selects the current MUD as the final RUD. Otherwise, the detection process continues until no further potential MUD is detected. In this case, the reward threshold in the k^{th} phase is expressed as

$$\Xi_{k}^{*}=\mathbb{E}\left[\Phi_{eff}^{k+1}\left(T,\tau_{m_{(k+1)}}\boldsymbol{\Omega}\left(m_{(k+1)}\right)\right)\right] \tag{5.32}$$

Note that if the final phase is the $|M|^{th}$ phase ($k^{*}=|M|$), i.e., there are no more relays to be detected, then we set $\Xi_{|M|}^{*}=-\infty$ to represent that the controller terminates the detection process after the $|M|^{th}$ phase. Consequently, we can derive the optimal stopping policy for relay selection in the social-physical layers as described in Theorem 2 below.

Theorem 2: The optimal choice is for the controller to stop detection in phase k^{*} if the social-physical relay selection problem satisfies the following condition:

$$k^{*}=\min_{k\in\mathcal{M}}\left\{k\geqslant 1\text{: }T_{eff}^{k}\left[T,\tau_{m_{(k)}}\boldsymbol{\Omega}\left(m_{(k)}\right)\right]\geqslant\Xi_{k}^{*}\right\} \tag{5.33}$$

where the thresholds $\{\Xi_k^*\}$ of the optimal stopping policy are given by

$$\begin{aligned}
&\Xi_{|M|}^* = -\infty, \\
&\Xi_{|M|-1}^* = (\tau_{\max} - \tau_{\min}) \int_{T_{\min}}^{T_{\max}} \frac{t^{(\mu-1)} e^{\left(-\frac{t}{\rho}\right)}}{\Gamma(\mu)\rho^{\mu}} dt \\
&- \sum |M| \int_{T_{\min}}^{T_{\max}} \int_{\tau_{\min}}^{\tau_{\max}} \tau \frac{t^{(\mu-1)} e^{\left(-\frac{t}{\rho}\right)}}{\Gamma(\mu)\rho^{\mu}} d\tau dt, \\
&\vdots \\
&\Xi_k^* = \left[\tau_{\max} + \left(\Xi_{k+1}^* - 1\right)\Xi_k - \Xi_{k+1}^* \tau_{\min}\right] \int_{T_{\min}}^{T_{\max}} \frac{t^{(\mu-2)} e^{\left(-\frac{t}{\rho}\right)}}{\Gamma(\mu)\rho^{\mu}} dt \\
&- \sum |k+1| \int_{T_{\min}}^{T_{\max}} \int_{\Xi_k}^{\tau_{\max}} \frac{t^{(\mu-2)} e^{\left(-\frac{t}{\rho}\right)}}{\Gamma(\mu)\rho^{\mu}} d\tau dt, \\
&\forall k = 0,1,..., \ |M| - 2
\end{aligned} \tag{5.34}$$

with $\Xi_k = \frac{(\Xi_{k+1} - \sum |k+1|)}{k} + (k+1)\tau$ and $\sum |k| = \sum_{i=1}^{|k|} \tau_{m_{(k)}} \boldsymbol{\Omega}\left(m_{(k)}\right)$.

Proof. As mentioned above, $\Xi_{|M|}^* = -\infty$ means that it is always optimal for the controller to stop detecting in the $|M|^{th}$ phase. According to (5.32), for the $|M-1|^{th}$ phase, we can derive $\Xi_{|M|-1}^*$ as follows:

$$\begin{aligned}
\Xi_{|M|-1}^* &= \mathbb{E}\left[\Phi_{eff}^{|M|}\left(T, \tau_{m_{(|M|)}} \boldsymbol{\Omega}\left(m_{(|M|)}\right)\right)\right] \\
&= \int_{\tau}\int_{T} \Phi_{eff}^{|M|} f_{\tau T}(\tau, t) d\tau dt \\
&= (\tau_{\max} - \tau_{\min}) \int_{T_{\min}}^{T_{\max}} \frac{t^{(\mu-1)} \exp^{\left(-\frac{t}{\rho}\right)}}{\Gamma(\mu)\rho^{\mu}} dt \\
&- \sum |M| \int_{T_{\min}}^{T_{\max}} \int_{\tau_{\min}}^{\tau_{\max}} \tau \frac{t^{(\mu-1)} \exp^{\left(-\frac{t}{\rho}\right)}}{\Gamma(\mu)\rho^{\mu}} d\tau dt
\end{aligned} \tag{5.35}$$

where $f_{\tau T}(\tau, t)$ is the joint PDF of $f_T(x)(\cdot)$ and $f_{\tau_{m_k}}(x)(\cdot)$. In particular, $\tau_{\max}$, $\tau_{\min}$, $T_{\max}$ and $T_{\min}$ denote the maximum and minimum values of the relay selection time and the

contact durations between the AP and FUDs, respectively. Likewise, we can obtain Ξ_k^* as

$$\begin{aligned}
\Xi_k^* &= \mathbb{E}\left\{\max\left[\Phi_{eff}^{k+1}\left(T, \tau_{m_{(k+1)}}\boldsymbol{\Omega}\left(m_{(k+1)}\right)\right), \Xi_{k+1}^*\right]\right\} \\
&= \mathbb{E}\left\{\Phi_{eff}^{k+1}\left(T, \tau_{m_{(k+1)}}\boldsymbol{\Omega}\left(m_{(k+1)}\right)\right)\right\}|\Delta_1 + \mathbb{E}\left\{\Xi_{k+1}^*\right\}|\Delta_2 \\
&= \iint_{\Delta_1} \Phi_{eff}^{k+1} f_{\tau T}(\tau, t)\, d\tau dt + \Xi_{k+1}^* \iint_{\Delta_2} f_{\tau T}(\tau, t)\, d\tau dt \\
&= \int_{T_{\min}}^{T_{\max}} \int_{\Xi_k}^{\tau_{\max}} \left(t - \sum |k+1|\right) \frac{1}{t} \frac{t^{(\mu-1)} e^{\left(-\frac{t}{\rho}\right)}}{\Gamma(\mu)\rho^{\mu}} d\tau dt \\
&+ \Xi_{k+1}^* \int_{T_{\min}}^{T_{\max}} \int_{\tau_{\min}}^{\Xi_k} \frac{1}{t} \frac{t^{(\mu-1)} e^{\left(-\frac{t}{\rho}\right)}}{\Gamma(\mu)\rho^{\mu}} d\tau dt \\
&= \left[\tau_{\max} + \left(\Xi_{k+1}^* - 1\right)\Xi_k - \Xi_{k+1}^* \tau_{\min}\right] \\
&\times \int_{T_{\min}}^{T_{\max}} \frac{t^{(\mu-2)} e^{\left(-\frac{t}{\rho}\right)}}{\Gamma(\mu)\rho^{\mu}} dt \\
&- \sum |k+1| \int_{T_{\min}}^{T_{\max}} \int_{\Xi_k}^{\tau_{\max}} \frac{t^{(\mu-2)} e^{\left(-\frac{t}{\rho}\right)}}{\Gamma(\mu)\rho^{\mu}} d\tau dt
\end{aligned} \tag{5.36}$$

where Δ_1 and Δ_2 denote the integral intervals under the conditions of $\Phi_{eff}^{k+1} \geqslant \Xi_{k+1}^*$ and $\Phi_{eff}^{k+1} < \Xi_{k+1}^*$, respectively. □

Remark 5.4.4. *The thresholds $\{\Xi_k^*\}_{k=1}^{|M|-2}$ can be interpreted as the maximal expected reward that the controller can find by seeking a better relay from phase $k+1$ to phase $|M|$ rather than performing data transmission after the k^{th} phase. Thus, the controller will compute the sequence of thresholds $\{\Xi_k^*\}_{k=1}^{|M|-2}$ in accordance with* ***Theorem 6*** *before relay signal detection. Once relay detection starts, the controller in the AP compares the instantaneous reward $T_{eff}^k\left[T, \tau_{m_{(k)}}\boldsymbol{\Omega}\left(m_{(k)}\right)\right]$ against the expected threshold Ξ_k^*. If the threshold is greater than this instantaneous reward, then the controller continues to detect the next relay; otherwise, it terminates the detection process and decides to proceed to the multiuser cooperative mobility phase. In such a case, the indicator function $\boldsymbol{\Omega}(m_i)$ for relay selection can be obtained as*

$$\begin{aligned}
&\boldsymbol{\Omega}(m_i) = \left(\mathcal{A}^T, \mathcal{B}^T\right), \\
&\mathcal{A}^{|\widehat{R}|\times 1} \triangleq \left(\mathbf{1}_{(0)}, ..., \mathbf{1}_{(k^*)}, ..., \mathbf{1}_{\left(|\widehat{R}|\right)}\right)^T, \\
&\mathcal{B}^{\left(|M|-|\widehat{R}|\right)\times 1} \triangleq \left(\mathbf{0}, ..., \mathbf{0}_{(j)}, ..., \mathbf{0}\right)^T, \\
&k^* := \underset{k}{arg\min}\left(\Xi_k^*\right), j \in \mathcal{M} \setminus \{k^*\}
\end{aligned} \tag{5.37}$$

where $\boldsymbol{\Omega}(m_i)$ indicates that each relay is selected in accordance with the optimal stopping policy, i.e., the previously described process of comparison against an expected threshold Ξ_k^* in the k^{th} phase needs to be repeated $|F|$ times until a sufficient number of relays are selected, and the label of each selected relay is k.

To summarize, our relay selection scheme can be described in two steps. The first step is to select feasible relays to ensure stable social links such that each link's intimacy is greater than a predefined threshold. In the second step, the relays with the longest effective transmission times are selected on the basis of the optimal stopping problem.

5.4.2 Link interference degree graph

After relay selection, problem (5.27) is transformed into a relay-location-based optimization problem, in which the relay coordinates that maximize the throughput can be attained through multiuser cooperative mobility. Therefore, the optimization problem based on the RUD distance variables $\boldsymbol{D}$ can be expressed as

$$
\begin{aligned}
(\mathbf{P2}): \quad & \max_{\boldsymbol{D}} \frac{|F|}{\sum_{i=1}^{|F|} \frac{1}{R_{eff,f_i}(\boldsymbol{D})}} \\
\text{s.t.} \quad & p(\boldsymbol{D}) \geqslant \overline{p}, \\
& \frac{\gamma_{\mathrm{AP},\widehat{r}_i}\gamma_{\widehat{r}_i,f_i}}{\gamma_{\mathrm{AP},\widehat{r}_i}+\gamma_{\widehat{r}_i,f_i}+1} \geqslant \overline{\gamma}, \\
& \gamma_{\widehat{r}_i,f_i} \geqslant \overline{\gamma}, \\
& \gamma_{\mathrm{AP},\widehat{r}_i} \geqslant \overline{\gamma}, \\
& D_{\widehat{r}_i,f_i} \leqslant 2L, \\
& D_{\widehat{r}_i,m_j} \leqslant 2L, \\
& \widehat{r}_i \in \widehat{\mathcal{R}}, f_i \in \mathcal{F}, m_j \in \widetilde{\mathcal{R}} \cup \widehat{\mathcal{R}} \backslash \{\widehat{r}_i\}
\end{aligned}
\tag{5.38}
$$

The goal of this problem can be characterized as choosing the optimal coordinates for the RUDs to achieve the highest transmission rate and throughput performance with limited distance and interference between nodes while satisfying all physical constraints and reliability requirements. Since **P2** is a nonconvex optimization problem, we would like to transform it into a convex problem using graph theory concepts. Therefore, we introduce the definition of the link interference degree graph. Within the limited circular space $\mathbb{C}$, the communication links established with the D2D technique in the ad hoc network can be represented by a physical graph $\boldsymbol{G}_p = (\mathcal{H}, E)$, where $\mathcal{H}$ is the set of all device nodes and edge $(u, v) \in E$ exists only if the SINR of the link between nodes u and v is no less than a threshold value $\overline{\gamma}$.
Definition 1: (Link interference degree graph (LIDG)): Given a communication graph $\boldsymbol{G}_p = (\mathcal{H}, E)$, the corresponding LIDG $\boldsymbol{G}_{LIDG} = (\mathcal{V}, \mathcal{E})$ in a sense quantitative extension of the conflict graph, that is:

- $\mathcal{V} := E$; that is, a vertex $v \in \mathcal{V}$ is introduced for each link $e \in E$ in $\boldsymbol{G}_p = (\mathcal{H}, E)$. A weighted edge $e \in \mathcal{E}$ is inserted between nodes $u, v \in \mathcal{V}$ that interfere with each other, where u and v correspond to links $e_1, e_2 \in E$ in the physical graph. Specifically, the weights of the edges represent the degrees of interference at the receiver nodes.

- $\boldsymbol{G}_{LIDG} = (\mathcal{V}, \mathcal{E})$ is a directed graph, and each directed edge $e_i = (u, v) \in \mathcal{E}$ is assigned a weight $W^i_{u,v}$, where $W^i_{u,v} = W^j_{v,u}$ does not always hold. This means that two vertices $e_i = (u, v)$ and $e_j = (v', u)$ in $\boldsymbol{G}_{LIDG} = (\mathcal{V}, \mathcal{E})$ generally do not have equal link interference degrees as a result of the channel states and fading coefficients.

- Each vertex $v \in \mathcal{V}$ has an incoming degree I_v and an outgoing degree O_v, where the incoming degree represents the level of interference from other nodes with that node and the outgoing degree represents its level of interference to other nodes. Node $v \in \mathcal{V}$ in $\boldsymbol{G}_{LIDG} = (\mathcal{V}, \mathcal{E})$ is feasible if and only if

$$\frac{P^i_v}{n_0 + \sum_{v' \in \mathcal{V} \setminus \{v\}} I_{v'}} \geqslant \overline{\gamma} \tag{5.39}$$

  where P^i_v is the received power, which depends on d_v, i.e., the geometric distance of this link in the communication graph $\boldsymbol{G}_p$.

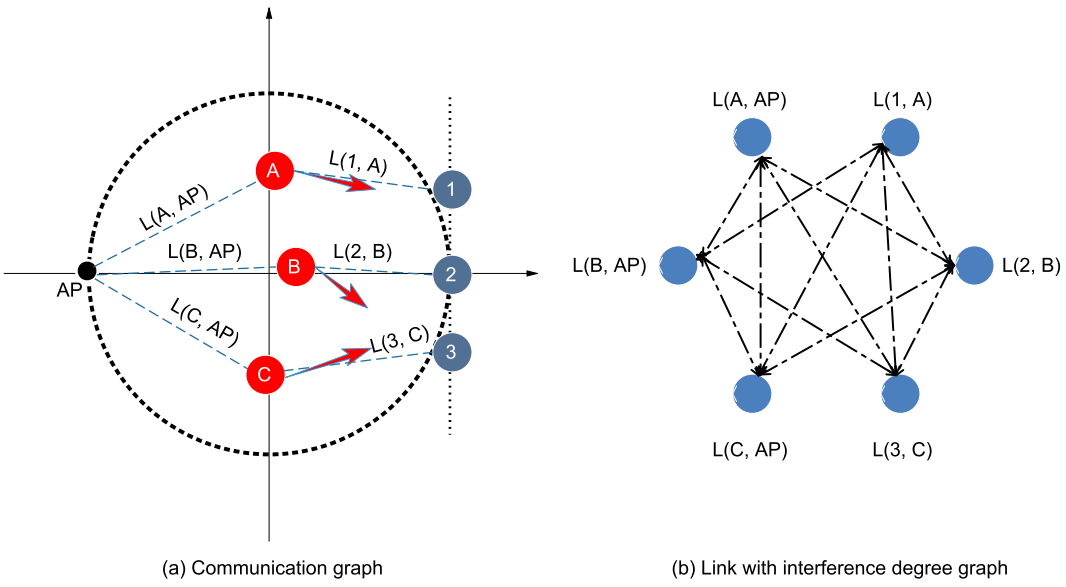

(a) Communication graph (b) Link with interference degree graph

Fig. 5.4 A specific illustration explains the definition and attributes of the LIDG: (a) Communication graph; (b) Link interference degree graph.

A specific illustration is given, as shown in Fig. 5.4, to better characterize the definition and attributes of the LIDG. In Fig. 5.4(a), the RUDs (nodes A, B and C) act as transmission intermediaries connecting the AP and the FUDs (nodes 1, 2 and 3), ultimately forming six communication links, L (A, AP) , ...L (3, C). These links correspond to nodes in Fig. 5.4(b), and the weighted edges between these nodes are bidirectional, representing the corresponding degrees of interference. Specifically, $\boldsymbol{G}_{LIDG} = (\mathcal{V}, \mathcal{E})$ is a directed complete graph in which all edges are directed and two edges with opposite directions connect every pair of vertices. For an arbitrary pair of bidirectional edges $e_i = (u, v) \in \mathcal{E}$ and $e_j = (v', u) \in \mathcal{E}$,

their weights $W_{u,v}^{i}$ and $W_{v',u}^{j}$ are generally not equal in value, that is, $W_{u,v}^{i} \neq W_{v',u}^{j}$. Therefore, the set of weights for these bidirectional edges forms a weight matrix with zeros on the diagonal, $\boldsymbol{\Theta}^{2|F|\times 2|F|}$, which is expressed as

$$\boldsymbol{\Theta} = \begin{pmatrix} 0 & W_{2,1}^{1} & \cdots & W_{u,1}^{1} & \cdots & W_{2|F|-1,1}^{1} & W_{2|F|,1}^{1} \\ W_{1,2}^{1} & 0 & \cdots & W_{u,2}^{2} & \cdots & W_{2|F|-1,2}^{2} & W_{2|F|,2}^{2} \\ \cdots & \cdots & \cdots & \cdots & \cdots & \cdots & \cdots \\ W_{1,v}^{i} & W_{2,v}^{i} & \cdots & W_{u,v}^{i} & \cdots & W_{2|F|-1,v}^{i} & W_{2|F|,v}^{i} \\ \cdots & \cdots & \cdots & \cdots & \cdots & \cdots & \cdots \\ W_{1,2|F|-1}^{2|F|-1} & W_{2,2|F|-1}^{2|F|-1} & \cdots & \cdots & \cdots & 0 & W_{2|F|,2|F|-1}^{2|F|-1} \\ W_{1,2|F|}^{2|F|} & W_{2,2|F|}^{2|F|} & \cdots & W_{u,2|F|}^{2|F|} & \cdots & W_{2|F|-1,2|F|}^{2|F|} & 0 \end{pmatrix} \tag{5.40}$$

Furthermore, for any node $v \in \mathcal{V}$, the incoming degree I_v and the outgoing degree O_v are given by

$$I_v = \sum_{u=1}^{2|F|} W_{u,v}^{i} = \sum_{n} \boldsymbol{\Theta}\left(m,n\right) \tag{5.41}$$

$$O_v = \sum_{u=1}^{2|F|} W_{v,u}^{j} = \sum_{m} \boldsymbol{\Theta}\left(m,n\right) \tag{5.42}$$

According to (5.6) and (5.8), $W_{u,v}^{i}$ and $W_{v,u}^{j}$ can be expressed as

$$W_{u,v}^{i} = \left|H_{u,v}^{i}\right|^{2} P_{u}^{i} K d_{u,v}^{-\alpha} \tag{5.43}$$

$$W_{v,u}^{j} = \left|H_{v,u}^{j}\right|^{2} P_{v}^{j} K d_{v,u}^{-\alpha} \tag{5.44}$$

where $H_{u,v}^{i}$ is the channel fading coefficient from node u to node v; P_{u}^{i} is the transmission power of node u, $P_{u}^{i} = P_0 K d_{u}^{-\alpha}$; and $d_{u,v}$ denotes the distance between nodes u and v, $d_{u,v} = d_{v,u}$, i.e., the interference power of the transmitting node on link u with respect to the receiving node on link v in the physical graph $\boldsymbol{G}_p = (\mathcal{H}, E)$.

Theorem 3: A sufficient and necessary condition for achieving the maximum system throughput is to minimize the sum of the incoming and outgoing degrees for all nodes in $\boldsymbol{G}_{LIDG} = (\mathcal{V}, \mathcal{E})$. To this end, the following should be satisfied:

$$\max_{\boldsymbol{D}} \frac{|F|}{\sum_{i=1}^{|F|} \frac{1}{R_{eff,f_i}(\boldsymbol{D})}} \rightleftharpoons \min_{d_u, d_v, d_{u,v}} \sum_{\substack{u,v \in \mathcal{V} \\ e_i, e_j \in \mathcal{E}}} \left(I_v + O_v\right) \tag{5.45}$$

where d_u and d_v represent the geometric distances of links e_1 and e_2, respectively, that is, $d_u \sim e_1$ and $d_v \sim e_2$, for $e_1, e_2 \in E$ in the communication graph $\boldsymbol{G}_p$.

Proof. On one hand, the maximum throughput of this ad hoc network is equivalent to the maximum transmission rate per unit time for adequacy. In other words, the transmission rate of the whole system is globally optimal for the locations of the relay nodes after mobility within the limited circular space $\mathbb{C}$. At this point, globally, the total SINR among nodes is

maximized. Thus, with a known constant transmission power, the total interference among nodes is minimized. The minimization of the total interference implies the minimization of the sum of all nodes' incoming and outgoing degrees, which reflects the total level of interference in the system. Therefore, the necessity has been proven.

On the other hand, when the sum of the incoming and outgoing degrees of all nodes is minimized, the global interference level is minimized, which means that the SINR of this ad hoc network is maximized. The effective transmission rate of the nodes is also maximized, implying that the maximum throughput can be obtained at the locations after the relay nodes have moved. Hence, the sufficiency has been proven. □

Remark 5.4.5. *As mentioned, the objective function of this optimization problem is a nonconvex function, and therefore,* ***P2*** *is obviously a nonconvex optimization problem. According to* ***Theorem 3****, instead of maximizing the system throughput, the objective function can be recast to minimize the sum of the incoming and outgoing degrees of all nodes in* $\boldsymbol{G}_{LIDG} = (\mathcal{V}, \mathcal{E})$*. Thus, we obtain the following optimization problem:*

$$
\begin{aligned}
(\mathbf{P3}): \quad & \min_{d_u, d_v, d_{u,v}} \quad \sum_{\substack{u,v \in \mathcal{V} \\ e_i, e_j \in \mathcal{E}}} (I_v + O_v) \\
\textit{s.t.} \quad & p_r\left(d_u, d_v, d_{u,v}\right) s_{u,v}\left(\boldsymbol{\Omega}\right) \geqslant \overline{p}, \\
& \frac{P_0 K d_u^{-\alpha} d_v^{-\alpha}}{d_u^{-\alpha}\left[I_v + n_0\right] + d_v^{-\alpha}\left[I_o + n_0\right] + \sigma} \geqslant \overline{\gamma}, \\
& 0 \leqslant d_u \leqslant 2L, \\
& 0 \leqslant d_v \leqslant 2L
\end{aligned}
\tag{5.46}
$$

where P_0 *is the transmission power,* $p_r\left(d_u, d_v, d_{u,v}\right)$*,* I_v*,* I_o *and* σ *are expressed as*

$$
\begin{aligned}
p_r\left(d_u, d_v, d_{u,v}\right) &= 1 - F_Y\left(2^{\frac{Z}{T - \sum_{i \in \mathcal{M}} \tau_i(\boldsymbol{V})}} - 1\right), \\
k_1 &= \frac{P_0 d_u^{-\alpha}}{I_v + n_0}, \\
k_2 &= \frac{P_0 d_v^{-\alpha}}{I_o + n_0}
\end{aligned}
\tag{5.47}
$$

$$
I_v = \sum_{u=1}^{2|F|} \left|H_{u,v}^i\right|^2 P_0 K d_{u,v}^{-\alpha} \tag{5.48}
$$

$$
O_v = \sum_{u=1}^{2|F|} \left|H_{v,u}^j\right|^2 P_0 K d_{v,u}^{-\alpha} \tag{5.49}
$$

$$
\sigma \triangleq \frac{\left(I_v + n_0\right)\left(I_o + n_0\right)}{P_0 K} \tag{5.50}
$$

According to the definition of convex optimization [101], **P3** is a convex optimization problem. Since the objective function and other inequality constraints are affine functions, according to Slatter's theory [102], the Karush-Kuhn-Tucker (KKT) conditions are necessary and sufficient conditions for the optimal solution to problem (5.46). We can obtain the approximate optimal solution by applying the KKT optimality conditions and the Lagrange multiplication method. For this purpose, the Lagrange function is given by

$$\begin{aligned}
&\mathcal{L}\left(d_u, d_v, d_{u,v}, \pi_1, \pi_2, \pi_3, \pi_4\right) \\
&= \sum_{\substack{u,v \in \mathcal{V} \\ i,j \in \mathcal{E}}} \left(I_v + O_v\right) + \pi_1 \left[p_r\left(d_u, d_v, d_{u,v}\right) s_{u,v}\left(\boldsymbol{\Omega}\right) - \overline{p}\right] \\
&+ \pi_2 \left(\frac{P_0 K d_u^{-\alpha} d_v^{-\alpha}}{d_u^{-\alpha}\left[I_v + n_0\right] + d_v^{-\alpha}\left[I_o + n_0\right] + \sigma} - \overline{\gamma}\right) \\
&+ \pi_3\left(2L - d_u\right) + \pi_4\left(2L - d_v\right)
\end{aligned} \tag{5.51}$$

where π_1, π_2, π_3 and π_4 are nonnegative Lagrange multipliers. The dual approach thus results in an elegant decomposition of the original problem. We introduce a dual function as follows:

$$\begin{aligned}
&\max_{\pi_1,\pi_2,\pi_3,\pi_4} \min_{d_u,d_v,d_{u,v}} \mathcal{L}\left(d_u, d_v, d_{u,v}, \pi_1, \pi_2, \pi_3, \pi_4\right) \\
&\text{s.t.} \quad p_r\left(d_u, d_v, d_{u,v}\right) s_{u,v}\left(\boldsymbol{\Omega}\right) \geqslant \overline{p}, \\
&\qquad \frac{P_0 K d_u^{-\alpha} d_v^{-\alpha}}{d_u^{-\alpha}\left[I_v + n_0\right] + d_v^{-\alpha}\left[I_o + n_0\right] + \sigma} \geqslant \overline{\gamma}, \\
&\qquad 0 \leqslant d_u \leqslant 2L, \\
&\qquad 0 \leqslant d_v \leqslant 2L.
\end{aligned} \tag{5.52}$$

As a result, the original optimization problem satisfies duality, which can be expressed as

$$\max_{\pi_1,\pi_2,\pi_3,\pi_4} \min_{d_u,d_v,d_{u,v}} \mathcal{L} = \min_{d_u,d_v,d_{u,v}} \max_{\pi_1,\pi_2,\pi_3,\pi_4} \mathcal{L} \tag{5.53}$$

Thus, the duality holds such that the globally optimal solution to (5.46) satisfies the KKT conditions, which are expressed as follows:

$$\begin{cases}
\frac{\partial \mathcal{L}}{\partial d_{u,v}} = 0 \\
\frac{\partial \mathcal{L}}{\partial d_u} = 0 \\
\frac{\partial \mathcal{L}}{\partial d_v} = 0 \\
\pi_1\left[p_r\left(d_u, d_v, d_{u,v}\right) s_{u,v}\left(\boldsymbol{\Omega}\right) - \overline{p}\right] = 0 \\
\pi_2\left(\frac{P_0 K d_u^{-\alpha} d_v^{-\alpha}}{d_u^{-\alpha}[I_v+n_0]+d_v^{-\alpha}[I_o+n_0]+\sigma} - \overline{\gamma}\right) = 0 \\
\pi_3\left(2L - d_u\right) \geqslant 0 \\
\pi_4\left(2L - d_v\right) \geqslant 0
\end{cases} \tag{5.54}$$

The optimal distance between nodes in $\boldsymbol{G}_{LIDG} = (\mathcal{V}, \mathcal{E})$ is given by

$$
\begin{aligned}
d_{u,v}^{\ell} &= \left[\sqrt[\alpha]{\frac{e^{\frac{-0.5\lambda Z}{T-\sum_{i\in\mathcal{M}}\tau_i(\boldsymbol{V})}}\left(\Psi_1\left(1-\frac{Z}{T-\sum_{i\in\mathcal{M}}\tau_i(\boldsymbol{V})}\right)-\sqrt{\Psi_2\left(\left\{d_u^{\ell-1}\right\}^{-\alpha}+\left\{d_v^{\ell-1}\right\}^{-\alpha}\right)}\right)}{\left(2^{\frac{Z}{T-\sum_{i\in\mathcal{M}}\tau_i(\boldsymbol{V})}}-1\right)\eta\left(2d_u^{\ell-1}+2d_v^{\ell-1}+KP_0\pi_2 d_u^{\ell-1}d_v^{\ell-1}\right)-\overline{\gamma}}} \right]^{+}, \\
\Psi_1 &\triangleq 2P_0\overline{p}\eta\left(d_u^{\ell-1}+d_v^{\ell-1}\right), \\
\Psi_2 &\triangleq P_0\pi_1\eta s_{u,v}\left(\boldsymbol{\Omega}\right)
\end{aligned}
\tag{5.55}
$$

where ℓ is the iteration index. Similarly, the optimal distance between nodes in $\boldsymbol{G}_{LIDG} = (\mathcal{V}, \mathcal{E})$ can be expressed as

$$
d_u^{\ell} = \left[\sqrt[\alpha]{\frac{\left\{d_v^{\ell-1}\right\}^{-\alpha}\left(\sqrt{KP_0\overline{p}\pi_2\pi_3\left\{d_{u,v}^{\ell-1}\right\}^{-\alpha}}-\pi_3\right)}{\overline{\gamma}\pi_3}} \right]^{+} \tag{5.56}
$$

$$
d_v^{\ell} = \left[\sqrt[\alpha]{\frac{\left\{d_u^{\ell-1}\right\}^{-\alpha}\left(\sqrt{KP_0\overline{p}\pi_2\pi_4\left\{d_{u,v}^{\ell-1}\right\}^{-\alpha}}-\pi_4\right)}{\overline{\gamma}\pi_4}} \right]^{+} \tag{5.57}
$$

Additionally, the remaining Lagrange multipliers can be updated in accordance with the gradient descent method [103], as follows:

$$
\begin{cases}
\pi_1^{\ell+1} = \pi_1^{\ell} - \xi_1\left[\, p_r\left(d_u, d_v, d_{u,v}\right) s_{u,v}\left(\boldsymbol{\Omega}\right) - \overline{p}\right]^{+} \\
\pi_2^{\ell+1} = \pi_2^{\ell} - \xi_2\left[\frac{P_0 K d_u^{-\alpha} d_v^{-\alpha}}{d_u^{-\alpha}[I_v+n_0]+d_v^{-\alpha}[I_o+n_0]+\sigma} - \overline{\gamma}\right]^{+} \\
\pi_3^{\ell+1} = \pi_3^{\ell} - \xi_3\left[2L - d_u\right]^{+} \\
\pi_4^{\ell+1} = \pi_4^{\ell} - \xi_4\left[2L - d_v\right]^{+}
\end{cases}
\tag{5.58}
$$

where ξ_1, ξ_2, ξ_3 and ξ_4 are positive step lengths. The iterative process is guaranteed to converge to yield an approximately optimal solution when these step sizes are sufficiently small.

Since the approximately optimal solution must be obtained via an iterative approach, we design an iterative algorithm, named the iteration algorithm for multiuser cooperative mobility, to represent the execution process of the equations and the implemented entities, which is elaborated in **Algorithm 6**.

In the first stage of Algorithm 6 (lines 1-4), $\boldsymbol{G}_{LIDG} = (\mathcal{V}, \mathcal{E})$ as defined in Definition 1 is derived from the input data (the communication graph and the CSI), and then, the parameters and control thresholds of the iterative process are initialized. In the second stage (lines 6-19),

the objective parameters ($d_{u,v}^{\ell}$, d_u^{ℓ} and d_v^{ℓ}) and Lagrange multipliers are iteratively updated until $\ell > \ell_{\max}$. During the iterative process, a judgment condition aims to ensure that the difference between the objective parameters and the optimal solution is sufficiently small to approximate the optimal solution. Finally, the algorithm outputs the final optimal distances $d_{u,v}^{*}$, d_u^{*} and d_v^{*} in the LIDG, from which the optimal position coordinates of the RUDs in the communication graph can be determined.

Lines 5-21 will be executed $\lceil \ell_{\max} \rceil$ times. Additionally, lines 16-20 will be executed $\lceil \max\left\{\log_2 \frac{d_{u,v}^{\ell}}{\vartheta_{u,v}}, \log_2 \frac{d_u^{\ell}}{\vartheta_u}, \log_2 \frac{d_v^{\ell}}{\vartheta_v}\right\} \rceil$ times, where $\vartheta_{u,v}$, ϑ_u and ϑ_v denote control thresholds. Note that the distances between nodes are less than $2L$ in each iteration, i.e., $\max\left\{d_u^{\ell}, d_v^{\ell}\right\} \leqslant 2L$. This implies that lines 16-20 should be executed $\lceil \max\left\{\log_2 \frac{d_{u,v}^{\ell}}{\vartheta_{u,v}}, \log_2 \frac{2L}{\vartheta_u}, \log_2 \frac{2L}{\vartheta_v}\right\} \rceil$ times. However, due to lines 7-11, the worst-case complexity of this algorithm is $\lceil \ell_{\max} \rceil$ executions. Thus, the complexity of **Algorithm 6** is $\mathcal{O}\left(\ell_{\max}\right)$. If $\ell_{\max}$ is too large, the complexity of the algorithm is too high; if it is too small, then the accuracy of the solution will not be sufficient to approximate the optimal solution. Therefore, to achieve a desirable tradeoff, we set $\ell_{\max}$ in the range of $[10^5, 10^6]$ in the following simulation study [104].

Algorithm 6: Iteration Algorithm for Multiuser Cooperative Mobility

Input: Communication graph $\boldsymbol{G}_p = (\mathcal{H}, E)$ and channel state information (CSI).

1 Convert $\boldsymbol{G}_p = (\mathcal{H}, E)$ into $\boldsymbol{G}_{LIDG} = (\mathcal{V}, \mathcal{E})$ in accordance with **Definition 1** and then obtain $d_{u,v}^{(0)}$, $d_u^{(0)}$ and $d_v^{(0)}$ in $\boldsymbol{G}_{LIDG} = (\mathcal{V}, \mathcal{E})$;
2 Initialize $\ell = 0$ and the Lagrange multipliers π_1^0, π_2^0, π_3^0 and π_4^0;
3 Initialize the maximum number of iterations $\ell_{\max}$ [33] and the control thresholds $\vartheta_{u,v}$, ϑ_u and ϑ_v;
4 Let $d_{u,v}^{*} = d_{u,v}^{(0)}$, $d_{u,v}^{*} = d_{u,v}^{(0)}$ and $d_{u,v}^{*} = d_{u,v}^{(0)}$;
5 **while** $\ell \leqslant \ell_{\max}$ **do**
6 **if** $\ell + 1 > \ell_{\max}$ **then**
7 $d_{u,v}^{*} = d_{u,v}^{\ell}$;
8 $d_u^{*} = d_u^{\ell}$;
9 $d_v^{*} = d_v^{\ell}$;
10 **else**
11 Update $d_{u,v}^{\ell}$ using (5.55);
12 Update d_u^{ℓ} using (5.56);
13 Update d_v^{ℓ} using (5.57);
14 Update the Lagrange multipliers π_1^{ℓ}, π_2^{ℓ}, π_3^{ℓ} and π_4^{ℓ} using (56);
15 **end**
16 **if** $\left\{d_{u,v}^{\ell} - d_{u,v}^{\ell-1} < \vartheta_{u,v}\right\} andand \left\{d_u^{\ell} - d_u^{\ell-1} < \vartheta_u\right\} andand \left\{d_v^{\ell} - d_v^{\ell-1} < \vartheta_v\right\}$ **then**
17 $d_{u,v}^{*} = d_{u,v}^{\ell}$;
18 $d_u^{*} = d_u^{\ell}$;
19 $d_v^{*} = d_v^{\ell}$;
20 **end**
21 **end**

Output: $d_{u,v}^{*}$, d_u^{*} and d_v^{*}.

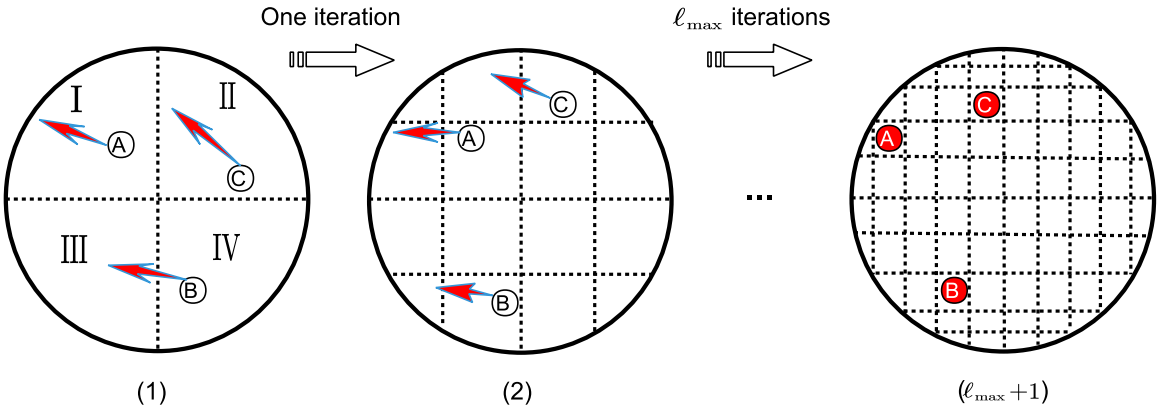

Fig. 5.5 Iteration of the multiuser cooperative mobility process involved three RUDs (A, B, C).

Although Algorithm 6 describes the method of calculating the optimal locations of the relay nodes in detail, the multiuser cooperative mobility process for the RUDs has not been elaborated. To facilitate its description, we present a vivid example for illustration in Fig. 5.5. Initially, three RUDs, A, B and C, are randomly distributed in a limited circular active area divided into four blocks. Thus, we can roughly record the RUDs' position coordinates in accordance with the distribution of the blocks. As shown in Fig. 5.5(1), A, B, and C are located in three different blocks, denoted by $\boldsymbol{U}_A = \{\text{I}\}$, $\boldsymbol{U}_B = \{\text{IV}\}$ and $\boldsymbol{U}_C = \{\text{III}\}$. Fig. 5.5(2) depicts that in the next iteration, the number of blocks increases exponentially, with an exponent of 2, to sixteen, and the positions of the RUDs are also updated based on the algorithm. By the $\ell_{\max}^{th}$ iteration, the number of blocks is $2^{2\ell_{\max}}$, and these nodes have moved to their optimal positions, and the positions of the small blocks are the final coordinate representations of each node.

5.4.3 Overall algorithm

In this section, the overall RS-LIDG algorithm is proposed, which combines the relay selection scheme and the user cooperative mobility strategy as follows.

As described in **Algorithm 7**, the selection variables and parameters are first initialized, and potential RUDs are then selected from among the feasible MUDs whose social intimacy values are larger than a predefined threshold (lines 1-2). Lines 3-19 describe the iterative process of selecting $\left|\widehat{R}\right|$ relays. For the selection of each relay, the instantaneous reward is compared against the expected threshold. If the instantaneous reward is larger than the threshold, this potential node is selected as a new relay; otherwise, the process of detecting potential nodes continues until the last one is detected. During this process, if no node satisfying the abovementioned constraints is selected, then the last detected node is selected as a new relay, i.e., $k^* = |M|$. Finally, as shown in lines 20-24, the best relay selection

Algorithm 7: RS-LIDG Algorithm

Input: Communication graph $\boldsymbol{G}_p = (\mathcal{H}, E)$, social intimacy graph $\boldsymbol{G}_s = \{\mathcal{H}, \mathcal{S}\}$, channel gain information (CSI known).

Select feasible MUDs with social intimacy greater than the predefined threshold $\overline{s}$ as potential relays in $\boldsymbol{G}_s = \{\mathcal{H}, \mathcal{S}\}$;
Initialize the number of selected RUDs $j = 0$, the set of selected RUDs $\Re = \{\oslash\}$, and the stopping phase index $k = 0$;
while $j = |F|$ **do**
    Calculate the thresholds Ξ_k^* using (34);
    Calculate the instantaneous reward $\Phi_{eff}^k \left(T, \tau_{m_{(k)}} \boldsymbol{\Omega}\left(m_{(k)}\right)\right)$ using (31);
    if $\Phi_{eff}^k \left(T, \tau_{m_{(k)}} \boldsymbol{\Omega}\left(m_{(k)}\right)\right) < \Xi_k^*$ **then**
        Go back to step (5);
        if $|k| < |M|$ **then**
            $k = k + 1$;
        else
            Select the RUD with index $|M|$ as a new relay;
            Go to step (16);
        end
    else
        Select the RUD with index k^* as a new relay;
        $\Re = \Re \cup \{k^*\}$;
    end
    $j = j + 1$;
end
Map to the indicator function $\boldsymbol{\Omega}^*$ based on the index of set $\Re$, where $\exists m_i = \mathbf{1}$, $i = k^* \in \Re$;
Obtain the indicator function $\boldsymbol{\Omega}^*$ using (5.37);
Obtain $d_{u,v}^*$, d_u^* and d_v^* using Algorithm 1;
Obtain the optimal MUD position coordinates $\boldsymbol{U}^*$ based on $d_{u,v}^*$, d_u^* and d_v^*;
Calculate the optimal throughput Th_{sys}^* using (5.19);

Output: $\boldsymbol{\Omega}^*$, $\boldsymbol{U}^*$, and Th_{sys}^*.

scheme $\boldsymbol{\Omega}^*$ is obtained, and the optimal MUD position coordinates $\boldsymbol{U}^*$ are determined based on **Algorithm 6**.

Now, we present a simple analysis of the complexity of our proposed RS-LIDG algorithm. The original optimization problem (5.27) is decomposed into two subproblems, **P1** and **P2**. The first corresponds to the relay selection scheme and is solved by identifying the optimal stopping phase; hence, the complexity is $\mathcal{O}\left(k^* \left|\widehat{R}\right|\right)$. Furthermore, the index k^* is less than or equal to the number of MUDs $|M|$, meaning that the complexity is $\mathcal{O}\left(|M| \left|\widehat{R}\right|\right)$ in the worst case. As a result, the computational complexity of the proposed algorithm is $\mathcal{O}\left(\max\left\{\ell_{\max}, |M| \left|\widehat{R}\right|\right\}\right)$.

5.5 Simulation and performance analysis

In this chapter, the proposed algorithm is evaluated and compared with five conventional algorithms in terms of throughput performance and complexity.

- Intuitive method (IM) [9]: A mobile relay with sufficient social intimacy moves along a link to the midpoint location between the transmitter and receiver.
- Direct transmission (DT): As the name implies, direct D2D communication does not require any relay; instead, communication is sent directly from the AP to the receiver. However, considering the channel fading and distance factors, this method's performance is relatively low and can serve as a benchmark reference.
- Social-trust-based selection and random mobility (STS-RM) [6]: Relays are selected on the basis of the inherent social intimacy between users, regardless of the physical-layer characteristics. The selected RUDs move randomly within the limited circular mobility space.
- Physical-based selection and random mobility (PHS-RM) [7]: Relays are selected on the basis of the interference and SINR between users, regardless of the social-layer characteristics. Subsequently, the selected RUDs also move randomly.
- Random selection and random mobility (RS-RM): The controller randomly selects a relay without detection or valid algorithm checks. The cooperative mobility of the RUDs is also haphazard, without any explicit strategy.

5.5.1 Network parameter settings

In this ad hoc network, the activity scope of the RUDs is a circular area with radius L. The FUDs and AP are located on either side of this circular area, and the devices' initial coordinates follow a random distribution. Considering the actual mobility distance and relay requirements, we set L to range from 100 m to 200 m. Since the randomness of the initial locations may affect the results, we conducted more than 1,000 experiments and summarized the resulting statistics. Additionally, since social relationships vary with social domains and inherent trust, we set the link reliability threshold $\overline{p}$ to range from 0 to 1. We defined the mobility velocity for each RUD to be 1.5 m/s, which is the average speed of a pedestrian. Recall that our goal is to find the best selected relays and the optimal positions for cooperative mobility; hence, the mobility velocity will not affect the final throughput result. The variance of the exponential distribution in Rayleigh fading channels was considered to be 8 dB or 10 dB, so $\lambda = 0.4$ and $\eta = 0.9$, and we set $\frac{Z}{T_{eff}}$ to 7.5 [106]. We set the random variable of contact durations T to follow the gamma distribution $G_T \sim Gamma\left(4.43, \frac{1}{1088}\right)$ [107]. The detailed configuration of the simulation parameters is shown in Table 5.2.

Table 5.3 Parameter values for simulation.

Parameter	Value
Communication standard	IEEE 802.11g [105]
Number of FUDs ($\|F\|$)	10
Transport protocol	UDP
Path-loss exponent (α)	4.00
Path-loss constant (K)	1.00
Maximum D2D transmission power	10 dBm
White Gaussian Noise (N_0)	-90 dBm
D2D decoding threshold ($\overline{\gamma}$)	20 dB
Initial social intimacy threshold ($\overline{s}$)	0.4
Initial link reliability threshold ($\overline{p}$)	0.5
Wave frequency	2.4 GHz
System bandwidth ($\mathscr{B}$)	10 MHz
Rayleigh fading standard deviation (Ω)	8 dB

5.5.2 Throughput performance analysis

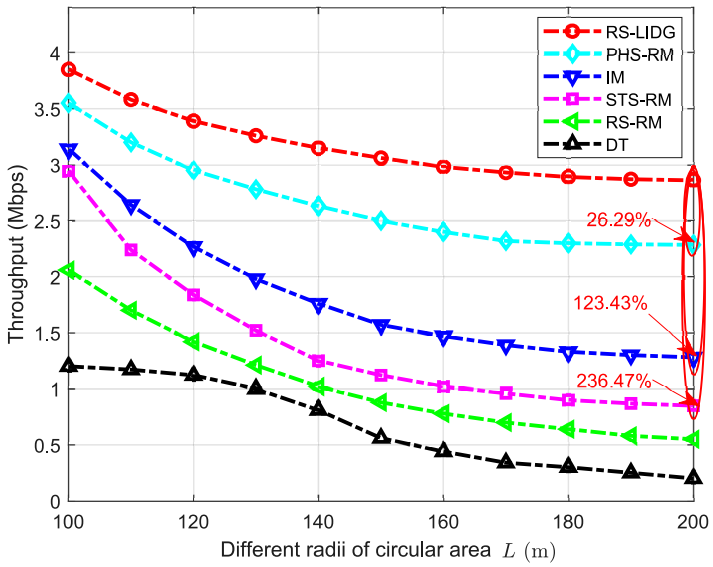

Fig. 5.6 System throughput comparison under the different radius of the mobile circular area L.

First, we evaluate our proposed RS-LIDG algorithm's throughput performance by comparing it with the above five conventional methods. Fig. 5.6 shows the system throughput obtained as the harmonic mean of all users' effective transmission rates, where $|M| = 20$, $\overline{s} = 0.4$ and $\overline{p} = 0.5$. From these results, one can observe that the throughput decreases as the mobility area's radius L increases for all six algorithms. For the DT method, the curve drops rapidly from 100 m to 140 m and then tends to stabilize up to 200 m. This is because

a larger L leads to stronger channel fading and lower received power for direct transmission. In contrast to that for DT, the curves for the other algorithms decline more smoothly, and our proposed algorithm shows the least degradation in throughput performance. The reason is that the number of available trunks per unit area is reduced; meanwhile, both the SINR and transmission rate are increased due to the relay selection scheme and user mobility, leading to positive feedback. Compared with PHS-RM, IM, and STS-RM, the proposed RS-LIDG algorithm achieves maximum throughput improvements of 26.29%, 123.43%, and 236.47%, respectively.

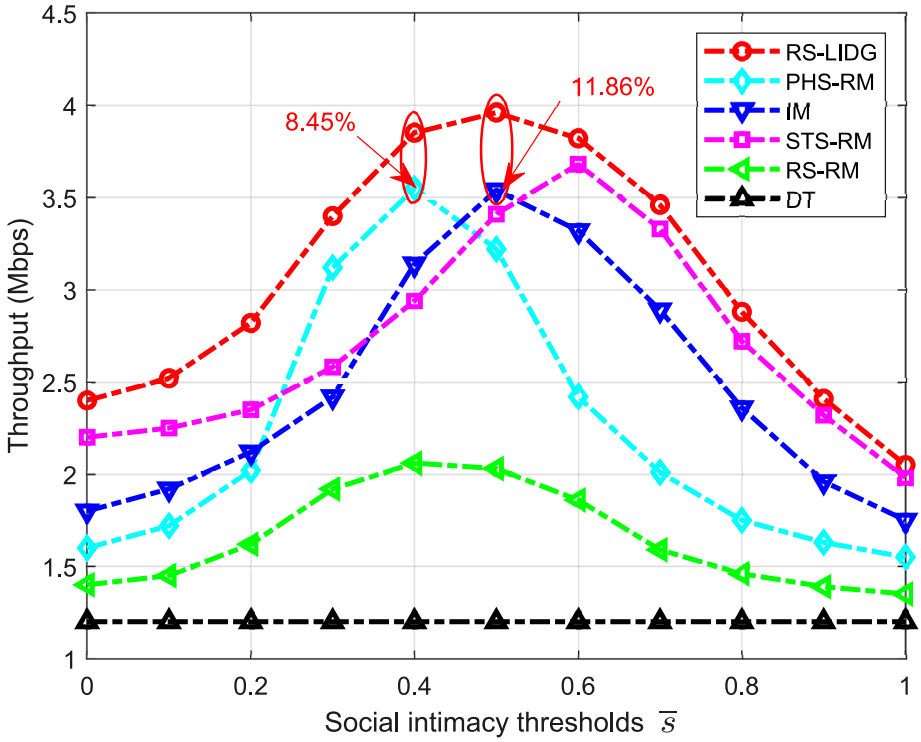

Fig. 5.7 System throughput comparison under different social intimacy thresholds $\overline{s}$.

Fig. 5.7 and Fig. 5.8 evaluate the impact of different social intimacy thresholds $\overline{s}$ and link reliability thresholds $\overline{p}$ on the system throughput, both of which are concave functions for all algorithms. As illustrated Fig. 5.7, the proposed RS-LIDG algorithm improves the throughput by 11.86% and 8.45% compared to IM and PHS-RM, respectively, where $L = 100$ m, $|M| = 20$ and $\overline{p} = 0.5$. For RS-LIDG and IM, the throughput reaches a maximum of $\overline{s} = 0.4$. For PHS-RM and STS-RM, the maximum points lie at $\overline{s} = 0.4$ and $\overline{s} = 0.6$. As illustrated in Fig. 5.8, the proposed RS-LIDG algorithm improves the throughput by 20.07%, 8.07% and 7.39% at the maximum points compared to IM, STS-RM and PHS-RM, respectively, where $L = 100$ m, $|M| = 20$ and $\overline{s} = 0.4$.

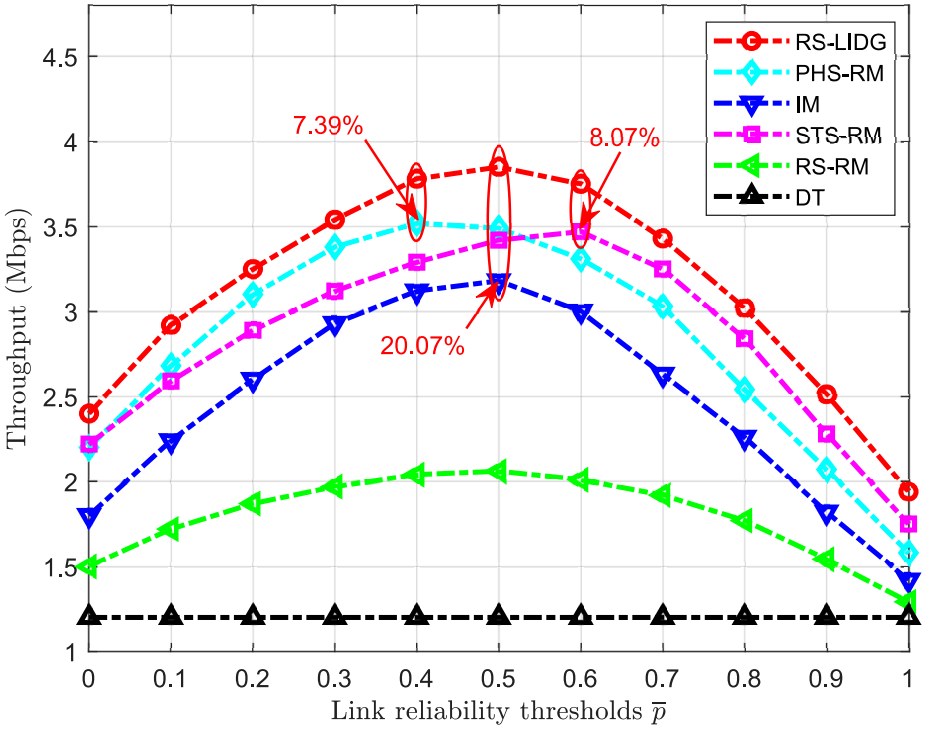

Fig. 5.8 System throughput comparison under different link reliability thresholds $\overline{p}$.

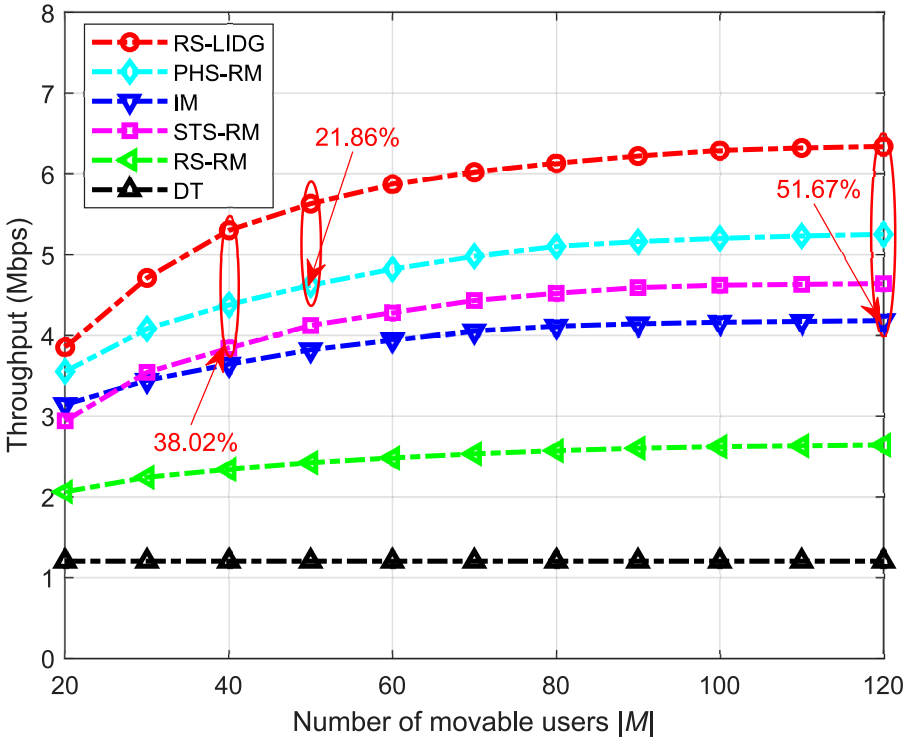

Fig. 5.9 System throughput comparison under different numbers of MUDs $|M|$.

This is because RUDs with low intimacy and low transmission success rates are eliminated while also ensuring the link reliability, resulting in an increase in the effective transmission time and SINR of each relay. After the peak point, the number of available MUDs is reduced such that a longer time is needed to select favorable relays while also incurring a reduction in link reliability. For RS-RM and DT, it can be seen that both $\overline{s}$ and $\overline{p}$ have little or no effect on the throughput. The reason is that due to the absence of relays or the random nature of the relay selection process, social attributes have almost no impact on throughput in either scenario.

Fig. 5.9 depicts the impact of different numbers of MUDs $|M|$ on the throughput, where $L = 100$ m and $\overline{s} = 0.4$. It can be observed that the throughput curves are increasing functions of $|M|$. We also observe that our proposed RS-LIDG algorithm achieves higher throughput than the other methods. The reasons are as follows. As the number of MUDs that can be selected grows, the probability of selecting an effective relay increases, allowing the transmission links selected for relaying to be stable, which effectively improves the transmission time and throughput. On the other hand, since the proposed method considers both physical and social constraints, the cooperative multiuser mobile strategy can effectively reduce user interference and improve the SINR. Finally, compared with PHS-RM, STS-RM, and IM, the throughput of RS-LIDG is increased by 21.86%, 38.02%, and 51.67%, respectively.

5.5.3 Relay selection cost and algorithm complexity analysis

In addition to evaluating the throughput performance, we also need to consider the relay selection cost and algorithm complexity. Fig. 5.10 shows a comparison of the system throughput throughout the iterative process. Note that the CPU of the computer used for simulation was an Intel(R) Core i7-8700 3.20 GHz. It can be seen from Fig. 5.10 that RS-LIDG reduces the relay selection time by 47.88% compared to PHS-RM. From the column chart in Figure 5.11, we can see that the RS-LIDG algorithm is faster than PHS-RM and close to STS-RM in terms of relay selection time.

This, in essence, can be attributed to the proposed relay selection scheme, particularly the calculation of the optimal stopping phase based on an instantaneous payoff greater than a preset threshold, while the process of preselecting potential RUDs guarantees that the social intimacy constraints are met. On the other hand, as expected, the complexity of the proposed multiuser cooperative mobility strategy, i.e., Algorithm 1, is relatively low, validating our algorithm complexity analyses above ($\mathcal{O}\left(\max\left\{\ell_{\max}, |M|\left|\widehat{R}\right|\right\}\right)$).

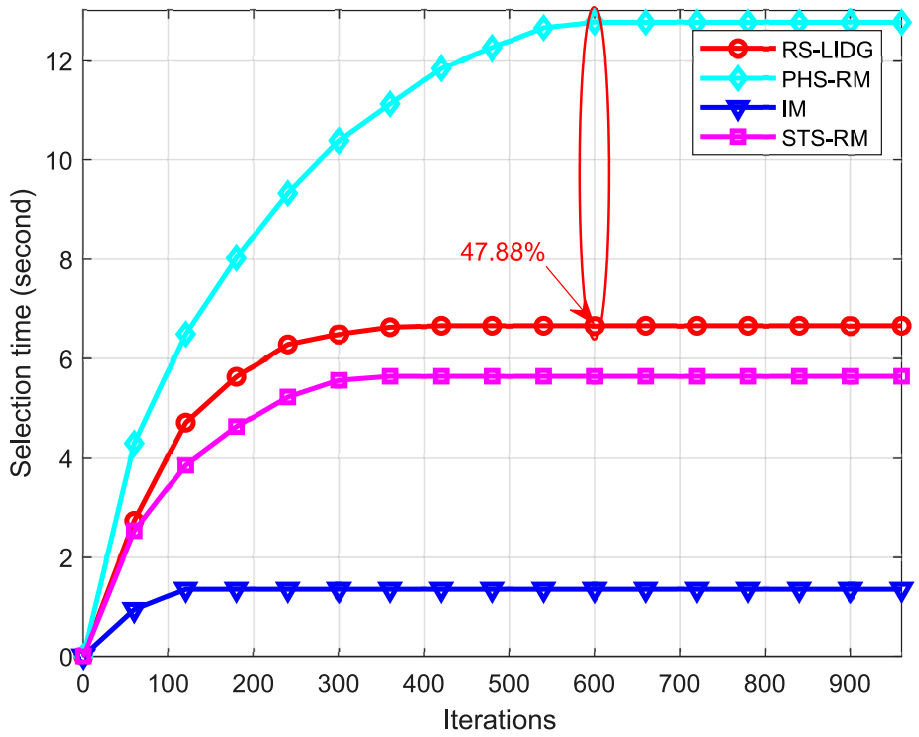

Fig. 5.10 Comparison of system throughput during iterations.

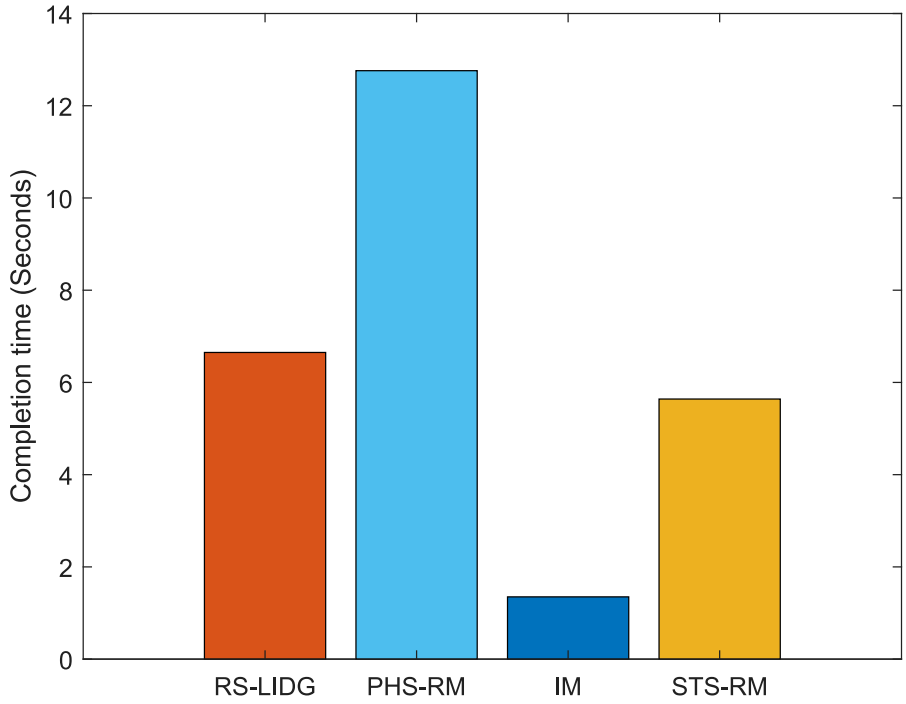

Fig. 5.11 Comparison histogram of system throughput for four algorithms: RS-LIDG, PHS-RM, IM, and STS-RM.

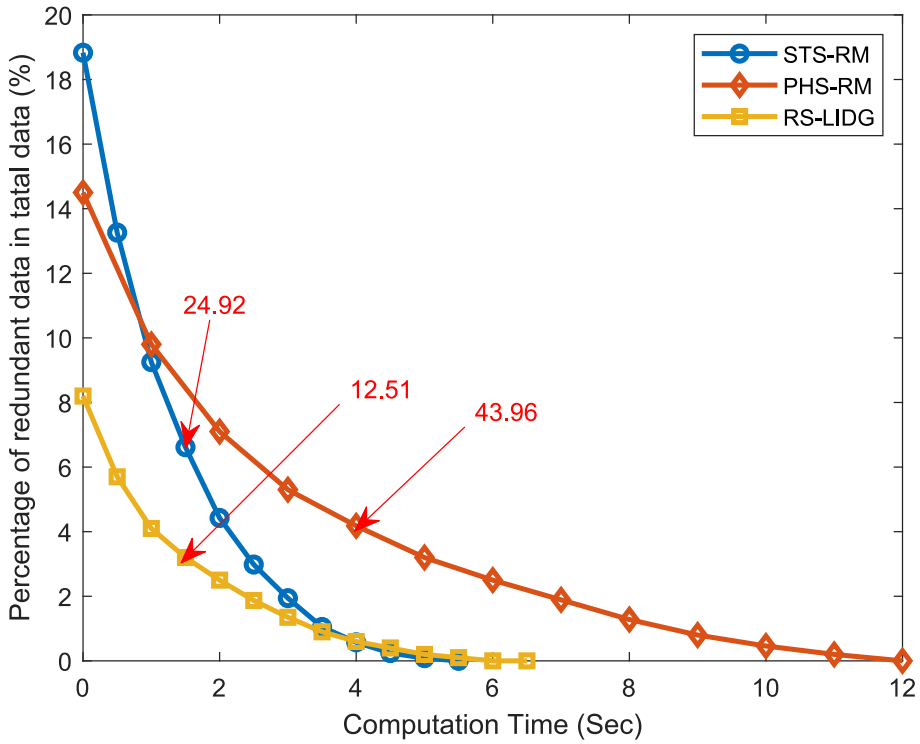

Fig. 5.12 Comparison histogram of system throughput for four algorithms: RS-LIDG, PHS-RM, IM, and STS-RM.

5.5.4 Communication overhead analysis

In a real network, the communication overhead of algorithm execution has a significant impact on the actual amount of data transferred. Here, the percentage of redundant data in the total is set as an evaluation indicator of the communication overhead, which consists of control information, user's location information, and valid policy information. The comparison of communication overhead among STS-RM, PHS-RM, and RS-LIDG is depicted in Fig. 5.12, where X-axis represents the computational time cost and Y-axis denotes the percentage of redundant data in total transferred. Therefore, the communication overhead is the area enclosed by the curve and the X-axis, whose value is equal to the definite integral in a finite computation time.

We observe that the curve gradually decreases and finally converges to zero at the maximum computation time. The reason is that the control strategies and location information required by these algorithms are degressive until the relay selection is finally confirmed. It is noted that the communication overhead of STS-RM, PHS-RM, and RS-LIDG is 24.92, 43.96, and 12.51, respectively. The results show that our proposed RS-LIDG reduces the communication overhead by 49.80% and 71.54% compared to STS-RM and PHS-RM. The main reasons are as follows: i) in the relay selection scheme, RS-LIDG only requires to select the optimal stopping phase according to the known control information, instead of traversing

all phases for the traditional algorithms; ii) RS-LIDG can iteratively partition the mobility region to obtain the optimum in the multiuser cooperative mobility strategy, while the traditional algorithm must exhaust all locations cases. Thus, STS-RM and PHS-RM require more redundant data than RS-LIDG.

5.6 Summary

In this chapter, we formulate a social-physical ad hoc network model based on multiuser cooperative mobility. The impacts of social intimacy and the probability of physical-layer data transmission success on link reliability are illustrated in this model. Accordingly, the system throughput maximization problem is constructed to optimize the selection of potential mobile relays and their geographic locations through a relay selection scheme and a cooperative mobility strategy. Moreover, we propose the Relay Selection and Link Interference Degree Graph (RS-LIDG) algorithm to address this NP-hard problem. It is proven that the proposed relay selection scheme can minimize the relay selection time while maintaining a high throughput gain. Furthermore, we define a graph representing the degrees of interference between links and verify that optimizing the mobile relays' locations with the proposed mobility strategy results in the maximization of the throughput performance. Numerical results show that our proposed RS-LIDG algorithm can increase the throughput gain by 26.29%, 123.43%, and 236.47% compared to IM, STS-RM, and PHS-RM, respectively.

Chapter 6

Conclusion and Future Prospects

6.1 Conclusion

This thesis focused on throughput performance maximization based on multiuser cooperative mobility in ad hoc networks. Previous approaches are limited to considering the single user mobility, i.e., an *independent* mobility strategy. In the case of multiuser cooperative mobility, the impact of user interference and signal strength on throughput is not considered simultaneously. Additionally, due to the huge diversity of the solution space, its complexity is very high and it is necessary to propose an algorithm with high throughput and low complexity. Finally, the motivation for cooperation of movable users needs to be considered, i.e., the social attributes of users. Only if certain social intimacy is reached, movable users are willing to cooperate.

We challenged multiuser cooperative mobility approach for maximizing throughput considering the signal attenuation and interference with different positions of users, low algorithmic complexity and social intimacy requirements. Most related work have only evaluated the features and performance of single-user mobility without jointly considering the problem of multiuser cooperative mobility and user interference in ad hoc networks. No related work jointly considered different geographical places and distances among all of the users to maximize throughput. Additionally, most previous algorithms for improving throughput performance have high complexity and high communication overhead. The high throughput and low complexity algorithms for cooperative multi-user mobility schemes have not been explored due to the complex transmission strategies and optimization conditions. Finally, an effective collaboration scheme that can achieve both high throughput and a low relay selection cost in practice has not yet been proposed.

To this end, we studied the following three contents: seeking a multiuser cooperative mobility approach for maximizing throughput considering the signal attenuation and interference with different positions of users; proposing a feasible and effective approach to achieve high throughput and low algorithmic complexity for larger number of user application scenarios; exploring an approach to improve the system throughput of social networks through multiuser cooperative mobility, i.e., to maximize throughput with high intimacy for relay selection.

In Chapter 3, we proposed an interaction position game (IPG) to maximize throughput based on multiuser cooperative mobility. Unlike conventional game-theoretic approaches, this game exploits cooperative behavior among movable users to obtain a global optimum

rather than a sub-optimum. The results showed that this game method improves the maximum throughput ratio evidently by 57.35% and 27.27% compared with the conventional intuitive method and SA algorithm, respectively. In Chapter 3, the proposed game is a remarkably effective method to improve system throughput in ad hoc networks.

In Chapter 4, we proposed a new algorithm, called Maximum Throughput algorithm for Optimal Position (MTOP), based on the known geographic location information of fixed users. Different from previous studies, the lower and upper bounds are derived to determine the search space domain based on feasible location assembles. The simulation results showed that the throughput of MTOP is increased by 298.81%, 37.91%, respectively, compared with the intuitive method, simulated annealing algorithm. Compared with game theory method and simulated annealing algorithm, MTOP reduces the computation cost by 44.12% and 237.97%, respectively. In Chapter 4, this proposed algorithm contributes to yielding an efficient multiuser cooperative mobility strategy in a large number of users to achieve high throughput performance and low algorithmic complexity.

In Chapter 5, we proposed the Relay selection and Link Interference Degree Graph (RS-LIDG) algorithm to obtain an optimal social relay selection scheme with high intimacy requirements to maximize the system throughput for social-physical ad hoc networks. Feasible relays and multiuser cooperative mobility with satisfactory link reliability for throughput maximization were jointly considered. Numerical simulations verified that the proposed RS-LIDG method improves the throughput gain by 26.29%, 123.43%, and 236.47% compared to the intuitive method (IM), the social-trust-based random mobility selection method (STS-RM), and the physical-based random mobility selection method (PHS-RM), respectively. In Chapter 5, this proposed algorithm contributed to maximizing throughput with satisfying high social intimacy in social-physical ad hoc networks.

In conclusion, this thesis achieved the improvement of the throughput based on multiuser cooperative mobility in ad hoc networks. This thesis contributes to advancing wireless networking, IoT and virtual reality of smart mobility. In particular, considering different application scenarios, including large number of users as well as social situations, we proposed three algorithms to achieve high throughput. The simulation results highlighted the performance of these proposed algorithms compared to previous methods.

6.2 Remaining problems and discussion

The current study has two problems that can be targeted for improvement in future work. Since this thesis primarily focuses on the theoretically achievable throughput performance, we have adopted several useful assumptions based on system modeling and ad hoc network modeling considerations.

First, we have not analyzed the data transmission loss of the relays during the mobility process of the developed model. Although the mobility time is short for existing communi-

cation systems, it does consume specific transmission slots for the relays, from disconnection to final access for the fixed users. Therefore, we needs to consider this contribution to the data throughput loss.

Second, the complexity of our proposed RS-LIDG algorithm is still high, making it difficult to meet the requirements of real-time systems with high accuracy. Compared with IM, our proposed cooperative mobility strategy has much space for improvement in terms of complexity. In the future, we will address these two issues by considering the data loss during relay mobility and reducing the degree of complexity. We hope to analyze the cases in which good throughput performance can be achieved without relay movement. Thus, the critical threshold conditions for the mobility and nonmobility of the relays can be derived.

6.3 Future prospects

In future research, we will continue to focus on the following three points.

- First, we will consider the impact of data throughput loss due to unstable communication connections while the user is moving. Although the mobility duration may be short, it can result in a loss of throughput performance. Therefore, the loss of system throughput due to this factor will be investigated in future studies, in terms of transmission time slots.

- Second, we want to propose a low complexity algorithm in the application scenario of social network. As we all know, computational complexity and system throughput performance are often two opposite indicators, both of which are often difficult to best at the same time. Thus, we expect to propose a new algorithm which can decrease the computation cost in real-time systems.

- Finally, we would like to propose a new method that can reduce the mobile distance of movable users and improve the system throughput. Our current study does not consider the costs of users' mobility, because it is difficult to measure by certain parameters, such as energy consumption or money, which are not appropriate. Therefore, we will consider how to reduce the users' mobility distance while also increasing the system throughput in future work.

In the short term, this research can greatly improve the user experience of anyone using mobile smart devices at any time and any place. Through further research, we will be able to achieve higher quality of ad hoc networks, which will help Augmented Reality (AR) and Virtual Reality (VR) technology implement. It can also be used in the future smart home system to bring convenience to people's family life.

In the long term, this research will improve the overall quality of life of people. The approach proposed in this research can be applied to other autonomous distributed communication systems. For example, in the future, many users may need high-quality communication

services at the same time in areas such as logistics and intelligent transportation. The results of this study can be applied to solve the multiuser interference problems that may arise from such cases.

Acknowledgement

With immense pleasure and deep sense of gratitude, I wish to express my sincere thanks to my supervisor **Prof. Tutomu Murase**, Information Technology Center, Nagoya University, without his motivation, continuous encouragement and elaborate guidance, this research would not have been successfully completed. He gave me a lot of help and support in my research, future planning, and life in Japan. In particular, **Prof. Tutomu Murase** instructed me how to be an excellent researcher and provided a platform for exchange and discussion with other professors. Through the study and exchange with other researchers, it helped me to open up research vision, expanded the research progress, and deepened my understanding of wireless network.

I am grateful to the various researchers for their assistance in my research. Especially, **Prof. Hiroyuki Seki**, Graduate School of Informatics in Nagoya University, **Prof. Yusheng Ji** in National Institute of Informatics, **Prof. Celimuge Wu** in University of Electro Communications, **Prof. Koji Nakazawa**, Graduate School of Informatics in Nagoya University, **Prof. Sumiko Miyata** in Shibaura Institute of Technology, and **Prof. Hiroyasu Obata** in Hiroshima City University, all of these professors played a great role in promoting my research, discussed with me and inspired me to explore the deeper principles of wireless communication.

I express my sincere thanks to all members in Murase and Shimada Laboratory. **Prof. Hajime Shimada** and **Prof. Yukiko Yamaguchi** supported me in my daily life and gave me kind support and encouragement in the laboratory. In particular, **Dr. Takeshi Hirai**, as my senior, often discussed academic issues with me and taught me how to make presentations and write project applications. In life, we are very good friends. He helped me to adapt daily life in Japan. **Prof. Yukihiro Tadokoro** and **Prof. Satoshi Makido** advised my research in team meeting. **Mrs. Junko Sakaguchi** administratively supported my reserach process and daily life in Japan. I like to acknowledge the support rendered by **Kosuke Okumura**, **Shoshin Nishibori**, **Sanya Kobayashi**, **Ryo Miyazaki**, **Takumi Ajiki**, and **Takumi Shiohara** in several ways throughout my research work and daily life in Japan. I also express my sincere thanks to my Chinese friends in Lab, **Yun Gao** and **Siyuan Su**, who made me feel the warmth from my motherland in Japan. **Yun Gao** helped me a lot in my daily life in Japan, and we are very close partners.

I wish to extend my profound sense of gratitude to **my parents** for all the sacrifices they made during my research and also providing me with moral support and encouragement whenever required. Without their constant encouragement and moral support along with patience and understanding, I can not finished the Doctoral course. Thanks to my former girlfriend, **Lufa Zeng**, who gave me a lot of encouragement. Even although we didn't get together in the end, I wish her better life in the future.

References

[1] E. Huang, W. Hu, J. Crowcroft, and I. Wassell, "Towards commercial mobile ad hoc network applications: A radio dispatch system," in *Proceedings of the 6th ACM international symposium on Mobile ad hoc networking and computing*, 2005, pp. 355–365.

[2] N. D. Han, Y. Chung, and M. Jo, "Green data centers for cloud-assisted mobile ad hoc networks in 5G,"*IEEE Netw.*, vol. 29, no. 2, pp. 70–76, 2015.

[3] B. Alawieh, Y. Zhang, C. Assi, and H. Mouftah, "Improving spatial reuse in multihop wireless networks-a survey," *IEEE Commun. Surv. Tutorials*, vol. 11, no. 3, pp. 71–91, 2009.

[4] Van Nee, Richard, et al. "The 802.11 n MIMO-OFDM standard for wireless LAN and beyond," *Wireless Personal Communications*, vol. 37, no. 3, pp. 445-453, 2006.

[5] S. Stefan, and M. Rupp. "Throughput maximizing feedback for MIMO OFDM based wireless communication systems," in *IEEE 12th International Workshop on Signal Processing Advances in Wireless Communications*, pp. 316-320, 2011.

[6] R. Daniels, C. Caramanis, R. Heath, "Adaptation in convolutionally coded MIMO-OFDM wireless systems through supervised learning and SNR ordering," *IEEE Trans. Veh. Technol.*, vol. 59, no. 1, pp. 114 - 126, 2010.

[7] B. Pankaj, D. Rajballav, C. Gwan, "Array like runtime re-configurable MIMO detectors for 802.11n WLAN: a design case study," *ASP-DAC*, pp 751 - 756, 2009.

[8] Michael Wu, et al. "High-throughput data detection for massive MU-MIMO-OFDM using coordinate descent," *IEEE Transactions on Circuits and Systems I: Regular Papers*, vol. 63, no. 12, pp. 2357-2367, 2016.

[9] H. Bolcskei, Moritz Borgmann, and Arogyaswami J. Paulraj, "Impact of the propagation environment on the performance of space-frequency coded MIMO-OFDM," *IEEE Journal on selected areas in communications*, vol. 21, no. 3, pp. 427-439, 2003.

[10] E. Charfi, L. Chaari and L. Kamoun, "Fairness of the IEEE 802.11n aggregation scheme for real time application in unsaturated condition," in *4th Joint IFIP Wireless and Mobile Networking Conference (WMNC)*, pp. 1-8, 2011.

[11] H. Lin, C. Wang and H. Wei, "Improving online game performance over IEEE 802.11n networks," in *9th Annual Workshop on Network and Systems Support for Games*, pp. 1-2, 2010.

[12] PK. Hazra, and D. Asok, "Performance Analysis of IEEE 802.11 e EDCA with QoS Enhancements through TXOP based Frame-concatenation and Block-acknowledgement," in *International Journal of Advancements in Technology*, vol. 2, no. 4, pp. 542-560, 2011.

[13] S. Chakraborty and S. Nandi, "Evaluating transport protocol performance over a wireless mesh backbone," *Perform. Eval.*, vol. 79, pp. 198–215, 2014.

[14] Z. Hu, X. Wen, Z. Li, Z. Lu, and W. Jing, "Modeling the TXOP sharing mechanism of IEEE 802.11 ac enhanced distributed channel access in non-saturated conditions," *IEEE Commun. Lett.*, vol. 19, no. 9, pp. 1576–1579, 2015.

[15] M. Aajami and J.-B. Suk, "Optimal TXOP sharing in IEEE 802.11 ac," *IEEE Commun. Lett.*, vol. 19, no. 7, pp. 1141–1144, 2015.

[16] M. Esslaoui, F. Riera-Palou, and G. Femenias, "A fair MU-MIMO scheme for IEEE 802.11 ac," in *2012 International Symposium on Wireless Communication Systems (ISWCS)*, 2012, pp. 1049–1053.

[17] M. Samih and E. Al-Hemiary, "Impact of TCP congestion control algorithms on IEEE802. 11n MAC frame aggregation," *Inter. J. Comput. Sci. Eng. Technol.*, vol. 2, no. 9, pp. 1410–1414, 2012.

[18] U. Akyol, M. Andrews, P. Gupta, J. Hobby, I. Saniee and A. Stolyar. "Joint scheduling and congestion control in mobile ad-hoc networks," *in Proc. IEEE INFOCOM*, Mar. 2008, pp. 619-627.

[19] Lichun Bao and Jose Juaquin Garcia-Luna-Aceves. "Topology management in ad hoc networks," *in Proc. 4th ACM int. sym. on Mob. ad hoc net and com (MobiHoc)*, Jun. 2003, pp. 129-140.

[20] M. Rajesh and J. M. Gnanasekar. "Path observation based physical routing protocol for wireless ad hoc networks," *Wireless Personal Communications.*, vol. 97, no. 1, pp. 1267-1289, Jun. 2017.

[21] Shigang Chen and K. Nahrstedt, "Distributed quality-of-service routing in ad hoc networks," *IEEE Journal on Selected Areas in Communications*, vol. 17, no. 8, pp. 1488-1505, Aug. 1999,

[22] S. De et al., "Trigger-Based Distributed QoS Routing in Mobile Ad Hoc Networks," in *ACM SIGMOBILE Mobile Comp. and Commun. Rev.*, vol. 6, no. 3, pp. 22–35, July 2002.

[23] T. Goff et al., "Preemptive Maintenance Routing in Ad Hoc Networks," in *Proc. ACM MobiCom.*, pp. 43–52, 2001.

[24] M. Grossglauser and D. N. C. Tse, "Mobility increases the capacity of ad hoc wireless networks," *IEEE/ACM Trans. Netw.*, vol. 10, no. 4, pp. 477–486, 2002.

[25] B. Baron, P. Spathis, M. D. de Amorim, Y. Viniotis, and M. H. Ammar, "Mobility as an alternative communication channel: A survey," *IEEE Commun. Surv. Tutorials*, vol. 21, no. 1, pp. 289–314, 2018.

[26] T. Murase, "User cooperative mobility for better multimedia communication quality," in *Proceedings of the ACM SIGCOMM workshop on Future human-centric multimedia networking*, 2013, pp. 39–40.

[27] A. Chaintreau, P. Hui, J. Crowcroft, C. Diot, R. Gass, and J. Scott, "Impact of human mobility on opportunistic forwarding algorithms," *IEEE Trans. Mob. Comput.*, vol. 6, no. 6, pp. 606–620, 2007.

[28] S. Miyata, T. Murase, and K. Yamaoka, "Novel access-point selection for user QoS and system optimization based on user cooperative moving," *IEICE Trans. Commun.*, vol. E95-B, no. 6, pp. 1953–1964, 2012.

[29] Ryo HAMAMOTO, Tutomu MURASE, Chisa TAKANO, Hiroyasu OBATA, and Kenji ISHIDA. "A Proposal of Access Point Selection Method Based on Cooperative Movement of Both Access Points and Users," *IEICE Transactions on Information and Systems.*, vol. 98, no. 12, pp. 2048-2059, Dec. 2015.

[30] Tianran Luo and Tutomu Murase. "User cooperative mobility for QoS improvement in ad-hoc networks," in *Proc. 14th IEEE Annual Cons. Comm. and Net. Conf. (CCNC)*, pp. 276-279, Jan. 2017.

[31] Tianran Luo and Tutomu Murase. "Validation of theoretical evaluation on user cooperative mobility for QoS improvement in ad-hoc networks," in *Proc. 6th Glob. Conf. on Cons. Elec. (GCCE)*, pp. 1-2, Oct. 2017.

[32] Prasant Mohapatra, Jian Li and Chao Gui. "QoS in mobile ad hoc networks," *IEEE Wireless Communications.*, vol. 10, no. 3, pp. 44-53, Jun. 2003.

[33] Riku Ohmiya, Hiroyasu Obata, and Tutomu Murase. "Optimal placement considering interference in multiple ad hoc networks," *in Proc. Int. Conf. on Infor. Net. (ICOIN)*, Jan. 2018, pp. 694-699.

[34] Jiquan Xie and Tutomu Murase, "Multiple User Cooperative Mobility in Mobile Ad Hoc Networks: An Interaction Position Game," *IEEE Access.*, vol. 8, pp. 126297 - 126314, Jul. 2020.

[35] Jiquan Xie and Tutomu Murase, "An Optimal Location Allocation by Multi-User Cooperative Mobility for Maximizing Throughput in MANETs," *IEEE Access.*, vol. 8, pp. 226089 - 226107, Dec. 2020.

[36] Jiquan Xie and Tutomu Murase, "Effective collaboration to maximize throughput based on multiuser cooperative mobility in social-physical ad hoc networks," *IEEE Open Journal of the Communications Society.*, vol. 2, pp. 818-835, Apr. 2021.

[37] S. Zhang, J. Liu, H. Guo, M. Qi and N. Kato, "Envisioning Device-to-Device Communications in 6G," *IEEE Network*, vol. 34, no. 3, pp. 86-91, May/June 2020.

[38] P. Yuan, R. Huang, "Integrating the device-to-device communication technology into edge computing: A case study," *Peer-to-Peer Networking and Applications*, vol. 14, no. 2, pp. 599-608, 2021.

[39] N. Kim, W. Na and S. Cho, "Dual-Channel-Based Mobile Ad Hoc Network Routing Technique for Indoor Disaster Environment," *IEEE Access*, vol. 8, pp. 126713-126724, 2020.

[40] F. Liu, K. W. Shum, Y. Zhang and W. S. Wong, Schedule Sequence Design for Broadcast in Multi-Channel Ad Hoc Networks, *IEEE Transactions on Vehicular Technology*, vol. 70, no. 5, pp. 4767-4783, May 2021.

[41] M.T. Mamaghani, A. Kuhestani, and H. Behroozi, Can a multi-hop link relying on untrusted amplify-and-forward relays render security? *Wireless Netw.*, vol. 27, pp. 795-807, 2021.

[42] Xuening Liao, et al. Buffer-aided relay selection for secure two-hop wireless networks with decode-and-forward relays and a diversity-combining eavesdropper, *Ad Hoc Networks*, vol. 98, pp. 102039, 2020.

[43] Shuokang Huang, and Kai Lei. IGAN-IDS: An imbalanced generative adversarial network towards intrusion detection system in ad-hoc networks, *Ad Hoc Networks*, vol. 105, pp.102177, 2020.

[44] E. Charfi, L. Chaari and L. Kamoun, "PHY/MAC Enhancements and QoS Mechanisms for Very High Throughput WLANs: A Survey," *IEEE Communications Surveys and Tutorials*, vol. 15, no. 4, pp. 1714-1735, Fourth Quarter 2013.

[45] K. Okumura and T. Murase, "User Cooperative Mobility with Optimal Node Selection for High Throughput in Multiple Ad-Hoc Networks," in *14th International Conference on Ubiquitous Information Management and Communication (IMCOM)*, 2020, pp. 1–7.

[46] Quang Duy Lã, Yong Huat Chew, and Boon-Hee Soong. "Potential Games," *in Potential Game Theory*, Switzerland: Springer, 2016, pp. 23-68. [Online]. Available: https://morawa.at/annotstream/2244009860229/PDF/L

[47] Koji Yamamoto. "A comprehensive survey of potential game approaches to wireless networks," *IEICE Transactions on Communications.*, vol. 98, no. 9, pp. 1804-1823, Sep. 2015.

[48] Zhangyu Guan, Tommaso Melodia, Dongfeng Yuan and Dimitris A. Pados. "Distributed resource management for cognitive ad hoc networks with cooperative relays," *IEEE/ACM Transactions on Networking.*, vol. 24, no. 3, pp. 1675-1689, Jun. 2015.

[49] Yuhua Xu, Jinlong Wang, Qihui Wu, Alagan Anpalagan and Yu-Dong Yao. "Opportunistic spectrum access in cognitive radio networks: Global optimization using local interaction games," *IEEE Journal of Selected Topics in Signal Processing.*, vol. 6, no. 2, pp. 180-194, Apr. 2011.

[50] Zhang, Yan, and Mohsen Guizani. "Game theory for wireless communications and networking," in *CRC press*, 2011, pp. 3-27.

[51] D. Goodman and N. Mandayam, "Power control for wireless data," *IEEE Personal Commun. Mag.*, vol. 7, pp. 48–54, Apr. 2000.

[52] E. E. Tsiropoulou, T. Kastrinogiannis, and S. Papavassiliou, "QoS-Driven Uplink Power Control in Multi-Service CDMA Wireless Networks - A Game Theoretic Framework," *Journal of Communications, Academy Publisher.*, vol. 4, no. 9, pp. 654-668, Oct. 2009.

[53] S. Ramanathan and E. L. Lloyd, "Scheduling algorithms for multihop radio networks," *IEEE/ACM Trans. Netw.*, vol. 1, no. 2, pp. 166–177, 1993.

[54] K. Jain, J. Padhye, V. N. Padmanabhan, and L. Qiu, "Impact of interference on multihop wireless network performance," *Wirel. networks*, vol. 11, no. 4, pp. 471–487, 2005.

[55] L. Chen, S. H. Low, and J. C. Doyle, "Joint congestion control and media access control design for ad hoc wireless networks," *Proc. - IEEE INFOCOM*, vol. 3, pp. 2212–2222, 2005.

[56] S. Lv, X. Wang, and X. Zhou, "Scheduling under SINR model in ad hoc networks with successive interference cancellation," *GLOBECOM - IEEE Glob. Telecommun. Conf.*, no. December 2010, 2010.

[57] J. Luo, A. Iyer, and C. Rosenberg, "Throughput-lifetime trade-offs in multihop wireless networks under an SINR-based interference model," *IEEE Trans. Mob. Comput.*, vol. 10, no. 3, pp. 419–433, 2010.

[58] T. Igarashi, J. Takai, and T. Yoshida, "Gender differences in social network development via mobile phone text messages: A longitudinal study," *J. Soc. Pers. Relat.*, vol. 22, no. 5, pp. 691–713, 2005.

[59] R. Jurdak, C. V. Lopes, and P. Baldi, "A survey, classification and comparative analysis of medium access control protocols for ad hoc networks," *IEEE Commun. Surv. Tutorials*, vol. 6, no. 1, pp. 2–16, 2004.

[60] M. Zhang, X. Chen, and J. Zhang, "Social-aware relay selection for cooperative networking: An optimal stopping approach," *IEEE Int. Conf. Commun. ICC*, pp. 2257–2262, 2014.

[61] X. Pan and H. Wang, "On the performance analysis and relay algorithm design in social-aware D2D cooperated communications," *IEEE Veh. Technol. Conf.*, vol. 2016-July, pp. 0–4, 2016.

[62] Z. Fang and X. Li, "A novel relay selection algorithm based on mobile social networks for device-to-device cooperative communications," *ICNC-FSKD 13th Int. Conf. Nat. Comput. Fuzzy Syst. Knowl. Discov.*, pp. 2755–2761, 2018.

[63] U. S. Khwakhali, S. Gordon, and P. Suksompong, "Social-Aware relay selection for device to device communications in cooperative cellular networks," *Int. Electr. Eng. Congr. iEECON*, pp. 9–12, 2017.

[64] H. Mao, W. Feng, and N. Ge, "Performance of Social-Position Relationships Based Cooperation Among Mobile Terminals," *IEEE Trans. Veh. Technol.*, vol. 65, no. 5, pp. 3128–3138, 2016.

[65] H. Zhang, Q. Du, P. Ren, and Z. Wang, "Social stability enhanced mobile D2D relay networks: An optimal stopping approach," in *IEEE International Conference on Communications*, 2017, pp. 1–6.

[66] Satoka Fujii, Tutomu Murase, Masato Oguchi and Eng Keong Lua. "Architecture and characteristics of social network based ad hoc networking," *in Proc. Int. Symp. on Loc. and Metro. Area Net (LANMAN)*, Jun. 2016, pp. 1-3.

[67] Tsiropoulou, E.E., Vamvakas, P., Papavassiliou, S. "Resource Allocation in Multi-tier Femtocell and Visible-Light Heterogeneous Wireless Networks," *Resource Allocation in Next-Generation Broadband Wireless Access Networks. IGI Global: Hershey*, PA, USA, 2017. [Online]. Available: https://www.igi-global.com/gateway/chapter/178143

[68] Illya Stepanov, Daniel Herrscher, Kurt Rothermel. "On the impact of radio propagation models on MANET simulation results," *in Proc. 7th IFIP Int. Conf. on Mob. and Wire. Comm. Net. (MWCN)*, Sep. 2005, pp. 1-7.

[69] Patrick Stuedi, Oscar Chinellato, Gustavo Alonso. "Connectivity in the presence of shadowing in 802.11 ad hoc networks." *IEEE Wireless Communications and Networking Conference*, Apr. 2005, Vol. 4, pp. 2225-2230.

[70] K. Medepalli and F.A. Tobagi. "Throughput analysis of IEEE 802.11 wireless LANs using an average cycle time approach," *in Proc. IEEE GLOBECOM*, St. Louis, MO, USA, Nov. 2005, pp. 3007-3011.

[71] S. Lasaulce and H. Tembine. "Fundamentals of game theory," *in Game theory and learning for wireless networks: fundamentals and applications*, Academic Press, 2011, pp. 3-66. [Online]. Available: https://hal.archives-ouvertes.fr/hal-00661625/.

[72] Bo Yin, Shotaro Kamiya, Koji Yamamoto, Takayuki Nishio, Masahiro Morikura and Hirantha Abeysekera. "Starvation mitigation for dense WLANs through distributed channel selection: Potential game approach," *in Proc. 14th Annual Cons. Comm. and Net. Conf. (CCNC)*, Jan. 2017, pp. 548-553.

[73] D. Monderer and L. S. Shapley, "Potential games," *Games Econ. Behav.*, vol. 14, no. 1, pp. 124–143, May 1996.

[74] Takashi Ui. "A Shapley value representation of potential games," *Games and Economic Behavior.*, vol. 31, no. 1, pp. 121-135, Apr. 2000.

[75] H. Peyton Young. *Individual strategy and social structure: An evolutionary theory of institutions.* Princeton, NJ: Princeton University Press, Jan. 2001.

[76] Minghua Chen, Soung Chang Liew, Ziyu Shao and Caihong Kai. "Markov approximation for combinatorial network optimization," *IEEE Transactions on Information Theory.*, vol. 59, no. 10, pp. 6301-6327, Jun. 2013.

[77] S. Bandyopadhyay. "Simulated annealing using a reversible jump Markov chain Monte Carlo algorithm for fuzzy clustering," *IEEE Transactions on Knowledge and data Engineering.*, vol. 17, no. 4, pp. 479-490, Mar. 2005.

[78] P. J. M. van Laarhoven and E. H. L. Aarts, *Simulated Annealing: Theory andApplications.* New York, NY, USA: Springer, 1987.

[79] S. Z. Selim and K. Alsultan, "A simulated annealing algorithm for the clustering problem," *Pattern Recognit.*, vol. 24, no. 10, pp. 1003-1008, Jan. 1991. [Online]. Available: https://www.sciencedirect.com/science/article/pii/003132039190090.

[80] K. Medepalli and F. A. Tobagi, "Throughput analysis of IEEE 802.11 wireless LANs using an average cycle time approach," in *GLOBECOM'05. IEEE Global Telecommunications Conference.*, 2005, vol. 5, pp. 5.

[81] S. P. Weber, X. Yang, J. G. Andrews, and G. De Veciana, "Transmission capacity of wireless ad hoc networks with outage constraints," *IEEE Trans. Inf. theory*, vol. 51, no. 12, pp. 4091–4102, 2005.

[82] Y.-W. P. Hong, W.-J. Huang, and C.-C. J. Kuo, *Cooperative communications and networking: technologies and system design.* Springer Science and Business Media, 2010, pp. 17-77. [Online]. Available: http://dl.merc.ac.ir/handle/Hannan/146#sthash.KzZwJ4wA.dpbs

[83] G. Kramer, M. Gastpar, and P. Gupta, "Cooperative strategies and capacity theorems for relay networks," *IEEE Trans. Inf. Theory*, vol. 51, no. 9, pp. 3037–3063, 2005.

[84] D. Chen and J. N. Laneman, "Modulation and demodulation for cooperative diversity in wireless systems," *IEEE Trans. Wirel. Commun.*, vol. 5, no. 7, pp. 1785–1794, 2006.

[85] I. Stepanov, D. Herrscher, and K. Rothermel, "On the impact of radio propagation models on MANET simulation results," in Proceedings of 7th International Conference on Mobile and Wireless Communications Networks (MWCN), Marrakech, Morocco, Sep. 2005, pp. 1-7.

[86] P. Stuedi, O. Chinellato, and G. Alonso, "Connectivity in the presence of shadowing in 802.11 ad hoc networks," in *IEEE Wireless Communications and Networking Conference*, 2005, vol. 4, pp. 2225–2230.

[87] G. Brar, D. M. Blough, and P. Santi, "Computationally efficient scheduling with the physical interference model for throughput improvement in wireless mesh networks," *Proc. Annu. Int. Conf. Mob. Comput. Networking, MOBICOM*, vol. 2006, pp. 2–13, 2006.

[88] S. Kirkpatrick, C. D. Gelatt, and M. P. Vecchi, "Optimization by simulated annealing," *Science (80-.).*, vol. 220, no. 4598, pp. 671–680, 1983.

[89] H. E. Romeijn and R. L. Smith, "Simulated annealing for constrained global optimization," *J. Glob. Optim.*, vol. 5, no. 2, pp. 101–126, 1994.

[90] T. Y. Lin and J. C. Hou, "Interplay of spatial reuse and SINR-determined data rates in CSMA/CA-based, multi-hop, multi-rate wireless networks," *Proc. - IEEE INFOCOM*, pp. 803–811, 2007.

[91] J. Li, C. Blake, D. S. J. De Couto, H. I. Lee, and R. Morris, "Capacity of ad hoc wireless networks," in *Proceedings of the 7th annual international conference on Mobile computing and networking*, 2001, pp. 61–69.

[92] M. Heusse, F. Rousseau, G. Berger-Sabbatel and A. Duda. "Performance anomaly of 802.11 b," *in Proc. IEEE INFOCOM*, Mar. 2003, pp. 836-843.

[93] A. Fathi, Q. Shafiee, and H. Bevrani, "Robust frequency control of microgrids using an extended virtual synchronous generator," *IEEE Trans. Power Syst.*, vol. 33, no. 6, pp. 6289–6297, 2018.

[94] Y. Li, S. Qiang, X. Zhuang, and O. Kaynak, "Robust and adaptive backstepping control for nonlinear systems using RBF neural networks," *IEEE Trans. Neural Networks*, vol. 15, no. 3, pp. 693–701, 2004.

[95] A. P. Aguiar and J. P. Hespanha, "Trajectory-tracking and path-following of underactuated autonomous vehicles with parametric modeling uncertainty," *IEEE Trans. Automat. Contr.*, vol. 52, no. 8, pp. 1362–1379, 2007.

[96] S. P. Weber, J. G. Andrews, X. Yang, and G. De Veciana, "Transmission capacity of wireless ad hoc networks with successive interference cancellation," *IEEE Trans. Inf. Theory*, vol. 53, no. 8, pp. 2799–2814, 2007.

[97] Y. Ma, G. Zhou, and S. Wang, "WiFi sensing with channel state information: A survey," *ACM Comput. Surv.*, vol. 52, no. 3, pp. 1–36, 2019.

[98] S. Berger, M. Kuhn, A. Wittneben, T. Unger, and A. Klein, "Recent advances in amplify-and-forward two-hop relaying," *IEEE Commun. Mag.*, vol. 47, no. 7, pp. 50–56, 2009.

[99] Z. Zhang, P. Zhang, D. Liu, and S. Sun, "SRSM-based adaptive relay selection for D2D communications," *IEEE Internet Things J.*, vol. 5, no. 4, pp. 2323–2332, 2017.

[100] S. Nam, M. Vu, and V. Tarokh, "Relay selection methods for wireless cooperative communications," in 2008 42nd Annual Conference on Information Sciences and Systems, 2008, pp. 859–864.

[101] S. Boyd and L. Vandenberghe, Convex Optimization. Cambridge, U.K.: Cambridge Univ. Press, 2004.

[102] S. Dempe, "Directional differentiability of optimal solutions under Slater's condition," *Math. Program.*, vol. 59, no. 1, pp. 49–69, 1993.

[103] S. Ruder, "An overview of gradient descent optimization algorithms," *arXiv Prepr. arXiv1609.04747*, 2016.

[104] Q. Wei, D. Liu, and H. Lin, "Value iteration adaptive dynamic programming for optimal control of discrete-time nonlinear systems," *IEEE Trans. Cybern.*, vol. 46, no. 3, pp. 840–853, 2015.

[105] IEEE Standard for Information Technology, 802.11g-2003, "Wireless LAN Medium Access Control (MAC) and Physical Layer (PHY) Specifications", 2003.

[106] L. Wang, H. Tang, and M. Čierny, "Device-to-device link admission policy based on social interaction information," *IEEE Trans. Veh. Technol.*, vol. 64, no. 9, pp. 4180–4186, 2014.

[107] A. Passarella and M. Conti, "Analysis of individual pair and aggregate intercontact times in heterogeneous opportunistic networks," *IEEE Trans. Mob. Comput.*, vol. 12, no. 12, pp. 2483–2495, 2012.

[108] George F. Riley, and R. Henderson. Thomas, "The ns-3 network simulator," *Modeling and tools for network simulation*, Springer, Berlin, Heidelberg, pp. 15-34, 2010.

List of Publications

Peer-reviewed Journals

1. Jiquan Xie and Tutomu Murase, "Effective Collaboration to Maximize Throughput Based on Multiuser Cooperative Mobility in Social-Physical Ad Hoc Networks," *IEEE Open Journal of the Communications Society*, vol. 2, pp. 818-835, Apr. 2021.

2. Jiquan Xie and Tutomu Murase, "An Optimal Location Allocation by Multi-User Cooperative Mobility for Maximizing Throughput in MANETs," *IEEE Access*, vol. 8, pp. 226089 - 226107, Dec. 2020.

3. Jiquan Xie and Tutomu Murase, "Multiple User Cooperative Mobility in Mobile Ad Hoc Networks: An Interaction Position Game," *IEEE Access*, vol. 8, pp. 126297 - 126314, Jul. 2020.

International Conference

1. Jiquan Xie and Tutomu Murase, "Potential Games for Improving Throughput of Social Relay Networks by Multi-User Cooperative Mobility," in *IEEE International Conference on Communications (ICC)*, Jun. 2021 (Accepted).

Domestic Conferences

1. Jiquan Xie and Tutomu Murase, "Multiple User Cooperative Mobility with An Interaction Position Game in Ad Hoc Networks for Improving Throughput," in *IEICE Technical Report*, vol. 120, no. 414, IN2020-89, pp. 208-213, Mar. 2021.

2. Jiquan Xie and Tutomu Murase, "Improvement of System Throughput by Multiple User Mobility in Multiple Ad Hoc Networks," in *IEICE Technical Report*, vol. 119, no. 460, NS2019-245, pp. 383-387, Mar. 2020.